Roles of Osteoclasts and Macrophages in Medication-Related Osteonecrosis of the Jaw Pathophysiology

Apichai Yavirach

A dissertation

submitted in partial fulfillment of the

requirements for the degree of

Doctor of Philosophy

University of Washington

2022

Reading Committee:

Cecilia M. Giachelli, Chair

Marta Scatena

Hai Zhang

Program Authorized to Offer Degree:

Oral Health Sciences

University of Washington

Abstract

Roles of Osteoclasts and Macrophages in Medication-Related Osteonecrosis of the Jaw Pathophysiology

Apichai Yavirach

Chair of the Supervisory Committee:
Cecilia M. Giachelli
Department of Bioengineering

Medication-related osteonecrosis of the jaw (MRONJ) is a serious side effect of antiresorptive drugs including bisphosphonates (BPs) and denosumab (anti-RANKL antibody) prescribed for osteoporosis and cancer treatments. MRONJ often occurs after tooth extraction as the presence of necrotic bone and impaired soft and hard tissue healing in oral cavity resulting in pain and affecting patients' quality of life. Although the risk of MRONJ is low, the numbers of patients taking these drugs are high (> 10 million worldwide) and still increasing making this a growing clinical problem. Importantly, the mechanisms underlying MRONJ pathophysiology have remained elusive, hence, the effective curative treatments have not been established. In this thesis, the effects of anti-RANKL antibody on several cell types which may potentially

contribute to MRONJ pathophysiology were investigated. First, osteoclasts, a bone resorbing cell, were studied. Utilizing tooth extraction and anti-RANKL antibody injections in nude mice, absence of osteoclasts and necrotic bone accumulation were observed in the MRONJ mouse model. I further showed that the replenishment of bone resorptive function by the local delivery of iRANK cells, the engineered cells whose osteoclast differentiation can be controlled by CID drug and is independent of RANKL, decreased necrotic bone area, but did not improve other MRONJ features. This suggests that other mechanisms besides osteoclast inhibition may play a role in MRONJ pathophysiology. Next, osteoblasts, a bone forming cell, were studied. Interestingly, anti-RANKL antibody did not have any significant effect on osteogenic differentiation of osteoblasts via RANKL autocrine/paracrine loop *in vitro* suggesting that it has no direct effect on mineralization. Lastly, macrophages, an immune cell involved in inflammation and wound healing, were studied. The effects of the presence and the absence of RANKL on macrophage polarization were determined. I showed that RANKL has only slight effects on macrophage polarization *in vitro*; it upregulated several genes similarly to M1 macrophages but in much lower level. However, the increased M1/M2 ratio was observed in the MRONJ mouse model. All these findings support bone remodeling inhibition and inflammation as potential mechanisms of MRONJ as well as paving the way for engineered osteoclasts cell therapy for MRONJ treatment.

TABLE OF CONTENTS

LIST OF FIGURES

LIST OF TABLES

LIST OF ABBREVIATIONS

α-MEM	minimum essential medium eagle - alpha modification
ALP	alkaline phosphatase
BMD	bone marrow derived
BMP	bone morphogenetic protein
BPs	bisphosphonates
BRONJ	bisphosphonate-related osteonecrosis of the jaw
CAII	carbonic anhydrase II
CCL	CC chemokine ligand
cDNA	complementary deoxyribonucleic acid
CID	chemical inducer of dimerization
DEGs	differentially-expressed genes
DMEM	dulbecco's modified eagle's medium
DRONJ	denosumab-related osteonecrosis of the jaw
EDTA	ethylenediaminetetraacetic acid
EtOH	ethanol
FACS	fluorescence-activated cell sorting
FBS	fetal bovine serum
GFP	green fluorescent protein
GO	gene ontology
H&E	hematoxylin and eosin

IFN	interferon
iRANK	inducible receptor activator of nuclear factor kappa-B
IL	interleukin
KEGG	Kyoto Encyclopedia of Genes and Genomes
LPS	lipopolysaccharide
M-CSF	macrophage-colony stimulating factor
MMP	matrix metalloproteinase
MRONJ	medication-related osteonecrosis of the jaw
MSC	mesenchymal stem cell
NaCl	sodium chloride
NaOH	sodium hydroxide
NDS	normal donkey serum
NF-κB	nuclear factor kappa-light-chain-enhancer of activated B cells
OC	osteoclast
ONJ	osteonecrosis of the jaw
OPG	osteoprotegerin
OSM	osteogenic media
P/S	penicillin/streptomycin
PBS	phosphate buffered saline
RANK	receptor activator of nuclear factor kappa-B
RANKL	receptor activator of nuclear factor kappa-B ligand
RNA	ribonucleic acid
RNA-seq	ribonucleic acid sequencing

RPM	RANKL-polarized macrophage
rRNA	ribosomal ribonucleic acid
SREs	skeletal-related events
TBS-T	TRIS-buffered saline with Tween
TGF	transforming growth factor
TNF	tumor necrosis factor
TRAP	tartrate resistant acid phosphatase
ZA	zoledronic acid

ACKNOWLEDGEMENTS

I know that pursuing PhD is a commitment, however, I did not truly know how long and challenging this journey could be until I embarked. It takes a village to be where I am today. First and foremost, I would like to sincerely thank Dr. Cecilia Giachelli for her encouragement and advice on research and career development. Coming from a clinical field with very limited research experience, I had been struggled with learning new skills and developing research questions. Her words, "Why would you need to come here if you already know them? You come here to learn things you do not know.", motivated me to embrace the process of getting out of the comfort zone and helped me become a better researcher today. I would like to also thank Elizabeth Soberg, a former lab manager of Giachelli lab, for her assistance and patience. She had been tremendously helpful and taught me literally everything about lab works from pipetting to designing experiments. Additionally, I would like to thank my committee members, Dr. Marta Scatena, Dr. Hai Zhang, Dr. Tracy Popowics, and Dr. Sue Herring for both academic advice and emotional support throughout these five years.

Pursuing PhD is hard, but pursuing PhD overseas away from my beloved family and friends makes it ten times harder. I am very grateful for an opportunity to work in Giachelli lab with wonderful friends and colleagues. I would like to thank former and current members of Giachelli and Scatena lab including Philip Walczak, Hao Zhou, Jessica Simon, Maristella Donato, Erica Ijeoma, Alex Rasch, Taleb Ahsan, Jessica Bretz, Annika Kumar, Elizabeth Leber, Meiting Wu, Subramanian Dharmarajan, Kat Pierce, Jake Lally, Chaoyang Tang, Li Fu, Nong Sirirat, and Ice Worakanya Buranaphatthana for both lab-related advice and mental support. Additionally, I would

like to give a shout out to Aditi Prabhala, my undergraduate student helper, for her help on RNA-seq analysis and macrophage quantitation. Lab happy hours were probably one of the things I looked forward to every week!

In addition to Giachelli and Scatena lab members, supports from my friends and colleagues outside of the lab also largely contribute to my success today. I would like to thank friends and faculties from the Oral Health Sciences Department especially Dr. Richard Presland, Dr. Robert Cornell, Lora Brewsaugh, Kathy Hobson, and Priti Mulimani. Moreover, I would like to thank my Fulbright friends for their emotional support and arrangement of enjoyable extracurricular activities throughout of my first two years in Seattle. Although I am glad that most of us have completed the master's degree and went back to their home countries to follow their dreams, I am happy that Mareldi Ahumada is still here with me to finish our PhD journey together. Furthermore, I would like to thank all my Thai friends in Seattle for Friday gathering and bringing me taste of home which I am much needed.

I would like to acknowledge my funding for both research and living throughout these five years including Thai government scholarship for Geriatrics study, Fulbright scholarship, and Magnuson scholarship. Also, many thanks to the faculties and staffs at Faculty of Dentistry, Chiang Mai University, Thailand who guided me through the application process and developing research ideas.

Most importantly, I would like to wholeheartedly thank my beloved parents and family for their understanding and unconditional love. Without a single word of complaint, they have sacrificed exceedingly to ensure that I will be alright. I am proud to say that this success does not only belong to me, but to every single one of them.

DEDICATION

To my beloved parents, family, and the Kingdom of Thailand

Chapter 1. INTRODUCTION

1.1 BACKGROUND

1.1.1 *Medication-related osteonecrosis of the jaw*

1.1.1.1 Definition

Medication-related osteonecrosis of the jaw (MRONJ), which was first described in 2003, is a potentially serious side effect of treatment of certain medications that often occurs in the oral cavity after traumatic dentoalveolar procedures such as tooth extraction.*(1, 2)* Those medications are 1.) antiresorptive drugs including bisphosphonates (BPs) and denosumab which are prescribed to treat osteoporosis and osteopenia, and to manage cancer-related conditions and 2.) antiangiogenic drugs which are prescribed to treat malignancies by disrupting the angiogenesis-signaling cascade.*(1)* The characteristics of MRONJ patients include 1.) current or previous treatment of antiresorptive or antiangiogenic drugs 2.) exposed bone or bone that can be probed through a fistula in the maxillofacial region persisting for more than 8 weeks and 3.) No history of radiation therapy and metastatic disease to the jaws **(Figure 1.1)**.*(1)*

In May 2022, the American Association of Oral and Maxillofacial Surgeons (AAOMS) published a position paper on MRONJ updating the one released in 2014.*(3)* The criteria of MRONJ remained almost the same, with the exception that the characteristics of MRONJ patients was broadened to include those with current or previous treatment with antiresorptive therapy alone or in combination with immune modulators or antiangiogenic medications. Moreover, romosozumab was introduced as another antiresorptive drug, in addition to BPs and denosumab. Romosozumab is a new monoclonal antibody used to prevent fracture in osteoporotic patients by

binding to and inhibiting sclerostin in the Wnt pathway, which results in increased bone formation and decreased bone resorption.*(3)*

1.1.1.2 Staging and treatment strategies

In 2009, AAOMS introduced a staging system to help establish proper treatment strategies for individuals, and to evaluate the prognosis and outcome of MRONJ.*(4)* It was modified in 2014*(1)* and has remained the same in the 2022 position paper.*(3)* Symptoms as well as clinical and radiographic findings of patients are used to classify the MRONJ stages as summarized in **Table 1.1**. In brief, patients are considered at risk when treated with antiresorptive drugs without any symptoms or visible necrotic bone, while stage 0 has nonspecific symptoms or findings without apparent necrotic bone. Stage 1 to 3 patients all have exposed necrotic bone with or without pain, infection, and extension to the nearby area according to the severity of MRONJ.*(3)*

Different treatment strategies are recommended, depending on the stage of MRONJ. To prevent patients at risk from developing MRONJ, optimizing the oral health and practicing a drug holiday prior to tooth extraction and other traumatic dentoalveolar procedures are recommended. However, whether a cessation of antiresorptive drugs should be performed routinely remains inconclusive as the risks of potential detrimental effects of suspending antiresorptive therapy may surpass a benefit.*(3)* Additionally, a rebound increase in bone resorption following the discontinuation of denosumab leading to higher risk of fracture has also been observed.*(5–7)* In later stages of MRONJ (stage 1 to 3), non-operative treatments including local wound care to exposed bone, antimicrobial rinse, sequestrectomy, systemic antibiotics, and pain control are suggested. If necessary, operative procedures such as segmental or marginal resection of the jaw should also be considered in the advanced stages of MRONJ (stage 1 to 3).*(3)* Despite the well-established staging system and treatment guideline, most of the approaches are only supportive or

palliative care, hence, effective preventive and curative treatments for MRONJ remain an unsolved problem in the field.

1.1.1.3 Pathophysiology

Since MRONJ was first discovered, its pathophysiology has remained elusive. Throughout the past decade, clinicians and researchers have investigated various potential mechanisms underlying pathophysiology of MRONJ utilizing both clinical and pre-clinical animal models. Recent studies suggest that MRONJ is a multifactorial disease and multiple mechanisms may potentially contribute to the overall pathophysiology.*(3)*

One of the potential mechanisms is bone remodeling inhibition. Although BPs and denosumab have different mechanisms of action, both medications inhibit osteoclast formation, differentiation, and functions. While osteoclast inhibition increases bone mineral density and decreases skeletal-related events, it also suppresses bone resorptive and bone remodeling activities leading to accumulation of necrotic bone, which is one of the important clinical features of MRONJ.*(3)*

Inflammation or infection along with macrophage alteration has also been hypothesized as a potential mechanism. MRONJ mostly occurs after extraction of teeth with pre-existing inflammatory conditions such as periodontal and periapical diseases. Animal models have shown that both a local increase in inflammatory cytokines in the oral cavity and systemic inflammation, such as rheumatoid arthritis, contribute to more severe MRONJ lesions. Moreover, bacteria accumulation on the exposed necrotic bone also contributes to MRONJ severity.*(3)*

In addition, angiogenesis inhibition, innate or acquired immune dysfunction, and genetic factors are also potential mechanisms underlying pathophysiology of MRONJ. Even though more studies need to be conducted to fully understand the overall pathophysiology, which is the key to

effective prevention and treatment, both recent animal and human studies suggest that the combination of antiresorptive treatment and inflammation or infection is most likely necessary and sufficient to induce MRONJ.*(3)*

1.1.2 *Healing following tooth extraction*

As MRONJ usually occurs after traumatic dentoalveolar procedures, especially tooth extraction *(1, 2)*, it is essential to first understand bone and soft tissue healing processes in order to further investigate the pathophysiology of MRONJ. In physiological wound healing following tooth extraction, various cell types play unique roles in different processes as shown in **Figure 1.2**. The socket healing process can be divided into three sequential and overlapping phases including inflammatory, proliferative, and bone modeling/remodeling.*(8, 9)* Macrophages are key inflammatory cells playing crucial roles in healing. They are heterogeneous and capable of polarizing into a broad spectrum of cell types including pro-inflammatory M1, which release several cytokines such as IL-1, IL-2, IL-6, IL-12, TNF-α, and IFN-γ playing roles in inflammation, pathogen clearance, and activation of immune system in the early phase of wound healing.*(10, 11)* In contrast, anti-inflammatory M2 promotes tissue repair, extracellular matrix deposition and new bone formation by releasing in IL-10, CCL-18, CCL-12, BMP-2, TGF-β, osteopontin, and 1,25-dihydroxy-vitamin D3 during the late phase of wound healing.*(12–14)* In the bone modeling/remodeling phase, osteoblasts and osteoclasts become key players. Damaged or necrotic bone at the extraction site as a result of traumatic force is first resorbed by osteoclasts *(15–18)*, while woven bone is rapidly formed within the tooth socket by osteoblasts.*(19)* Later on, woven bone is remodeled into lamellar bone which is more mineralized and stiffer, and both osteoclasts and osteoblasts are essential for the bone remodeling process which happens throughout a lifetime to maintain homeostasis of bone milieu.*(9, 19)*

In contrast, the equilibrium of populations and functions of inflammatory cells is disrupted in pathological healing conditions. It has been shown that zoledronic acid (ZA) enhances macrophages polarization towards M1 via several pathways and increases M1/M2 ratio, correlating to more severe ONJ lesions in MRONJ animal models and patients.*(20–22)* In addition to MRONJ, these changes are also observed in other oral bone diseases. In periodontitis, increased numbers of M1 and pro-inflammatory cytokines compared to healthy individuals are observed.*(23, 24)* Moreover, it has been shown that osteoclast deficiency concurrent with macrophage alteration potentially contributes to accumulation of necrotic bone and impaired new bone formation in MRONJ.*(25–27)* This pathological socket healing also leads to incomplete closure of the epithelium above.*(25–27)* Therefore, further investigation on how alterations in the inflammatory environment affects oral wound healing processes will be beneficial for studies on pathophysiology and pathogenesis of MRONJ, as well as, other oral bone diseases.

1.1.3 *Cell therapy approaches for MRONJ treatment*

Despite a better understanding of MRONJ pathophysiology in the past decade, effective curative treatments have not been established and remain in urgent need. Most of the treatment strategies of MRONJ nowadays are supportive care, for instance, pain control and antibiotics for infection control. Removal of the mobile/well-formed exposed necrotic bone or sequestrum is also recommended, however, surgical removal involving a large area of alveolar bone may affect the masticatory function, and prostheses and/or rehabilitation may be needed after the surgery.*(3)* Furthermore, the discontinuation of denosumab before dentoalveolar surgeries aiming to decrease the prevalence of MRONJ may have a rebound bone resorption effect and result in an increased risk of bone fracture.*(5–7)* The progression of the disease as well as the side effects of the current

treatments of MRONJ tremendously impact a quality of life of patients, hence, effective curative treatments are currently much needed in the field.

Recently, researchers have utilized cell therapy as a tool to study MRONJ mechanisms and progression as well as a potential treatment of MRONJ. As MRONJ usually occurs after tooth extraction, a delivery of certain types of cells involved in the healing processes has been utilized in several MRONJ animal models. It has been shown that both local and systemic delivery of various cells, including bone marrow-derived mesenchymal stem cells (BM-MSCs), peripheral blood mononuclear cells (PBMCs), adipose-derived stem cells (ASCs), stromal vascular fraction (SVF), and endothelial progenitor cells (EPCs), alleviate MRONJ lesions in animal models.*(28–32)* Moreover, the delivery of cell products, such as monocyte chemoattractant protein (MCP)-1, insulin growth factor (IGF)-1, and vascular endothelial growth factor (VEGF) which are cytokines released by MSCs, also improve MRONJ lesions in animal studies.*(33)* These findings suggest that cell therapy may potentially serve as a novel treatment modality for MRONJ. Nevertheless, current cell therapy strategies improve only several features, but do not completely cure MRONJ. Furthermore, systemic delivery of cells is limited since it does not specifically target MRONJ lesions, and thus may cause unintended side effects. Therefore, more studies on the effects of cell delivery on other sites besides oral cavity need to be invented. Additionally, most studies were conducted in BRONJ models, so their utility in DRONJ models is not known. Thus, more targeted or local cell delivery and studies in DRONJ models are essential to develop cell therapy as an effective treatment of MRONJ in the future.

1.2 SIGNIFICANCE

MRONJ is a serious side effect of the antiresorptive treatment which tremendously affects patients' quality of life. Although the risk of MRONJ is relatively low; 0-18% for BPs and 0-6.9% for denosumab in cancer patients, while 0.02-0.05% for BPs and 0.3% for denosumab in osteoporotic patients*(3)*, the numbers of patients taking these drugs are high (> 10 million worldwide)*(3)* and still increasing, making these a growing clinical problem. Most importantly, the mechanisms underlying MRONJ pathophysiology are not fully understood resulting in a lack of effective curative treatments. Therefore, investigating potential MRONJ mechanisms including bone remodeling inhibition and inflammation may shed light on MRONJ pathophysiology and progression leading to establishing effective treatments, which are currently much needed in the field. Specific aim 1, 2, and 3 explore the roles of osteoclast, osteoblast, and macrophage in MRONJ induced by anti-RANKL antibody treatment respectively. Additionally, our lab has developed engineered RAW264.7 murine monocytic cells with an inducible RANK (iRANK) construct to conditionally differentiate into osteoclasts under the control of a CID drug. This differentiation is independent of RANKL and M-CSF, and also resistant to OPG, a natural analog of denosumab.*(34)* In specific aim 1, I propose to use these cells to restore the inhibited bone resorptive function and improve MRONJ lesions. These findings provide proof-of-concept data and pave the way for osteoclast cell therapy as a potential treatment strategy for MRONJ.

1.3 INNOVATION

1.3.1 *Engineered osteoclasts to prevent diseases caused by osteoclast deficiency*

Osteoclasts are multinucleated cells playing a role in bone resorption by attaching to bone surface, forming resorption lacunae, and degrading bone minerals and organic matrix.*(35)* They differentiate from hematopoietic stem cells (HSCs) under the induction of M-CSF and RANKL produced by osteoblasts and osteocytes.*(36)* The balance of osteoclasts and osteoblasts, bone forming cells, is essential for maintaining physiological bone resorption and formation processes.*(37)* Therefore, the disruption of this equilibrium caused by osteoclast deficiency can lead to bone pathologies such as ectopic calcification and potentially MRONJ.

Our lab has developed a unique osteoclast differentiation system for a study tool and a potential therapeutic approach for bone pathologies related to osteoclast deficiency **(Figure 1.3)**. This system consists of two main components: a fusion protein and a drug (AP20187 or chemical inducer of dimerization; CID). F36V, the CID specific binding domain, and the specific CID-inducible intracellular RANK (iRANK) construct were utilized for this technology as shown in **Figure 1.4**.*(34)* Since trimerization of iRANK domains is required for CID-induced osteoclastogenesis*(38)* , we utilized two F36V domains fused to the iRANK domain in order to ensure successful oligomerization. In addition, a myristoylation signal was added to direct the protein to the cell membrane to maximize interaction with downstream signaling molecules as shown in **Figure 1.4**.*(34)* Moreover, the construct also contained the gene for green fluorescent protein (GFP), which allowed cell sorting to be performed. Cells were sorted twice by fluorescence-activated cell sorting (FACS) to obtain a purified (>98% GFP+) population for *in vitro* characterization.*(34)* We previously published that TRAP activity and ability to form

multinucleated osteoclasts of RAW264.7 cells, a murine monocytic cell line, engineered with this technology were observed in a dose dependent manner *in vitro* as shown in **Figure 1.5**.*(34)* These engineered osteoclasts also resorbed mineralized surface *in vitro* **(Figure 1.6)**. As one of the potential mechanisms underlying MRONJ pathophysiology is osteoclast inhibition, I propose to incorporate iRANK osteoclasts into a loss-and-gain of osteoclast function study in the MRONJ model and investigate if osteoclast replenishment alleviates the MRONJ lesions in my thesis. This is innovative as a loss-and-gain of osteoclast function study has not been conducted before. Furthermore, it will elucidate the puzzled mechanisms of MRONJ and introduce osteoclast cell therapy as a potential MRONJ treatment which is urgently required.

1.3.2 *RANKL-polarized macrophages (RPMs)*

In addition to osteoclast deficiency, macrophage alteration is also one of the potential mechanisms underlying MRONJ pathophysiology*(1, 39)* since macrophages play important roles in oral wound healing following traumatic dentoalveolar procedures including tooth extraction*(8, 9, 19)* and MRONJ usually occurs after tooth extraction.*(1, 2)* It has been shown that BPs induce macrophages to polarize toward M1, and increased M1/M2 ratio is observed in MRONJ patients and animal models and correlated with the severity of lesions.*(20–22)* On the other hand, Tamaki et al. recently showed that anti-RANKL antibody alone had no effects on macrophage phenotype when directly treated to isolated bone marrow derived macrophages (BMDMs) *in vitro(40)*, which is not surprising as BMDMs do not express RANKL.*(41)* However, BMDMs express RANK (RANKL receptor) and RANKL is expressed at the tooth extraction site during healing processes, thus suggesting that environmental RANKL possibly modulates the macrophage phenotype.*(8)* I have termed these cells RANKL-polarized macrophages (RPMs). In contrast to M1 and M2 macrophages, RPM's gene expression profile and cytokines have not been thoroughly investigated.

I hypothesize that RANKL regulates macrophages in a unique way which in turn may affect the surrounding tooth socket/injury microenvironment to promote bone and soft tissue healing. Treatment with denosumab, an anti-RANKL antibody, potentially inhibits RPM induction, thereby interrupting proper RPM-driven physiological healing. This is innovative as RPM and its functions have not been studied before. Exploring this novel macrophage phenotype will explain how anti-RANKL antibody affects macrophage polarization and healing processes which potentially explains the mechanisms of MRONJ as well as other bone diseases such as periodontitis.

Figure 1.1. Clinical manifestations of MRONJ

The exposed necrotic bone was observed in both maxilla and mandible six months after tooth extraction in the patient with metastatic breast cancer treated with zoledronic acid and denosumab.*(42)*

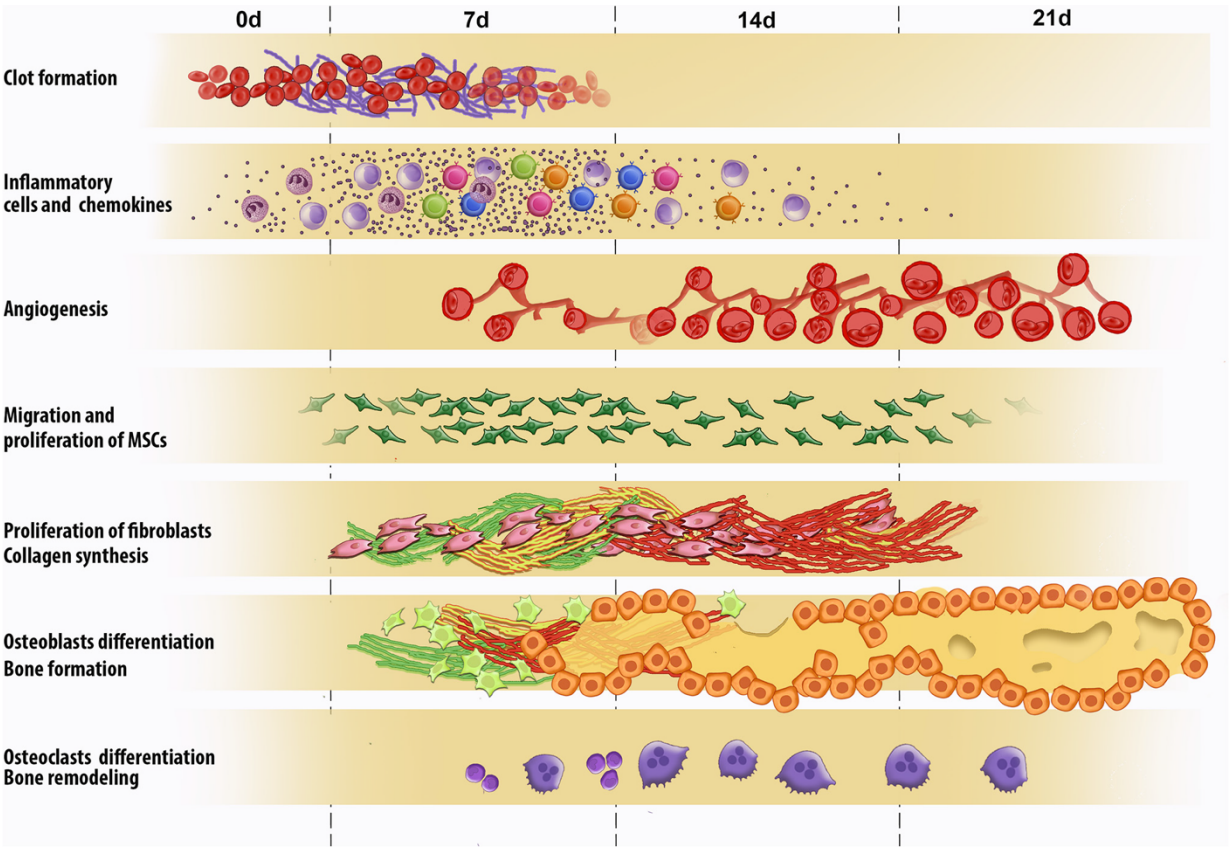

Figure 1.2. Inflammatory and healing events in the bone healing processes following tooth extraction*(8)*

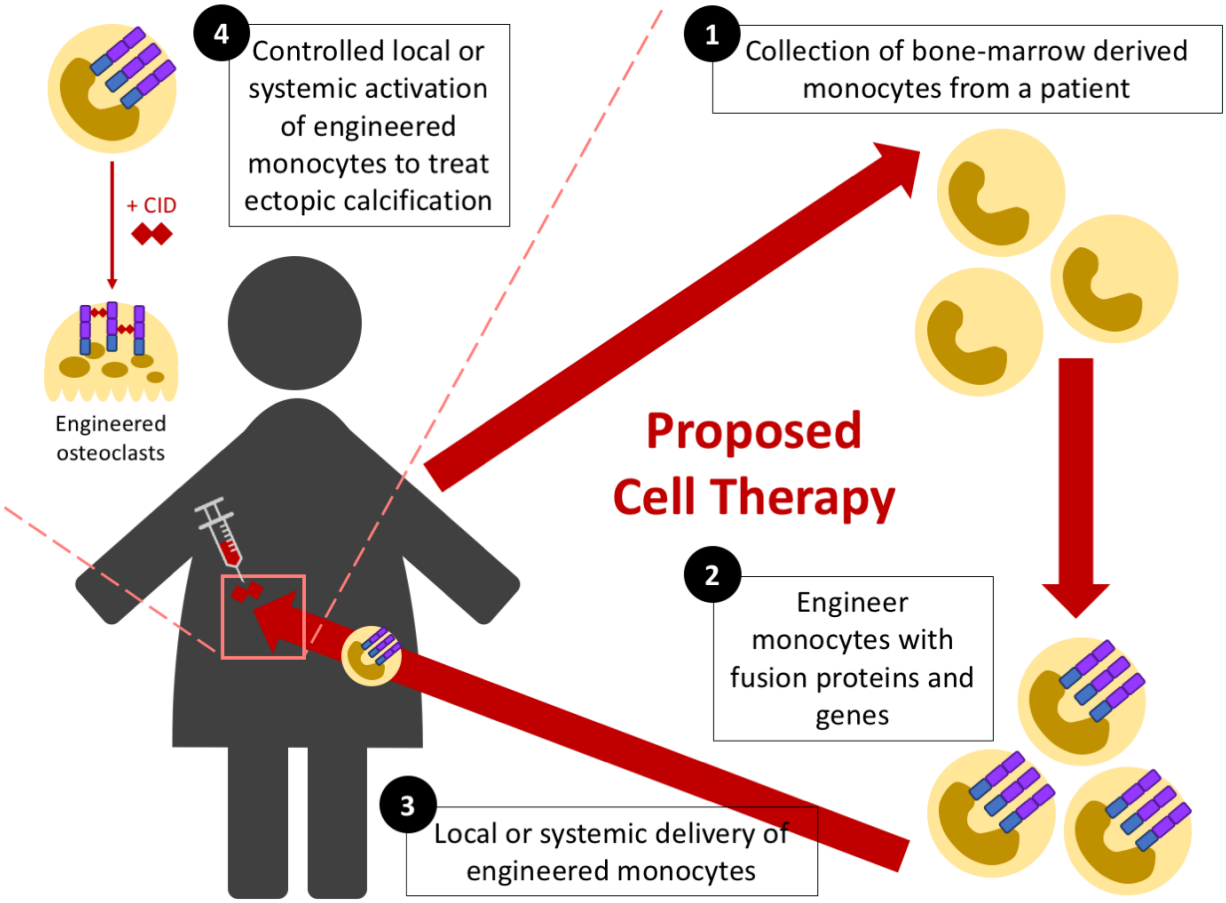

Figure 1.3. Proposed cell therapy of the engineered osteoclasts to prevent disease caused by osteoclast deficiency

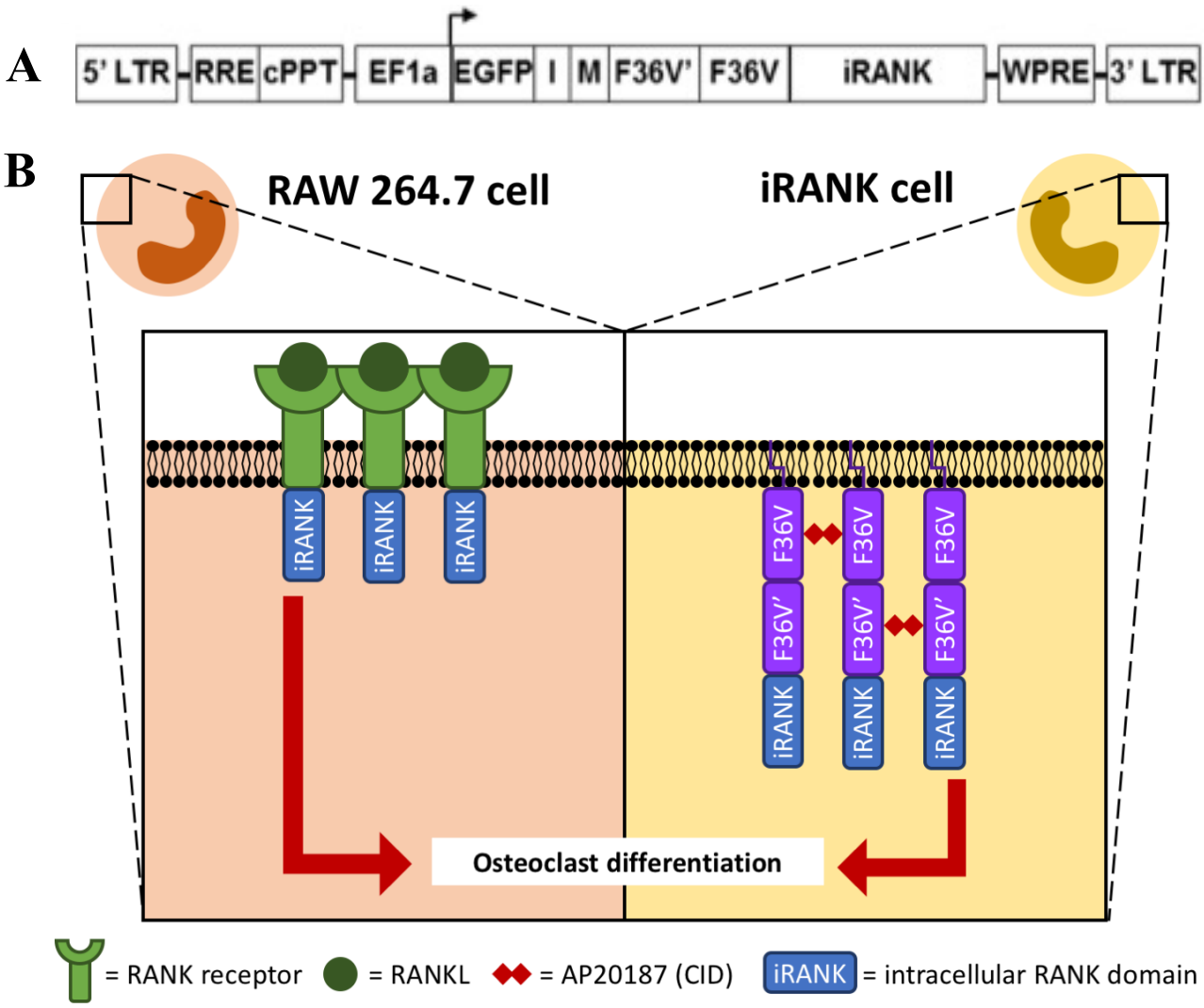

Figure 1.4. CID-iRANK lentiviral construct and comparison of osteoclast differentiation systems

(A) Schematic representation of CID-inducible intracellular RANK (iRANK) construct. LTR = long terminal repeat; RRE = rev response element; cPPT = central polypurine tract; EF1a = elongation factor 1-Alpha; EGFP = green fluorescent protein; I = IRES; M = myristoylation; F36V = FKBP12; F36V' = modified FKBP12; iRANK = intracellular domain of RANK; WPRE = WHP posttranscriptional regulatory element. **(B)** Comparison of RANKL- and CID-induced osteoclastogenesis in RAW264.7 and iRANK cells respectively

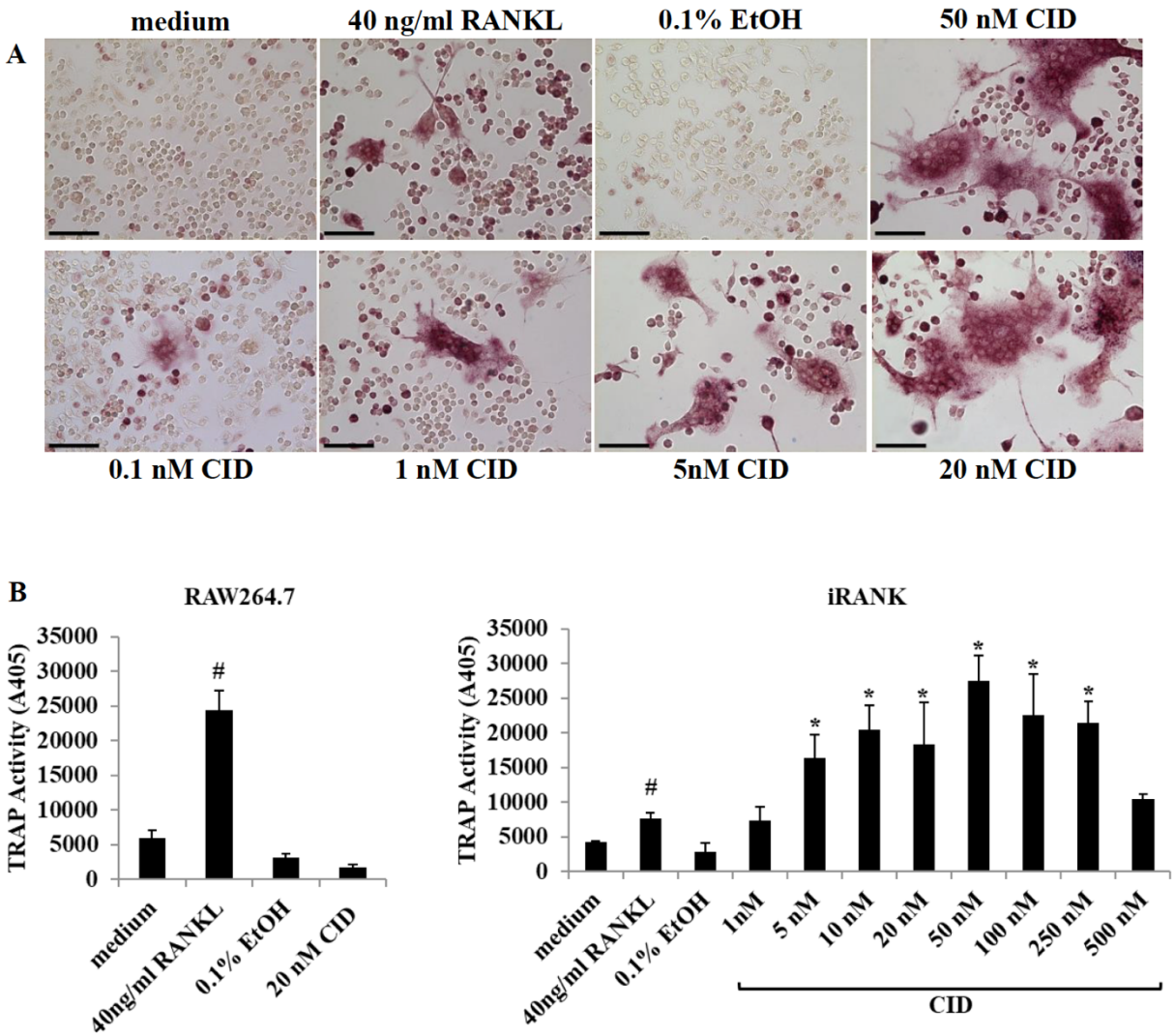

Figure 1.5. Response of iRANK cells to CID

(A) iRANK cells were differentiated into osteoclasts (TRAP+ multinucleated cells with three or more nuclei) by various doses of CID treatment. Higher CID concentration resulted in an increased size and number of osteoclasts. **(B)** TRAP activity of RAW264.7 and iRANK cells following osteoclast differentiation. The dose-dependent effect of CID on TRAP activity was observed in CID-induced osteoclastogenesis of iRANK cells. (Scale bar = 100 μm; #p<0.05 compared to medium, *p<0.05 compared to 0.1% EtOH)*(34)*

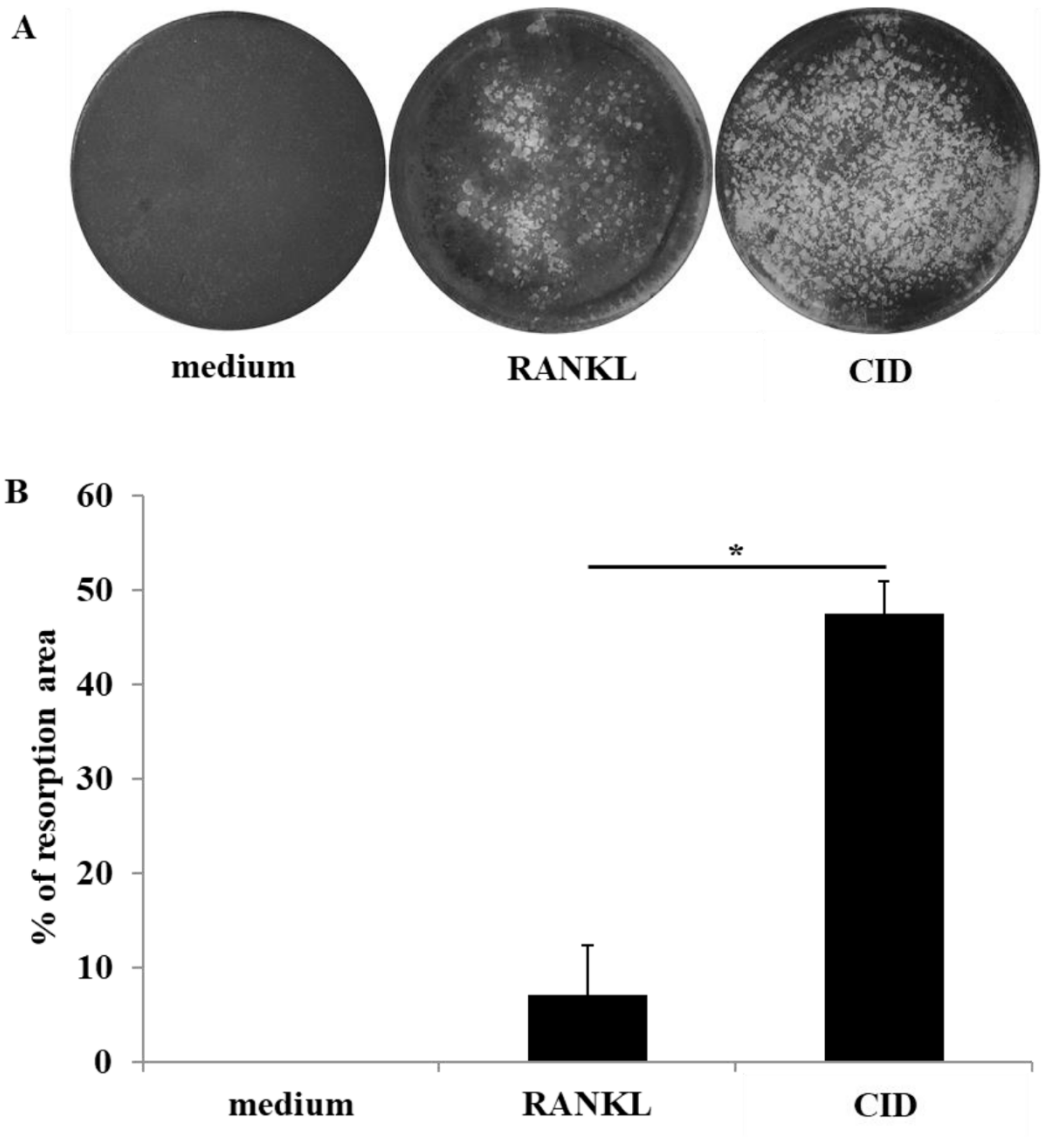

Figure 1.6. iRANK osteoclasts resorbed 2D-mineralized surface

(A) von Kossa staining of 2D-mineralized discs cultured with iRANK cells with either RANKL (100 ng/ml) or CID (50 nM) treatment for 10 days. White area represents the resorption area. **(B)** Quantitation of the resorption area (*$p<0.05$)*(34)*

	At risk	Stage 0	Stage 1	Stage 2	Stage 3
Treated with the medications	✓	✓	✓	✓	✓
Exposed necrotic bone/fistula that probes to necrotic bone	✗	✗	✓	✓	✓
Change in radiography	✗	✓	✓	✓	✓
Pain	✗	• No pain • Non-specific symptoms		✓	✓
Infection	✗	✗	✗	✓	✓
Other symptoms	✗	✗	✗	✗	Beyond the alveolar bone region

Table 1.1. MRONJ staging adapted from AAOMS's position paper*(1)*

Chapter 2. RESEARCH GOALS

The objective of this thesis is to investigate the roles of osteoclasts, osteoblasts, and macrophages in MRONJ pathophysiology. Additionally, I propose to identify the effects of RANKL on a novel macrophage polarization state, termed RANKL-polarized macrophages (RPMs). MRONJ is defined as an area of exposed necrotic bone that has persisted more than eight weeks with no history of radiation therapy.*(1, 43)* This is a serious side effect of the treatment of antiresorptive drugs including denosumab and BPs to prevent skeletal-related events, such as fracture, in osteoporosis and metastatic cancer.*(2, 43)* In addition, MRONJ often occurs in the oral cavity related to tooth extraction and periodontitis.*(1, 2)* Although MRONJ is relatively rare*(44)*, the number of patients prescribed antiresorptive agents is high (>10 million worldwide) and steadily increasing*(45)*, making this a growing clinical problem.*(39)* Importantly, the pathophysiology of MRONJ remains elusive resulting in the absence of effective preventive and curative approaches besides palliative treatments.*(39)* Several hypotheses have been focusing on the effects of these drugs on various cell types and events involved in new bone formation and oral wound healing.*(1, 39)* As impaired bone remodeling and inflammation are the potential mechanisms contributing to MRONJ pathophysiology, I propose to investigate the effects of antiresorptive drugs on osteoclasts, osteoblasts, and macrophages, as well as, to identify the roles of these cells in MRONJ pathophysiology. Based on the previous studies and our preliminary data, *the overall hypothesis is that the deficiency of osteoclasts, osteoblasts, and RPMs caused by antiresorptive drugs impairs bone healing processes and induces MRONJ*. To test this hypothesis, the following specific aims **(Figure 2.1)** are proposed:

Aim 1: To identify the roles of osteoclasts in MRONJ using the local delivery of engineered osteoclasts in the MRONJ mouse model

Osteoclast inhibition caused by antiresorptive drugs and accumulation of necrotic bone has been observed in MRONJ.*(46, 47)* However, the roles of the osteoclast deficiency on progression of MRONJ lesions, and whether replenishment of osteoclasts and their functions can ameliorate the lesions remain inconclusive. Our lab previously developed a unique osteoclast differentiation system which is independent of RANKL and M-CSF, resistant to the inhibition by OPG, and resorbs 2D calcium phosphate *in vitro*.*(34)* Thus, I propose to develop the MRONJ mouse model with tooth extraction and anti-RANKL antibody and perform a loss-and-gain of function study by delivering the engineered osteoclasts to the extraction site. *I hypothesize that the replenishment of osteoclasts improves MRONJ lesions.*

Aim 2: To determine the effects of antiresorptive drugs on osteogenic differentiation *in vitro*.

In addition to osteoclast deficiency, impaired new bone formation, which potentially affects connective tissue and epithelial healing above the tooth socket, has also been observed in MRONJ.*(46, 47)* Osteoblasts are a bone forming cell which directly plays a role in mineralization and new bone formation.*(9, 19)* In this aim, I propose to study the effects of anti-RANKL antibody on osteogenic differentiation via RANKL autocrine/paracrine loop of MC3T3 mouse pre-osteoblast cell line and compare them to the effects I observe in the MRONJ model in aim 1. *I hypothesize that anti-RANKL antibody inhibits osteogenic differentiation of MC3T3 cells.*

Aim 3: To investigate the roles of RANKL in macrophage polarization *in vitro* and *in vivo.*

It has been shown that macrophages have influences on osteoblasts*(48, 49)*, thus, the effects of antiresorptive drugs on macrophages potentially affect bone formation indirectly as well. Our *in vitro* preliminary data indicate that RANKL itself has unique polarizing effects on unstimulated macrophages (M0), and in addition, synergistically promotes M1 macrophage polarization while inhibiting M2 polarization suggesting the induction of a unique RANKL-polarized macrophage (RPM) phenotype. Moreover, our data also suggest that RPMs are likely to have distinct gene expressions compared to M1 and M2. Importantly, the roles of RPMs in bone healing and MRONJ have never been investigated before. Hence, I propose to utilize isolated bone marrow derived macrophages (BMDMs) to investigate RPM characteristics and functions *in vitro*. Additionally, the MRONJ mouse model will be used to identify the effects of antiresorptive drugs on macrophage population *in vivo*. *I hypothesize that RANKL induces RPM phenotype which is distinct from M0, M1, M2 macrophages and osteoclasts, and anti-RANKL antibody inhibits RPM differentiation leading to impaired bone formation.*

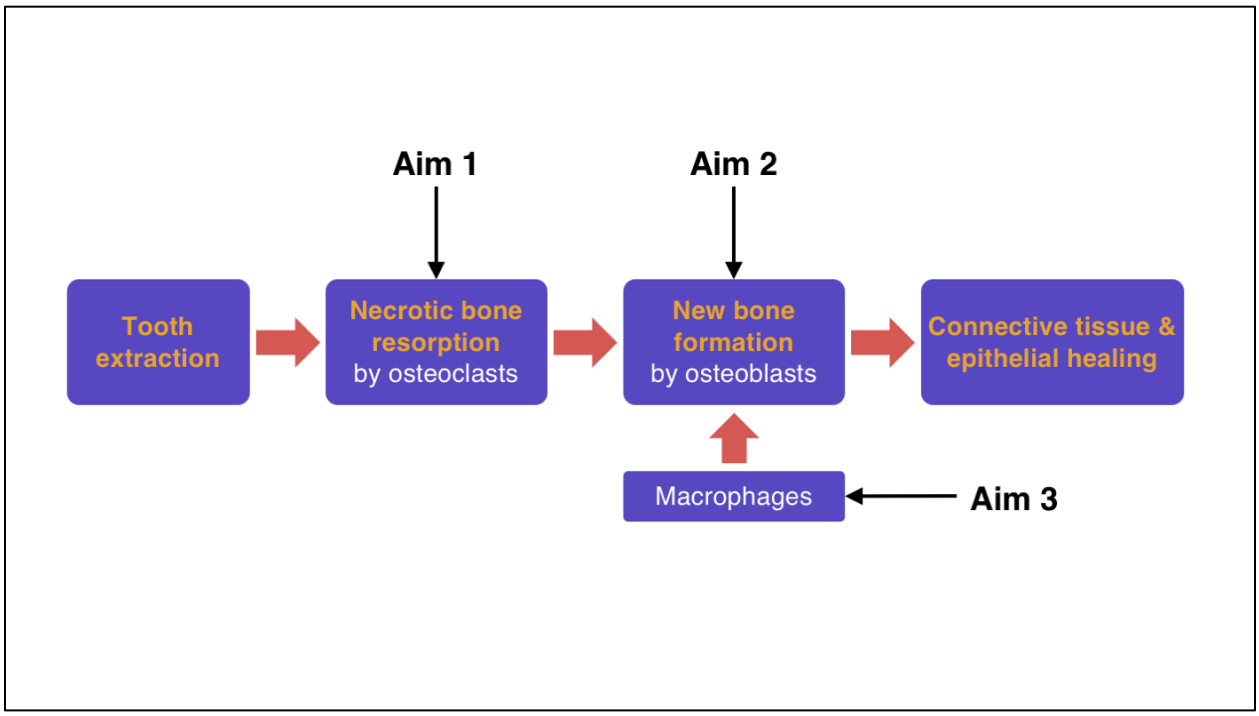

Figure 2.1. Specific aims focusing on different cell types and bone healing processes, and how they contribute to MRONJ pathophysiology

Chapter 3. ROLES OF OSTEOCLAST IN MEDICATION-RELATED OSTEONECROSIS OF THE JAW

Necrotic bone accumulation at the jaw is one of the clinical features observed in MRONJ.*(3, 50)* Therefore, inhibition of osteoclasts and their bone resorptive function has been proposed as one of potential mechanisms underlying MRONJ.*(3)* However, whether replenishing osteoclasts and their functions can improve MRONJ lesions remains elusive. In this chapter, I proposed to utilize iRANK cells, and MRONJ model established by injections of anti-RANKL antibody and tooth extraction to address this question. First, I determined if osteoclast differentiation of iRANK cells via CID system is resistant to the inhibition by anti-RANKL antibody *in vitro.* As we previously showed that osteoclast differentiation of iRANK cells is independent of OPG*(34)*, *I hypothesized that it is resistant to anti-RANKL antibody as well.* Next, I proposed to locally deliver iRANK cells at the tooth extraction site in the MRONJ mouse model to investigate if osteoclast replenishment can alleviate MRONJ. *I hypothesized that restoring the bone resorptive function by the engineered osteoclasts can reduce necrotic bone area, hence improves MRONJ lesions.* These data will shed light on the field regarding the roles of osteoclasts on MRONJ pathophysiology and also help paving the way of the engineered osteoclasts as a study tool and potential cell therapy for MRONJ. The findings in this chapter have already been published in *BONE* journal.*(50)*

3.1 INTRODUCTION

Medication-related osteonecrosis of the jaw (MRONJ), which was first described in 2003, is a potentially serious side effect of treatment with antiresorptive and antiangiogenic medications that often occurs in the oral cavity after traumatic dentoalveolar procedures such as tooth

extraction.*(1, 2)* These antiresorptive medications, including bisphosphonates (BPs) and denosumab, are used to decrease the risk of skeletal-related events in patients with severe osteoporosis, multiple myeloma and bone metastasis of other cancers.*(1)* MRONJ is clinically defined as accumulation of an area of exposed and necrotic bone that has persisted for more than eight weeks with no history of radiation therapy.*(2, 43)* Initially, lesions are asymptomatic but may become symptomatic when the surrounding tissues become inflamed. MRONJ incidence in patients with cancer receiving intravenous BPs is reported to range from 2% to 15%*(46, 51)*, whereas MRONJ development in osteoporotic patients still remains controversial. The incidences of ONJ from BPs and denosumab were comparable in cancer patients, suggesting that ONJ induced by both drugs adversely affects patients' quality of life and produces significant morbidity.*(46, 51)*

Denosumab is a human monoclonal antibody that binds to receptor activator of nuclear factor kappa-B ligand (RANKL) and prevents RANKL from activating its receptor, RANK, on the surface of osteoclasts and their precursors.*(52)* Prevention of the RANKL/RANK interaction inhibits osteoclast formation, function, and survival, thereby decreasing bone resorption and increasing bone mass and strength in both cortical and trabecular bone.*(53–55)* In contrast to denosumab, many potential mechanisms by which BPs inhibit osteoclastic bone resorption have been proposed. BPs, attached to hydroxyapatite on bony surfaces, are impregnated into osteoclasts when they begin to resorb bone and impair their ability to form the ruffled border, to adhere to the bony surface, and to produce protons necessary for bone resorption.*(56, 57)* Several studies also showed that BPs reduce osteoclast activity by decreasing osteoclast progenitor development and recruitment, and by inducing osteoclast apoptosis via the activation of caspases.*(58–60)* In addition to their inhibitory effect on osteoclasts, BPs appear to have an effect on osteoblasts. An in vitro study showed that zoledronic acid (ZA) can increase production of osteoprotegerin (OPG) in a

dose-dependent manner from primary human osteoblasts.*(61)* OPG then binds to RANKL and blocks the interaction with RANK, thereby inhibiting osteoclastogenesis. Another study also demonstrated that ZA markedly increased OPG protein secretion and reduced transmembrane RANKL protein expression in osteoblast-like cells.*(62)*

Despite the fact that the first case of MRONJ was described over a decade ago, the mechanism and pathophysiology of MRONJ still remain elusive. Proposed hypotheses that attempt to explain the unique localization of necrotic bone exclusively to the jaw include altered bone remodeling or oversuppression of bone resorption, angiogenesis inhibition, constant microtrauma, suppression of innate or acquired immunity, vitamin D deficiency, soft tissue toxicity, and inflammation or infection.*(1)* In addition, the management of MRONJ remains as a significant clinical challenge, with little progress having been made on treatment.*(63)* Patients with MRONJ are treated conservatively with mouth rinses, antibiotics and oral analgesics. Surgical debridement is typically not indicated unless it is absolutely necessary.*(1, 64)* Even with drug holiday before traumatic dentoalveolar procedures, many patients still experience a lot of pain and other side effects in later stages of MRONJ which tremendously affect their quality of life.*(1)* Therefore, it is critical to understand the pathophysiology of MRONJ and develop proper regimen for prevention and treatment of this disease.

Although osteoclast suppression has been observed in most MRONJ animal models, there is still no evidence to date whether restoring osteoclast and its bone resorptive function can alleviate MRONJ in animals that have received antiresorptive drugs. We previously engineered RAW264.7 murine myeloid precursor cells with an inducible intracellular RANK (iRANK) construct to allow differentiation into osteoclasts under the control of a chemical inducer of dimerization (CID) drug. This differentiation is independent of RANKL and macrophage colony-

stimulating factor (M-CSF), and also resistant to OPG.*(34)* In this study, we hypothesize that osteoclast formation, differentiation and function are impaired at the extraction site and normal bone healing is disturbed due to the inhibition of osteoclastic activities by antiresorptive drugs. Thus, we further hypothesize that locally-delivered engineered osteoclasts which are resistant to this inhibition may promote bone healing processes after tooth extraction in a MRONJ mouse model. This study determines the effects of restoring osteoclast functions on MRONJ development and also provides a new and innovative strategy to investigate mechanisms leading to different stages of MRONJ.

3.2 MATERIALS & METHODS

3.2.1 *In vitro osteoclast differentiation and mineral resorption*

RAW264.7 cells were purchased from American Type Culture Collection (ATCC). RAW264.7 cells containing a CID-inducible, intracellular RANK signaling domain (iRANK cells) were created as previously described.*(34)* RAW264.7 and iRANK cells were cultured in α-MEM containing 10% fetal bovine serum and 100 U/mL of penicillin/streptomycin and incubated at 37°C with 5% CO_2. RAW264.7 and iRANK cells were plated at 20,000 cells/well in 4-well Nunc™ Lab-Tek™ chamber slides. Four hours after plating, 2 nM recombinant mouse RANKL (R&D Systems) was applied to RAW264.7 cells for osteoclast differentiation concurrently with the treatment of 0 nM, 2 nM, 5 nM or 20 nM Ultra-LEAF™ purified rat anti-mouse CD254 (TRANCE, RANKL) IgG2a, κ monoclonal antibody (BioLegend) or 20 nM Ultra-LEAF™ purified rat IgG2a, κ isotype control antibody (BioLegend). Similarly, 10 nM AP20187 (CID; Clontech Laboratories) was applied to iRANK cells for osteoclast differentiation concurrently with the treatment of 0 nM, 10 nM, 25 nM or 100 nM of the same rat anti-mouse RANKL monoclonal antibody listed above

or 100 nM of the same rat IgG isotype control antibody also listed above. Cells were cultured for 5 days with media and treatments replaced once at day 3. Cells were washed twice with PBS, fixed with 10% neutral buffered formalin for 10 minutes and subjected to TRAP staining following the manufacturer's instructions (387A, Sigma-Aldrich). Slides were mounted with Aqua-Mount (Thermo Fisher Scientific) and images were obtained using an upright microscope (Nikon E800). The numbers of multinucleated TRAP-positive osteoclasts (with ≥ 3 nuclei) were quantified.

To determine the resorptive function of osteoclasts in the presence of anti-RANKL antibody *in vitro*, RAW264.7 and iRANK cells were cultured on an Osteo Assay (Corning Inc.) and treated with the inducers; 2 nM recombinant mouse RANKL (R&D Systems) and 10 nM CID (Clontech Laboratories) respectively. Concurrently, cells were treated with either 20 nM rat anti-mouse RANKL monoclonal antibody (BioLegend) or 20 nM rat IgG isotype control antibody (BioLegend). At day 10, all cells on the Osteo Assay plate were removed by 10% bleach and resorption pits were visualized using von Kossa staining. Images were taken by Nikon D5100 camera and the resorption area was quantified using ImageJ software version 1.52a (NIH, Bethesda, MD).

3.2.2 *MRONJ model in nude mice*

Animals and surgical procedures were handled in accordance with the University of Washington's Institutional Animal Care and Use Committee. A MRONJ model in athymic nude mice was utilized to allow delivery of allogeneic iRANK cells. Briefly, eight- to ten-week-old female nude mice were randomly divided into two groups (10 mice per group); IgG isotype control (Ct) and anti-RANKL antibody (Ab); same antibodies as in the *in vitro* experiments were used. Mice in Ct and Ab group were injected with 10 mg/kg rat IgG isotype control and 10 mg/kg of rat anti-mouse RANKL monoclonal antibody intraperitoneally respectively three times a week until

termination. One week after the first antibody injection, left maxillary first molar was extracted in both groups. Under general anesthesia using ketamine/xylazine, a rodent molar luxator (iM3) was used to separate the gingival attachment and a 25-gauge needle was used to gently luxate the tooth. Then, a curved hemostat was used to pull the tooth out. Approximately three weeks after tooth extraction, mice were sacrificed to harvest serum and maxilla.

3.2.3 *Cell delivery and CID treatment*

Eight- to ten-week-old nude mice were randomly divided into two groups (10 mice per group); anti-RANKL antibody with iRANK cells (Abc), and anti-RANKL antibody with iRANK cells and CID (Abcc); same antibodies used throughout study. Mice in both groups were injected with rat anti-mouse RANKL monoclonal antibody and tooth extraction was performed as described above. Immediately after tooth extraction, 100,000 iRANK cells in 0.5 mg/mL neutralized collagen were delivered to the tooth socket and covered with Gelfoam® (Pfizer Pharmaceutical) in both Abc and Abcc groups. Only the mice in Abcc group were injected with 10 mg/kg CID intraperitoneally for 3 consecutive days starting on the same day as cell delivery, then twice a week throughout the experiment to induce osteoclast differentiation. Mice were sacrificed to harvest serum and maxilla 3 weeks after tooth extraction. The tissue specimens from all groups were immediately fixed in 4% paraformaldehyde in PBS, pH 7.4, at 4°C for 48 hours and stored in 70% EtOH solution. Tissues were decalcified with 5% EDTA and 4% sucrose in PBS, pH 7.4 for 4 to 5 weeks at 4°C. Decalcification solution was changed daily. Tissue samples were then processed for paraffin embedding and sectioned for immunohistochemistry. Additionally, terminal blood was collected to measure the serum concentration of TRAP-5b and osteocalcin (OCN), biochemical markers for bone resorption and formation, respectively, using

the Mouse TRAP-5b (Immunodiagnostic Systems) and the Mouse Osteocalcin ELISA Kit (Immunotopics).

3.2.4 *H&E and TRAP staining*

4-µm-thickness tissue sections in sagittal plane were used for immunohistochemistry. For hematoxylin and eosin (H&E) staining, tissue sections were deparaffinized, rehydrated and placed in Harris hematoxylin solution for 3 minutes before rinsing. This was followed by 40 seconds in ammonium water (0.25% v/v). Finally, slides were dipped in eosin solution 10 times before dehydrating. The slides were mounted with Permount (Thermo Fisher Scientific). For TRAP staining, tissue sections were deparaffinized, rehydrated and incubated for 30 minutes with TRAP staining solution at 37°C, according to manufacturer's protocol (387A, Sigma-Aldrich). Nuclei were counterstained with 300 nM DAPI Dilactate (Life Technologies) for 5 minutes. Slides were mounted with Aqua-Mount (Thermo Fisher Scientific) and images were obtained using an upright microscope (Nikon E800).

3.2.5 *Immunofluorescence staining*

Engineered osteoclasts express green fluorescent protein (GFP), so we could visualize and distinguish them from endogenous osteoclasts. To detect GFP expression, tissue sections were deparaffinized and rehydrated with TBS-Tween (TBS-T; 0.05 M Tris buffer, 0.15 M NaCl, 0.1% Tween 20, pH 7.6) before permeabilization with 0.1% Triton X-100 in PBS, pH 7.4. for 10 minutes. Blocking was performed with 4% normal donkey serum (NDS) for 30 minutes. Rabbit anti-GFP polyclonal antibody (Thermo Fisher Scientific) was diluted to 10 µg/mL in 2% NDS and incubated at room temperature for 1 hour. Slides were rinsed 3 times in TBS-T for 5 minutes. Cy3 AffiniPure Donkey Anti-Rabbit IgG secondary antibody (Jackson ImmunoResearch Laboratories, Inc.) was

used to decrease autofluorescence in the green channel in order to accurately detect GFP expression. The secondary was diluted to 7.5 µg/mL in 2% NDS and incubated for 30 minutes at room temperature. In addition, tissue sections were used for double-staining of additional osteoclast markers including MMP-9, carbonic anhydrase II, and cathepsin K. For double-staining images in Figure 3.8, slides were incubated in primary antibodies: Goat Anti-Mouse MMP-9 at 5 µg/mL (Novus Biologicals) and Rabbit Anti-Carbonic Anhydrase II at 8 µg/mL (Abcam) or Goat Anti-Mouse MMP-9 at 5 µg/mL and Rabbit Anti-Cathepsin K at 10 µg/mL (Abcam) for 1 hour. Then, slides were incubated with appropriate secondary antibodies: Cy3 Donkey Anti-Goat at 7.5 µg/mL (Jackson ImmunoResearch) and Alexa Fluor 488 Donkey Anti-Rabbit at 7.5 µg/mL (Jackson ImmunoResearch) for 30 minutes at room temperature. Slides were then rinsed three times in TBS-T for 5 minutes and once in Milli-Q water. Nuclei were counterstained with 300 nM DAPI Dilactate (Life Technologies) for 5 minutes. Slides were rinsed with Milli-Q water and PBS before mounting with ProLong Gold Antifade Mountant (Thermo Fisher Scientific). Images were obtained using an upright microscope (Nikon E800) and overlaid using Adobe Photoshop to show double-staining of osteoclast markers in the same cell.

3.2.6 *Quantitation of epithelial closure, necrotic and new bone, and osteoclast number*

Several characteristics were used to evaluate the degree of ONJ-like lesions. After termination, the images of epithelial closure at the extraction site were taken before all the tissues were decalcified and processed for histochemistry. To Investigate necrotic bone area, newly formed bone, and number of osteoclasts at the extraction site, all the quantifications were done using ImageJ software version 1.52a (NIH, Bethesda, MD). To quantify necrotic bone area, four uniformly spaced (approximately 50 µm) H&E-stained sections were selected per sample. The area of interest covered the alveolar bone adjacent to the tooth sockets. The percentage of necrotic

area was calculated by the area containing 5 or more empty osteocytic lacunae divided by the total alveolar bone area. To quantify newly formed bone, four uniformly spaced (approximately 50 μm) H&E-stained sections were selected per sample. The newly formed bone was quantified only in the sockets without root fragments as the percentage of bone area in the socket/total socket area (%BA/TA). The number of osteoclasts was also quantified by using two uniformly spaced (approximately 100 μm) TRAP-stained sections per sample for Ct and Ab groups, and TRAP & GFP-stained sections for Abc and Abcc groups. Endogenous and engineered osteoclasts were defined as TRAP+ and TRAP+GFP+ cells with three or more nuclei respectively. Eight samples were excluded from the histological analysis due to tissue damage at the extraction site during embedding and sectioning process, except one sample from Abcc group which was because the CID system did not work, and osteoclast differentiation could not be induced.

3.2.7 *Blood chemistry*

Serum samples collected from each mouse were stored in −20°C and thawed once. The presence of TRAP-5b was detected by sandwich ELISA using the Mouse TRAP-5b ELISA Kit (Immunodiagnostic Systems). Serum levels of OCN were detected by sandwich ELISA using the Mouse Osteocalcin ELISA Kit (Immunotopics). The serum samples were assayed in triplicate and the procedure was performed according to the manufacturer's protocol.

3.2.8 *Statistical analysis*

Results are expressed as mean ± SD. GraphPad Prism version 8.4.1 was used to perform Kolmogorov-Smirnov test to test normality of data, student's *t*-test to compare means of two individual groups with equal variances, student's *t*-test with Welch's correction to compare means of two individual groups with unequal variances, one-way ANOVA with post-hoc Tukey test to

compare means of three or more individual groups, and Fisher exact's test to compare epithelial closure among groups. A value of $p < 0.05$ was considered statistically significant.

3.3 RESULTS

3.3.1 *iRANK engineered osteoclast differentiation and resorptive function were resistant to inhibition by anti-RANKL antibody*

RAW264.7 cells containing a CID-inducible, intracellular RANK signaling domain (iRANK cells) were created as previously described.*(34)* The main feature of CID technology is that induction of signaling is triggered only by the presence of the small molecule CID and is not affected by the presence of endogenous RANK/RANKL inhibitors, such as OPG. We previously showed that iRANK cell differentiation to osteoclasts in the presence of CID was OPG-resistant*(34)*, therefore, we hypothesized that this differentiation would not be inhibited by anti-RANKL antibody which binds to RANKL in a similar manner as OPG. As expected, iRANK cells formed multinucleated TRAP-positive osteoclasts following CID treatment even in the presence of the highest concentration of anti-RANKL antibody (100 nM). On the other hand, RANKL-mediated osteoclastogenesis of RAW264.7 cells was almost completely inhibited by anti-RANKL antibody even at the lowest concentration (2 nM) **(Figure 3.1)**.

Next, we determined the effect of anti-RANKL antibody on engineered osteoclast function *in vitro* by differentiating RAW264.7 and iRANK cells into osteoclasts directly on a 2D-mineralized well-plate using RANKL and CID respectively. Concurrently, both cell types were treated with 20 nM anti-RANKL antibody or control IgG antibody for 10 days. Visualized with von Kossa staining, there was no resorption in RANKL-treated RAW264.7 cells in the presence of anti-RANKL antibody. On the contrary, the resorption area in CID-treated iRANK cells in the

presence of anti-RANKL antibody was comparable to the group without treatment **(Figure 3.2)**. Interestingly, the resorption area in the IgG-treated iRANK group was significantly higher than the other iRANK groups **(Figure 3.2)** as IgG can interact with the Fc gamma receptors (FcγRs) on hematopoietic cells and facilitate osteoclastogenesis as well as phagocytosis/resorption.*(65, 66)* These *in vitro* data suggest that osteoclast differentiation of iRANK cells via CID system and their resorptive function are not inhibited by anti-RANKL antibody.

3.3.2 *Absence of osteoclasts and accumulation of necrotic bone were observed following tooth extraction in anti-RANKL antibody-treated nude mice*

As the osteoclast differentiation of iRANK cells and their resorptive function were resistant to anti-RANKL antibody *in vitro*, our next step was to develop the MRONJ animal model and locally deliver these cells hypothesizing that they would improve the MRONJ lesions.

Since iRANK cells are allogeneic, nude mice were required to develop the MRONJ model in order to avoid unfavorable host responses following cell delivery. Prior to establishing the MRONJ model, we first demonstrated that nude mice had normal wound healing compared to wild-type mice following tooth extraction **(Figure 3.3)**. Clinical presentation of maxilla at 3 weeks after tooth extraction showed that 100% of wild type and nude mice had complete closure of epithelium at the extraction site. Furthermore, connective tissue was observed directly above the bone-filled sockets in all mice, indicating normal healing process at the extraction site.

To establish the MRONJ model, nude mice were randomly divided into two groups (10 mice per group); Control IgG (Ct) and anti-RANKL antibody (Ab) as shown in **Figure 3.4**. Ct group received isotype control rat IgG, while Ab group received anti-RANKL antibody. Several features were studied at approximately three weeks following tooth extraction. In Ct group, we observed osteoclasts, identified as TRAP-positive cells with three or more nuclei, within the

extraction sites **(Figure 3.4)**. Osteoclasts were found within and around the tooth sockets demonstrating typical resorptive morphology near damaged bones. On the other hand, there were no osteoclasts detected in the tooth sockets of the Ab group **(Figure 3.4)**. These data indicated that the injections of anti-RANKL antibody inhibited osteoclast formation in nude mice.

Although tooth extraction has widely been used to induce ONJ-like lesions in rodents, root fracture is one of the most common complications following tooth extraction especially in mice with age of 8 weeks and older due to the accumulation of cementum at the root apices.*(67)* We excluded the samples with retained root fragments from the analysis of new bone formation since the bone formation process was complicated in those sockets.*(data not shown and 23, 24)* However, there has been no evidence showing that retained root fragments are associated with accumulation of necrotic bone around tooth sockets following tooth extraction in mice. To confirm this, we determined that no correlation existed between the retained root fragments and necrotic bone area in all groups **(Figure 3.5)**. Thus, we included all animals in the analysis of necrotic bone area.

As expected, Ct group showed significantly less % necrotic bone area at the extraction site compared to Ab group. H&E-stained sections displayed an osteoclast resorbing an alveolar bone next to the socket in Ct group, while the alveolar bone containing clusters of empty lacunae remained unresorbed in Ab group **(Figure 3.4)**. On the other hand, % newly formed bone area in the tooth socket (%BA/TA) showed no significant difference between Ct and Ab groups **(Figure 3.4)**. In addition, all of the samples in Ct and Ab groups, except one sample from Ab group which had a granulation tissue mass above the socket, exhibited normal soft tissue healing and complete epithelial closure at the extraction site **(Figure 3.4)**.

Lastly, we measured serum TRAP-5b and osteocalcin levels which are markers of bone resorption and bone formation, respectively. We found that Ab group showed significantly less

serum TRAP-5b and osteocalcin levels compared to Ct group **(Figure 3.6)**. According to all these findings, our MRONJ model developed in nude mice exhibited absence of osteoclasts and accumulation of necrotic bone following tooth extraction.

3.3.3 *iRANK cells were retained and differentiated into osteoclasts in anti-RANKL antibody and CID-treated mice*

To determine whether iRANK cells were retained following local injection, *in vivo* bioluminescence imaging was performed **(Figure 3.7)**. Bioluminescence was detected in all animals that received cells with or without Gelfoam®. As expected, no signal was detected in the animals that did not receive cells but received luciferin alone. Luciferase transfected iRANK cells were retained at the tooth socket up to 10 days following delivery.

Next, we locally delivered iRANK cells to the extraction sites of mice treated with anti-RANKL antibody to determine whether CID treatment would induce iRANK osteoclast differentiation and improve the healing of MRONJ-like lesions. Nude mice were randomly divided into two groups (10 mice per group); anti-RANKL antibody with iRANK cells (Abc), and anti-RANKL antibody with iRANK cells and CID (Abcc) as shown in **Figure 3.8**. Anti-RANKL antibody injections and tooth extraction were performed in all mice as described above. In this experiment, iRANK cells were delivered to the tooth sockets immediately after tooth extraction in both groups. However, only the mice in Abcc group were injected with CID drug intraperitoneally to induce osteoclast differentiation.

As shown in **Figure 3.8**, GFP-positive iRANK cells were observed in both Abc and Abcc groups. However, osteoclasts were only observed in Abcc group. These osteoclasts were not only TRAP-positive, but also GFP-positive, indicating that they differentiated from the delivered iRANK cells under the control of CID **(Figure 3.8)**. In addition to TRAP, the engineered

osteoclasts expressed other osteoclast markers including matrix metallopeptidase 9 (MMP-9), carbonic anhydrase II (CAII), and cathepsin K (CatK) **(Figure 3.8)**. Taking both *in vitro* and *in vivo* findings together, we demonstrated that iRANK cells delivered to the extraction sites were retained and successfully differentiated into osteoclasts via CID system despite the treatment of anti-RANKL antibody in nude mice.

3.3.4 *Necrotic bone resorption, but not new bone formation or epithelial closure, was restored by the iRANK engineered osteoclasts following tooth extraction in anti-RANKL antibody and CID-treated mice*

Next, we investigated how local replenishment of osteoclasts affected necrotic bone area, a main feature of MRONJ. Histologically, we observed engineered osteoclasts resorbing alveolar bone with empty lacunae in the Abcc group, while the alveolar bone containing clusters of empty lacunae remained unresorbed in the Abc group **(Figure 3.9)**. Furthermore, quantitative data indicated a statistically significant decrease in the necrotic bone area in Abcc group compared to Abc group, (p = 0.045) **(Figure 3.9)**. Thus, these data suggest that the osteoclasts' resorptive function could be restored by delivery of engineered osteoclasts.

In addition to necrotic bone area, we measured whether new bone formation and epithelial healing were altered in mice receiving anti-RANKL antibody and iRANK engineered osteoclasts. Interestingly, there was no significant difference between Abc and Abcc groups in %BA/TA **(Figure 3.9)** or epithelial closure **(Figure 3.9)**. However, in contrast to the mice that did not receive iRANK cells, the majority of the samples from Abc and Abcc groups exhibited partial or incomplete epithelial closure at the extraction site **(Figure 3.9)** as well as less newly formed bone in the sockets.

Finally, serum TRAP-5b and osteocalcin levels were reduced equally in Abc and Abcc groups, compared to Ct group, indicating that addition of engineered cells did not alter peripheral bone remodeling in general **(Figure 3.6)**.

3.4 DISCUSSION

Deficiency of osteoclastic bone resorption has been hypothesized as a main mechanism leading to MRONJ. In this study, we developed a tooth extraction-triggered MRONJ model in nude mice using anti-RANKL antibody to deplete osteoclasts. Replenishment of osteoclasts within sockets was achieved using engineered, inducible myeloid precursor cells. Lesions treated with iRANK cells + CID showed significantly decreased accumulation of necrotic bone in the sockets compared to those treated with iRANK cells alone. These data support the hypothesis that osteoclast deficiency leads to accumulation of necrotic bone, a major feature of MRONJ.

Throughout the past decade, many studies have shown that osteoclast inhibition is one of the potential mechanisms underlying MRONJ pathophysiology. In the normal healing processes following tooth extraction, osteoclasts play a role in resorption of damaged or necrotic bone caused by traumatic force in early stages, as well as, bone formation and remodeling in later stages.*(15, 19)* However, no study has shown whether replenishment of osteoclasts can restore these functions in MRONJ models. In this study, we are the first group to demonstrate that the bone resorptive function could be restored by delivered iRANK osteoclasts as decreased necrotic bone area was observed in Abcc group compared to Abc group.

Interestingly, the absence of osteoclasts caused by anti-RANKL antibody did not impair new bone formation (Ct vs. Ab group) and the local repletion of osteoclasts did not affect this process either (Abc vs. Abcc group). These findings suggest that new bone formation may not only

rely on the osteoclast-osteoblast interaction. Woven bone formation occurs in two ways: appositional formation from the existing bone surfaces primarily mediated by the coupling mechanism of osteoclast and osteoblasts, and *de novo* formation which is a new bone formation by osteoblasts without osteoclasts or any existing bone surfaces.*(70)* It is most likely that the appositional formation was inhibited in our model, leaving the *de novo* formation as the only source of new bone formation in the Ab group. These findings also raise another crucial point that osteoclast suppression alone may not be enough to induce severe-stage ONJ-like lesions. Other factors or mechanisms should also be considered toward the pathophysiology and different stages of MRONJ. Several hypotheses apart from osteoclast suppression, for instance, unbalanced M1 and M2 macrophages*(20, 22)* and angiogenesis inhibition*(71–73)*, have been studied in BP-treated animal models. Hence, further studies of those possibilities need to be investigated in anti-RANKL antibody-treated animal models in order to clearly understand the pathophysiology of MRONJ.

To investigate the clinical relevance between our MRONJ mouse models and patients, we categorized all the treated mice into different stages **(Table 3.1)** according to the MRONJ staging in humans.*(1)* The clinical manifestations at the extraction site of nude mice treated with anti-RANKL antibody (Ab group) are most similar to stage 0 MRONJ in humans, which presents some histological changes of alveolar bone at the extraction site with no evidence of exposed necrotic bone.*(1)* Several studies also observed stage 0 ONJ-like lesions in rodents treated with antiresorptive drugs.*(26, 46)* These lesions can be advanced to more severe stages by the induction of chemotherapy drugs concurrently to antiresorptive drugs.*(40, 47)* Also, we hypothesize that the mild stage of our model may be due to the extraction of healthy teeth. The major causes of tooth extraction in patients are caries, periodontal and pulpal disease*(74)*, and MRONJ is related to tooth extraction in patients with these diseases.*(75)* However, we extracted the healthy maxillary first

molars in this experiment which may result in less severity of ONJ-like lesions. Even though exposed necrotic bone area as well as other MRONJ characteristics including impaired bone formation and incomplete epithelial closure seen in later stages (stage 1-3) of MRONJ were not observed in Ab group, our model exhibited absence of osteoclasts and accumulation of necrotic bone at the extraction site histologically. These features were adequate for the cell delivery study to investigate whether bone resorptive function could be restored by the iRANK engineered osteoclasts. This is the first loss and gain of function study providing insights on specific osteoclast activities which can potentially contribute to future studies on pathophysiological mechanisms leading to different stages of MRONJ.

Nude mice which lack thymus were utilized in this study. They were necessary to avoid an immune rejection of the delivered cells since they lack normal T cells originating from the thymus. Several studies have shown that alteration of immune cells such as regulatory T cells (Tregs), T helper 17 cells (Th17), and dendritic cells may involve MRONJ pathophysiology*(76, 77)*, so it is possible that utilization of nude mice may have contributed to the mild-stage ONJ-like lesions in this study. However, nude mice still have intact innate immunity (such as natural killer (NK) cells), precursors of antibody forming cells, and T-cell precursors in their bone marrow which can differentiate to γδ T cells without antigen activation.*(78–80)* Therefore, the majority of immune cells besides thymus-dependent T-cells remain functional in nude mice. Indeed, Park *et al*. showed that the exposed bone area and open wound at the ONJ-like lesions were smaller in γδ T cell null (*Tcrd*$^{-/-}$) mice treated with zoledronic acid compared to treated wild-type mice.*(81)* This suggests that at least a few features related to MRONJ could potentially be induced in nude mice consisting of γδ T cells. In addition, we also showed that nude mice had normal wound healing compared to wild-type mice following tooth extraction. According to these data, utilization of nude mice should

not hinder the main objective of this study which focuses on the effects of delivered iRANK osteoclasts in the mouse model with the inhibition of endogenous osteoclasts, a common feature observed in all stages of MRONJ.

A limitation of this study is the use of a myeloid precursor cell line, rather than primary cells to create iRANK engineered osteoclasts. We delivered these cells directly to the tooth sockets in neutralized collagen which has been successfully used as a cell carrier to the periodontium without interfering healing processes.*(82)* However, primary osteoclasts could not be used in this model since they would be inhibited by anti-RANKL antibody treatment. In addition, we have been unable to transduce primary murine bone marrow precursors with iRANK constructs using either adenoviral or lentiviral vectors, most likely due to the size of the construct (unpublished data). In addition, undifferentiated myeloid precursor cells proliferate *in vivo* and therefore limited the duration of our experiments. These proliferated cells may potentially affect soft tissue healing at the delivery site resulting in the incomplete epithelial closure observed only in the cell-delivery groups (Abc and Abcc), but not in Ab group. Therefore, modifications such as delivery of purified iRANK osteoclasts should be considered for utilizing iRANK cells as a study tool and a potential therapeutic strategy for MRONJ in future studies.

In conclusion, we performed tooth extraction in nude mice treated with anti-RANKL antibody and developed iRANK cell and CID delivery methods to induce osteoclast formation *in vivo*. Our model captured the absence of osteoclasts and the clusters of empty lacunae representing necrotic bone area similarly to stage 0 MRONJ in human. However, new bone formation and epithelial closure were not affected by the complete inhibition of osteoclasts. We successfully used this model to demonstrate the roles of osteoclasts in healing following tooth extraction and potentially in MRONJ development. Our model suggests that the absence of osteoclasts affects the

process of necrotic bone resorption around the tooth sockets after tooth extraction which may contribute to MRONJ. This bone resorptive function can be restored by delivering the engineered osteoclasts to the extraction site. We are the first group to conduct a loss and gain of function study of osteoclasts *in vivo*, hence, we believe that the optimized engineered osteoclasts along with robust and reliable animal models would be beneficial tools to further study the pathophysiology and mechanisms leading to different stages of MRONJ.

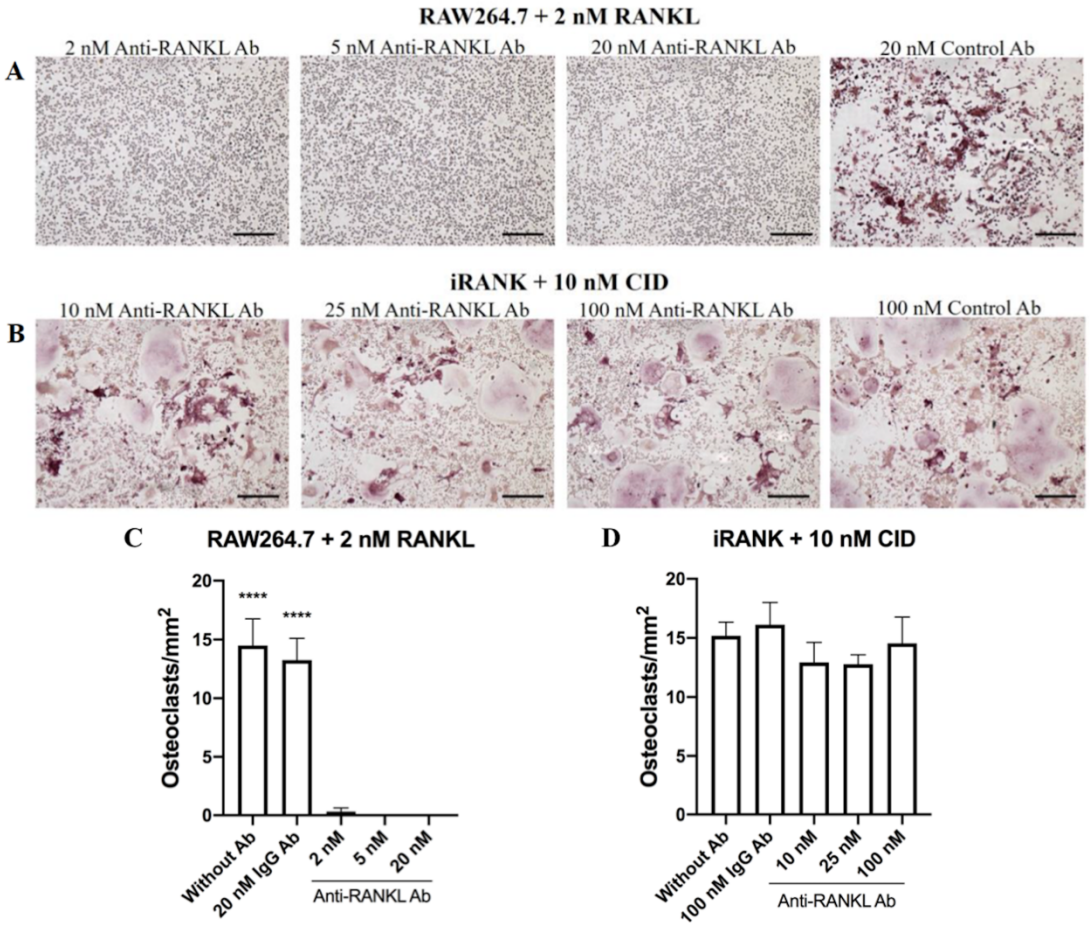

Figure 3.1. CID-induced osteoclastogenesis in iRANK cells was anti-RANKL antibody-independent.

(A), **(B)** TRAP staining of osteoclasts differentiated from RAW264.7 cells and iRANK cells treated with different concentration of anti-RANKL antibody **(C), (D)** Quantification of osteoclasts (n=3 per group; ****$p < 0.0001$; scale bar = 200 μM)

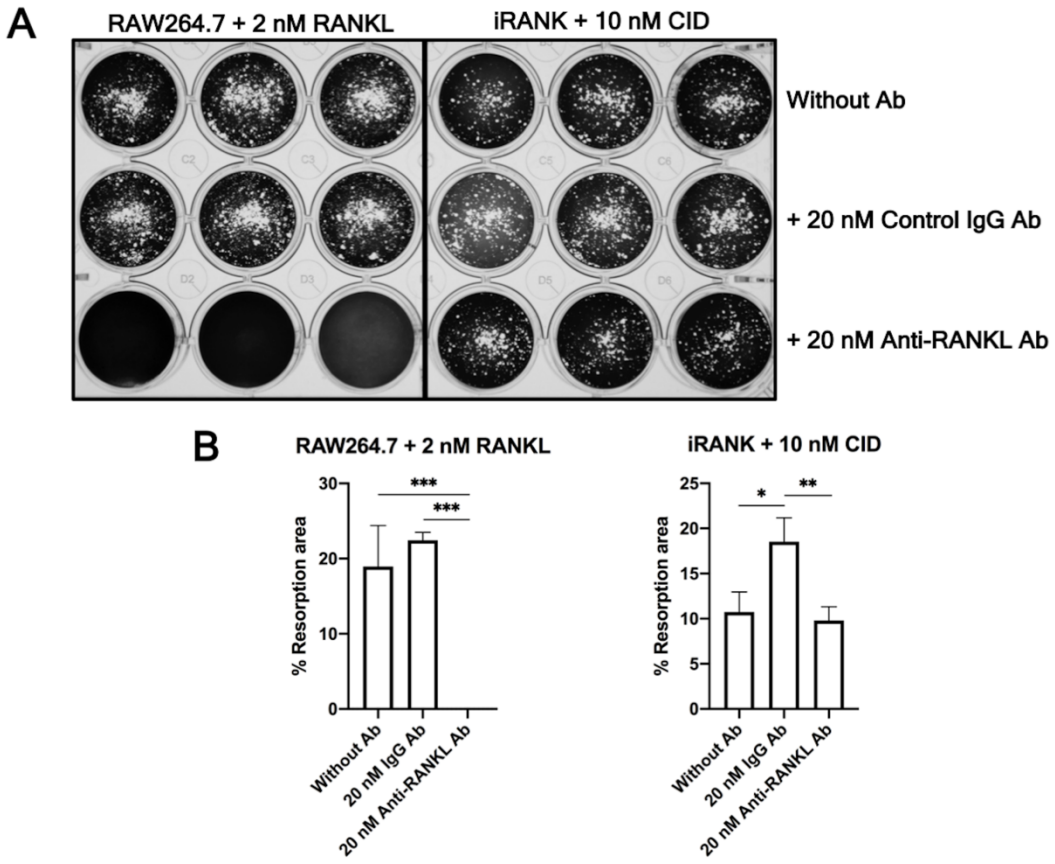

Figure 3.2. CID-induced osteoclasts resorbed 2D mineral substrate in the presence of anti-RANKL antibody.

(A) von Kossa staining of 2D mineral substrate (Osteo Assay) surfaces which osteoclasts differentiated from RAW264.7 cells and iRANK cells were cultured on **(B)** Quantification of resorption area (n=3 per group; *$p < 0.05$, **$p < 0.01$, and ***$p < 0.001$)

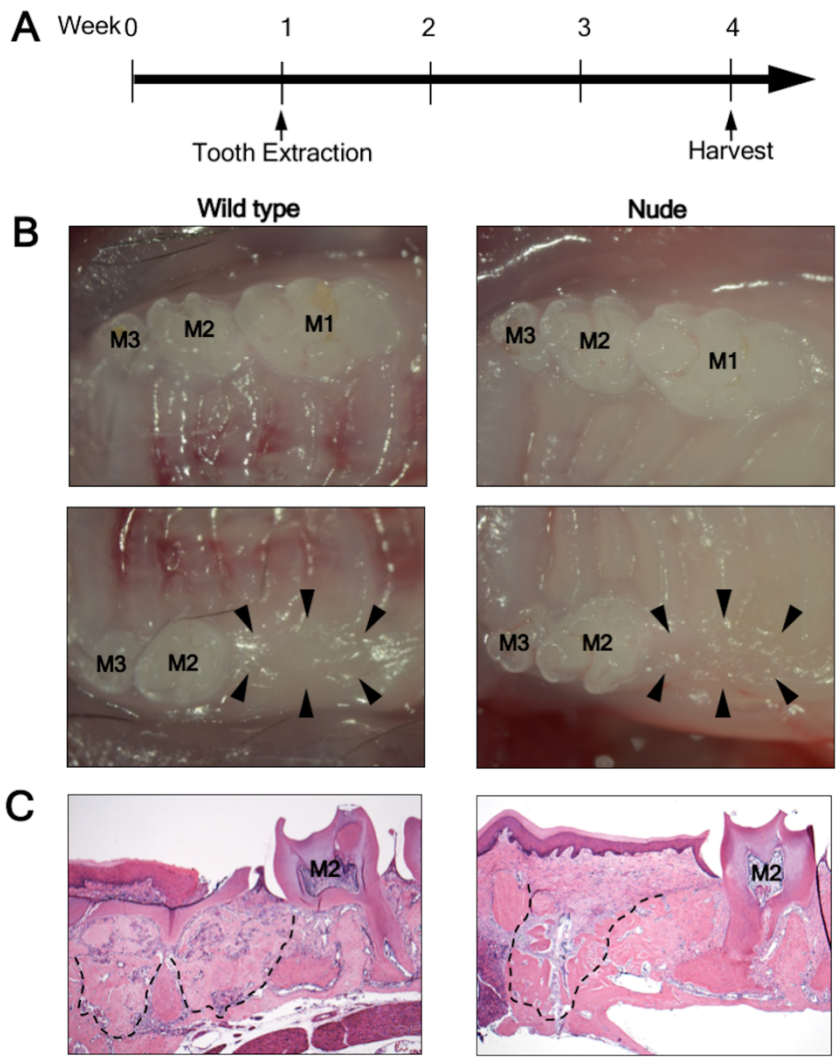

Figure 3.3. Nude mice had normal wound healing compared to wild type mice following tooth extraction.

Since iRANK cells are allogeneic, an MRONJ model with tooth extraction in nude mice was required to avoid an unfavorable host response following cell delivery. Therefore, we first determined if nude mice had normal wound healing after tooth extraction compared to wild type mice. **(A)** Experiment timeline; nude mice (n=5) and C57BL/6 wild type mice (n=5) were anesthetized with ketamine/xylazine through intraperitoneal injection and left maxillary first molar was extracted. Typical wound closure after an atraumatic tooth extraction usually occurs within 3 weeks. **(B)** Clinical presentation of maxilla at 3 weeks after tooth extraction showed that 100% of wild type and nude mice had complete closure of epithelium at the extraction site. (Black

arrowheads indicate the outline of the extraction site.; M1, first molar; M2, second molar; M3, third molar) **(C)** H&E staining showed that all mice had connective tissue directly above the bone-filled sockets which indicates normal healing process at the extraction site. (Black dot line indicates the tooth socket outline.; M2, second molar)

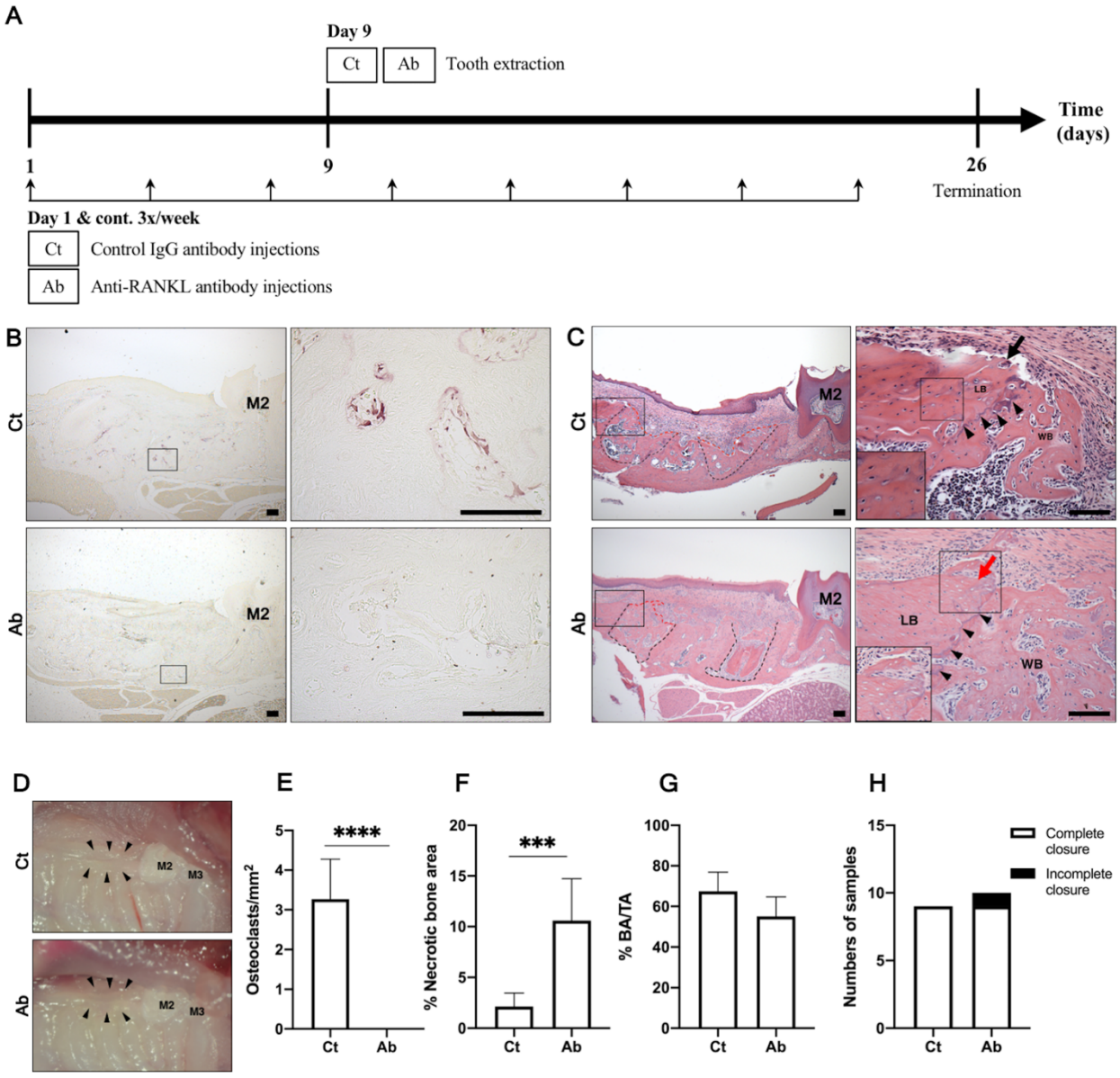

Figure 3.4. Absence of osteoclasts and presence of necrotic bone were observed following tooth extraction in anti-RANKL antibody-treated mice.

(A) Experiment timeline **(B)** TRAP staining; Osteoclasts, defined as TRAP+ cells with three or more nuclei, were observed in Ct group, but not in Ab group. **(C)** H&E staining; Clusters of empty lacunae locating at unresorbed alveolar ridge (red arrow) were observed with no sign of osteoclast in Ab group. On the contrary, osteoclasts (black arrow) were observed in Ct group. (Black dot line indicates the tooth socket outline. Red dot line indicates the level of newly formed woven bone.

Black arrowheads indicate reversal line.) **(D)** Clinical presentation at the extraction site (Black arrowheads indicate the outline of the extraction site.) **(E)** Quantification of osteoclasts, **(F)** % necrotic bone area, **(G)** % bone area/total socket area (%BA/TA), and **(H)** epithelial closure (M2, second molar; M3, third molar; LB, lamellar bone; WB, woven bone; scale bar = 100 μm; ***$p < 0.001$, ****$p < 0.0001$; $n \geq 7$ per group for osteoclast and % necrotic bone area; $n \geq 4$ per group for %BA/TA)

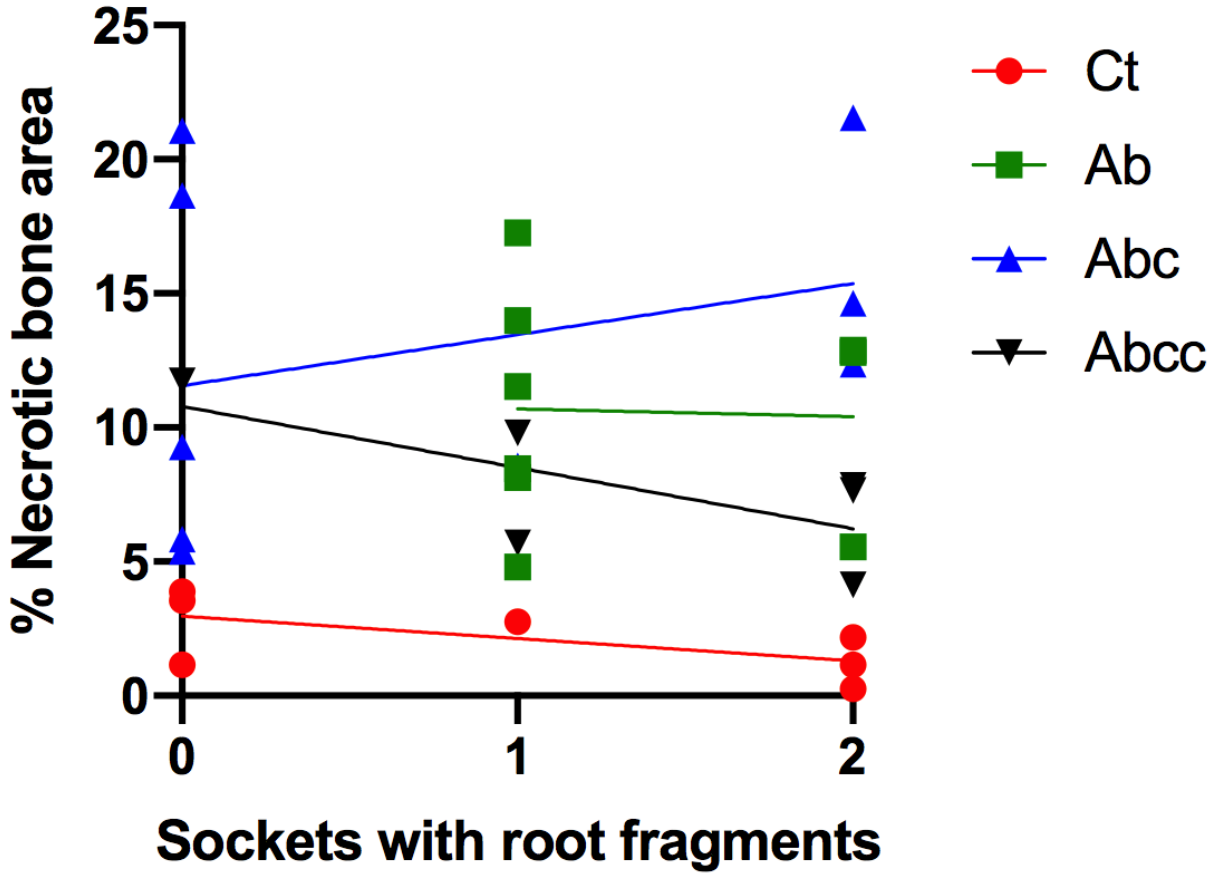

Figure 3.5. Correlation between the retained root fragments and necrotic bone area was not observed.

There was no statistically significant correlation between the retained root fragments and necrotic bone area in all groups. (Pearson correlation and simple linear regression; $p > 0.05$ in all groups)

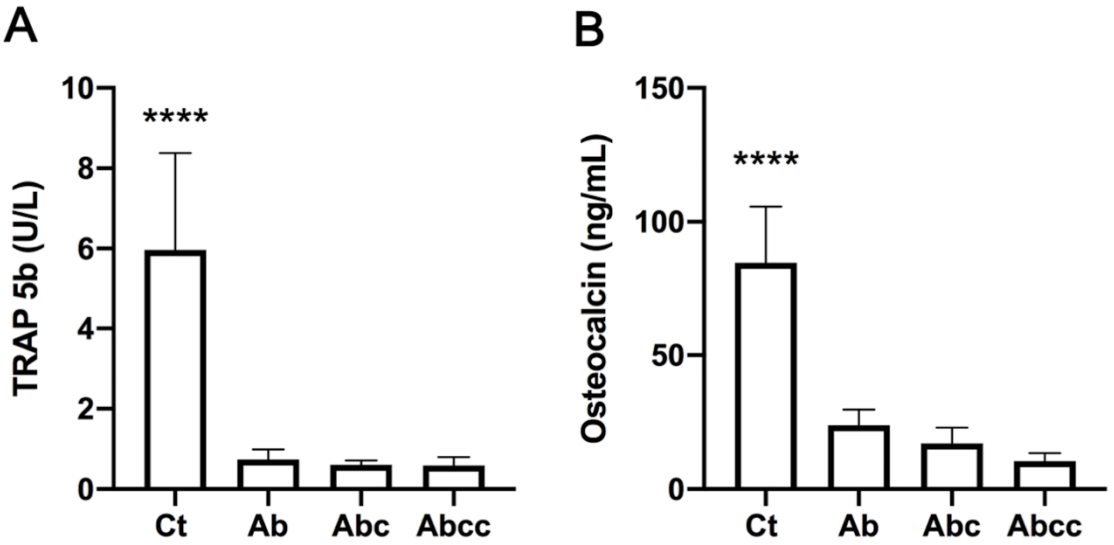

Figure 3.6. Serum markers of bone resorption and bone formation were decreased in anti-RANKL antibody-treated mice.

Blood was collected from the control IgG antibody-treated and anti-RANKL antibody-treated mice 4 weeks after initial administration. **(A)** The serum level of TRAP-5b **(B)** The serum level of osteocalcin (****$p < 0.0001$; $n \geq 9$ per group)

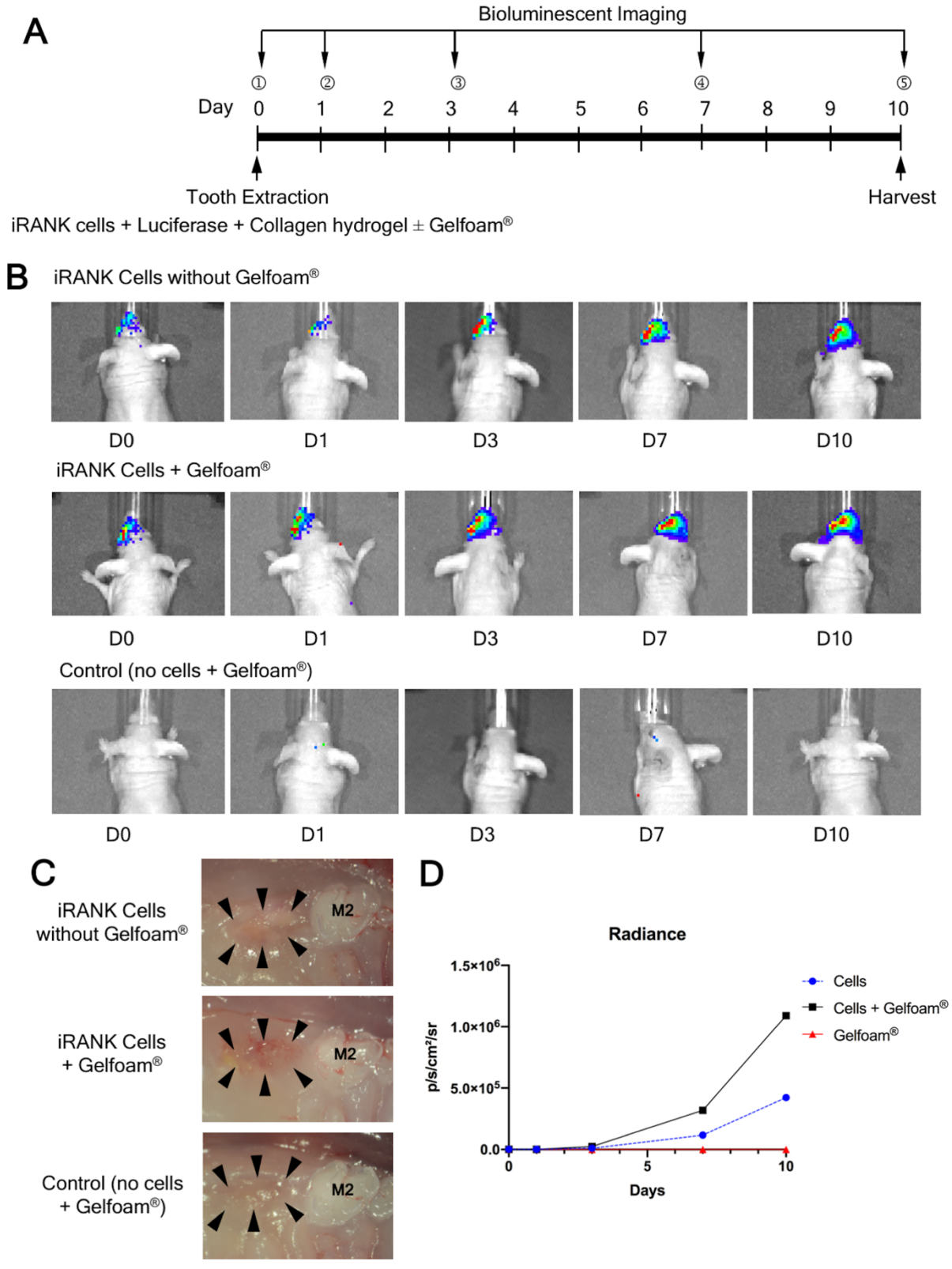

Figure 3.7. iRANK cells were retained at the tooth socket of nude mice.

(A) Experiment timeline; Luciferase transfected iRANK cells with collagen hydrogel were delivered to the socket and the socket was covered with Gelfoam® dental sponge to help keep the cells in place. To visualize luciferase transfected cells, luciferin was injected intraperitoneally 10 to 15 minutes prior to imaging with the Xenogen IVIS imaging system. Cell localization was assessed on the same day as cell delivery (day 0; D0). Additionally, mice were imaged 4 times (day 1, 3, 7 and 10; D1-10) following injection, at least 24 hours between imaging sessions. At day 10, the images of the extraction site were taken. **(B)** The bioluminescence data showed that the signal was detected and increased over time in all animals that received cells with or without Gelfoam®. As expected, no signal was detected in the animals that did not receive cells but received luciferin. This suggests that iRANK cells were retained at the tooth socket and the cells proliferated, which was expected as the engineered cells were derived from a cell line and were injected into athymic nude mice. **(C)** Clinical presentation of the extraction site showed that all groups had complete closure of epithelium. (n=1 per group; Black arrowheads indicate the outline of the extraction site.; M2, second molar) **(D)** The radiance unit as the number of photons per second that leave a square centimeter of tissue and radiate into a solid angle of one steradian (sr) ($p/s/cm^2/sr$) as the quantitative data of the bioluminescence imaging shown in Fig. 3.7B.

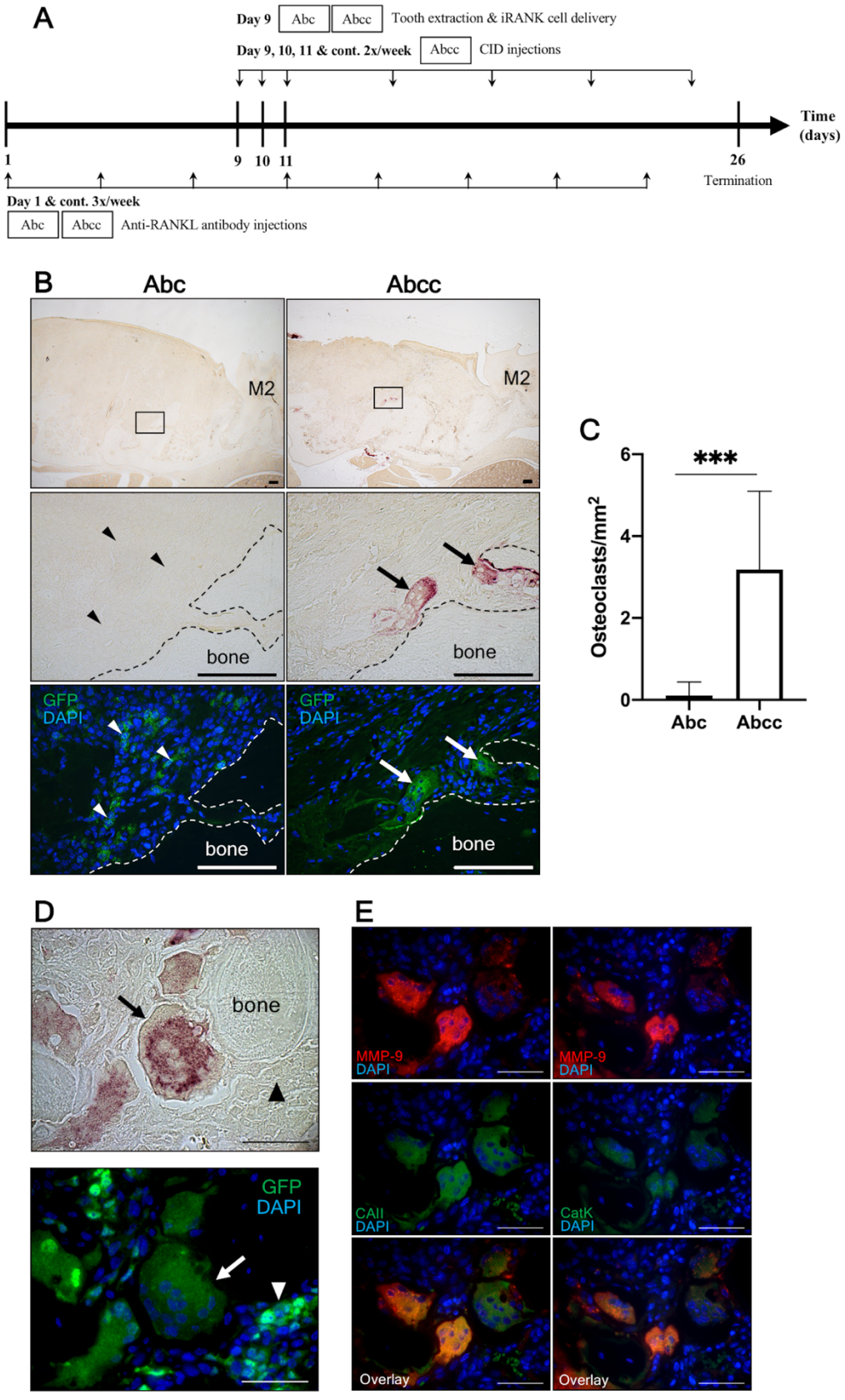
A
Day 9
Abc
Abcc
Tooth extraction & iRANK cell delivery
Day 9, 10, 11 & cont. 2x/week
Abcc
CID injections
Time (days)
1
9
10
11
26
Termination
Day 1 & cont. 3x/week
Abc
Abcc
Anti-RANKL antibody injections
B
Abc
Abcc
M2
M2
bone
bone
GFP
DAPI
GFP
DAPI
bone
bone
C
***
Osteoclasts/mm2
6
4
2
0
Abc
Abcc
D
bone
GFP
DAPI
E
MMP-9
DAPI
MMP-9
DAPI
CAII
DAPI
CatK
DAPI
Overlay
Overlay

Figure 3.8. iRANK cells were retained and differentiated into osteoclasts in anti-RANKL antibody and CID-treated mice.

(A) Experiment timeline **(B)** TRAP and immunofluorescence staining; GFP+ cells (arrowheads) indicating delivered iRANK cells were found in the sockets of both Abc and Abcc groups. However, only Abcc group exhibited osteoclasts (arrows) which are TRAP+GFP+ with three or more nuclei. (Dot line indicates outline of alveolar bone; M2, second molar; scale bar = 100μm) **(C)** Quantification of TRAP+GFP+ osteoclasts (***$p < 0.001$; $n \geq 7$ per group) **(D)** High magnification of iRANK osteoclasts; In Abcc group, engineered iRANK osteoclasts are positive for TRAP as indicated by red granules (black arrow). Un-fused iRANK cells are TRAP-negative as depicted by the absence of red staining (black arrowhead). Engineered iRANK cells also express GFP showing that these cells are the implanted iRANK cells which have differentiated into osteoclasts indicated by double-labeling of the same cell with TRAP enzyme and GFP antibody (black and white arrows). Osteoclast at center has 13 nuclei. Undifferentiated implanted iRANK cells also express GFP as expected (white arrowhead). 60X oil immersion images; scale bar = 50μm **(E)** Immunofluorescence of iRANK osteoclasts in the extraction site of adjacent sections double-labeled with antibodies to either MMP-9 and carbonic anhydrase II, or MMP-9 and cathepsin K. (MMP-9 = matrix metalloprotease 9; CAII = carbonic anhydrase II; CatK = cathepsin K. 60X oil immersion images; scale bar = 50μm)

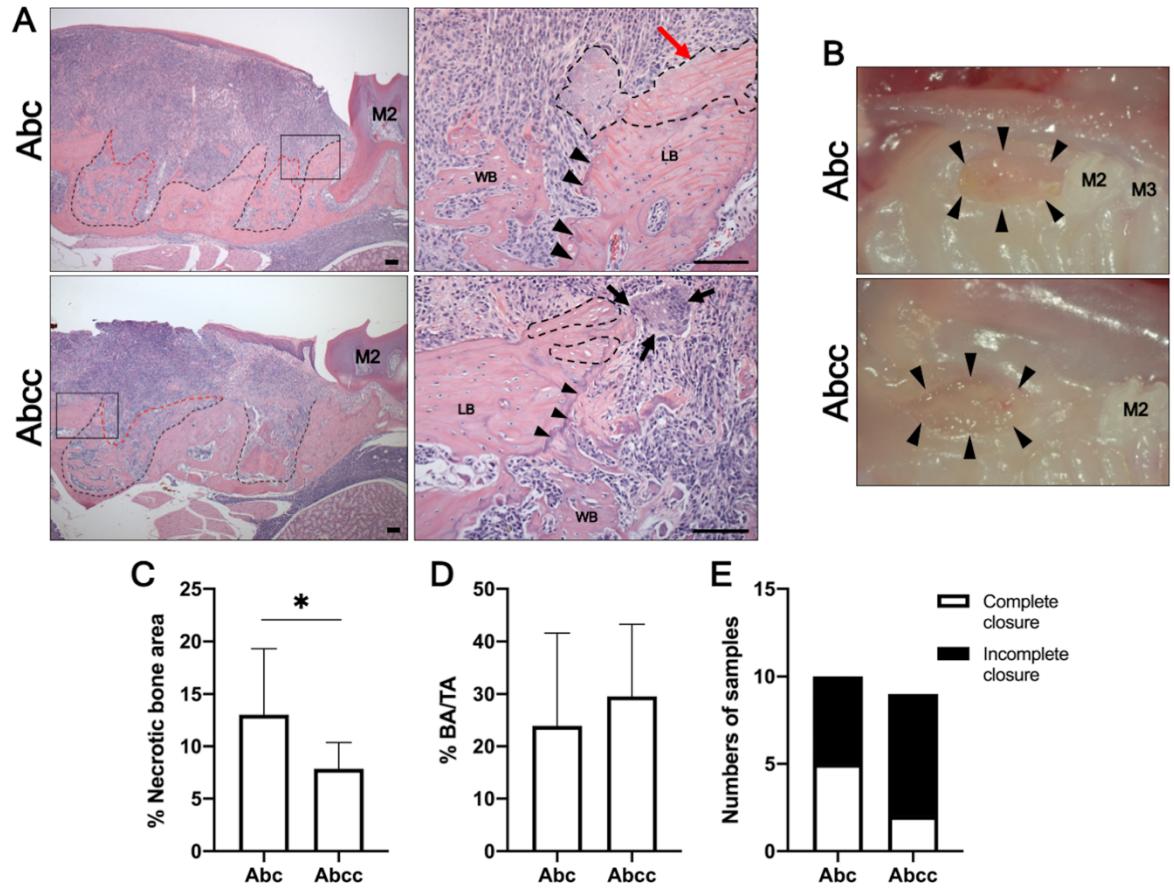

Figure 3.9. Bone resorptive function, but not new bone formation and epithelial closure, was restored by the engineered osteoclasts in anti-RANKL antibody-treated mice.

(A) H&E staining; Left panels: low magnification images of the extraction site. Black dotted line indicates the tooth socket outline. Red dotted line indicates the level of newly formed woven bone. The boxed areas represent alveolar bone adjacent to the tooth sockets. Scale bar = 100 µm. Right panels: Higher magnification images of the boxed areas in left panels. Large clusters of empty lacunae located at unresorbed alveolar ridge (red arrow) were observed with no sign of osteoclasts in Abc group. In contrast, iRANK engineered osteoclasts (black arrows) located next to smaller clusters of empty lacunae were observed in Abcc group. Black dotted line indicates the necrotic bone area. Black arrowheads indicate reversal line. LB, lamellar bone; WB, woven bone. Scale bar = 100 µm. **(B)** Clinical presentation at the extraction site. Black arrowheads indicate the outline of the extraction site. **(C)** Quantification of necrotic bone area, **(D)** % bone area/total socket area (%BA/TA), and **(E)** epithelial closure (M2, second molar; M3, third molar; *$p < 0.05$; $n \geq 7$ per group for % necrotic bone area; $n \geq 3$ per group for %BA/TA)

Clinical Features	Ct group	Ab group	Abc group	Abcc group
Osteoclasts	+	-	-	+
Accumulation of necrotic bone	-	+	+++	++
New bone formation	+	+	-	-
Epithelial closure	+	+	-	-
MRONJ stages	**No disease**	**Stage 0**	**Stage 1**	**Stage 1**

Table 3.1. Staging of the MRONJ mouse models regarding the staging in humans by S. L. Ruggiero et. al., 2014*(1)* (+ indicates the presence, while – indicates the absence of the features. For necrotic bone, the numbers of + also indicates the degrees of the feature.)

Chapter 4. EFFECTS OF ANTI-RANKL ANTIBODY ON OSTEOBLASTS

4.1 INTRODUCTION

In the last chapter, I showed that osteoclast inhibition led to accumulation of necrotic bone and restoring the osteoclast's bone resorptive function reduced the necrotic bone area in the MRONJ mouse model. However, other MRONJ characteristics including impaired bone formation and incomplete epithelial closure were not improved by osteoclast replenishment. This suggests that there are potentially other mechanisms underlying the impairment of these components of MRONJ pathophysiology.

Osteoblasts are bone forming cells which play a role in bone formation and bone remodeling process. Therefore, researchers have been investigating the effects of BPs and denosumab on osteoblast functions which may explain the impaired bone formation observed in MRONJ. While it has been shown that BPs have effects on cell viability of osteoblasts*(83)*, little is known about the effects of denosumab and/or anti-RANKL antibody. However, MSCs express RANK on their cell surface suggesting that the binding of RANKL released by MSCs themselves to RANK induces osteoblast differentiation via autocrine/paracrine regulatory loop both *in vitro* and *in vivo*.*(84)* In this chapter, I determined the effects of anti-RANKL antibody on osteogenic differentiation of MC3T3 cells which may contribute to a better understanding of DRONJ pathophysiology and *the hypothesis was that anti-RANKL antibody inhibits osteogenic differentiation of MC3T3 cells via autocrine/paracrine loop of RANKL in vitro*.

4.2 MATERIALS & METHODS

4.2.1 *Cell culture*

MC3T3 cells were purchased from American Type Culture Collection (ATCC) and were cultured in α-MEM (Gibco™, 12571063) containing 10% fetal bovine serum and 100 U/mL of penicillin/streptomycin and incubated at 37°C with 5% CO_2. MC3T3 cells were plated at 1×10^5 cells/well in 6-well plates. After reaching 80% confluency, MC3T3 cells were treated with osteogenic media (OSM) including 10 mM β-glycerophosphate (Sigma-Aldrich, G9422), 50 μg/mL L-ascorbic acid (Sigma-Aldrich, A4544), and 100 nM dexamethasone (Sigma-Aldrich, D4902) for 14 days to induce osteogenic differentiation. The media and inducers were changed every other day. Cells were washed twice with PBS and collected on Day 0, 7, and 14 for RT-qPCR.

To study the effects of anti-RANKL antibody on osteogenic differentiation, MC3T3 cells were plated at 1×10^4 cells/well in 48-well plates and treated with OSM concurrently to either anti-RANKL antibody or isotype control IgG antibody ranged from 0.5-100 nM for 14 days. The media and inducers were changed every other day. Cells were collected on Day 14 for ALP activity assessment.

4.2.2 *RNA extraction and reverse transcription-quantitative polymerase chain reaction (RT-qPCR)*

RNA extraction was performed with a RNeasy mini kit (Qiagen). MC3T3 cells were washed twice with PBS and lysed by Buffer RLT from the kit. Cell lysate was kept at -80 °C until further use. RNA was extracted from cell lysate following manufacturer's instructions. cDNA was synthesized from 500 ng RNA using an Omniscript RT Kit (Qiagen). qPCR was performed on

cDNA using TaqMan gene expression assays (Applied Biosystems) for *Rank*, *Rankl*, and *Opg* **(Table 4.1)**, and ABI Prism 7000 sequence detection system (Applied Biosystems). RNA expressions were reported as fold changes to Day 0 MC3T3 cells using ΔΔCT method normalized to 18s rRNA (Applied Biosystems, 4308329). RAW 264.7, a murine monocyte/macrophage-like cell line was used as a positive control for *Rank* and negative controls for *Rankl* and *Opg*.

4.2.3 *ALP activity assessment*

For qualitative assessment of alkaline phosphatase (ALP) activity, cells were fixed with 10% neutral buffered formalin for 15 minutes at room temperature, then stained with ImmPACT™ Vector® Red (Vector laboratories) for 20-30 minutes. For quantitative assessment, cells were lysed with 0.2% Triton X-100 on a shaker for 20 minutes and measured for ALP activity using a QuantiChrom™ ALP Assay kit (BioAssay Systems) following manufacturer's instructions. ALP activity was normalized to total proteins measured by a Micro BCA Protein Assay kit (Thermo Fisher Scientific).

4.3 RESULTS

4.3.1 *MC3T3 cells expressed Rankl and Opg, but not Rank*

To understand the roles of *Rank*, *Rankl*, and *Opg* in osteogenic differentiation, the expression of these genes was first investigated in MC3T3 cells using RT-qPCR. Interestingly, *Rank* expression of MC3T3 cells was undetectable at all timepoints, while the average CT values of *Rank* in RAW264.7 cells was 25.14. As expected, both *Rankl* and *Opg* were expressed at all timepoints in MC3T3 cells, while they were undetectable in RAW264.7 cells **(Figure 4.1)**. Though not significantly different, a trend towards upregulation of *Rankl* and downregulation of *Opg* was

observed as MC3T3 cells differentiated into mature osteoblasts. These results suggest that RANKL, as well as its inhibition by anti-RANKL antibody, is unlikely to affect osteogenic differentiation of MC3T3 cells.

4.3.2 *Anti-RANKL antibody treatments did not affect ALP activity of MC3T3 cells*

ALP activity was measured to investigate the effects of anti-RANKL antibody on osteogenic differentiation. According to the qualitative assessment, ALP activity represented in red areas was not different among all antibody-treated groups **(Figure 4.2)**. Likewise, there was no significant difference in ALP activity normalized to total proteins among all antibody-treated groups **(Figure 4.3)**. The ALP activity was also comparable between the cells treated with anti-RANKL antibody and isotype control IgG antibody at the same concentration. Moreover, there was no significant difference in total proteins among all antibody-treated groups suggesting that anti-RANKL antibody has no effect on cell viability of osteoblasts.

4.4 DISCUSSION

Impaired new bone formation is a common feature observed in MRONJ in addition to osteoclast deficiency and accumulation of necrotic bone. In the previous chapter, I showed that the delivery of iRANK osteoclasts restored bone resorptive activity and reduced necrotic bone area in the MRONJ model, however, it did not improve new bone formation. These data suggest that osteoclast deficiency may not be the only effect of the inhibition of RANKL on MRONJ pathophysiology. Therefore, I investigated the effects of anti-RANKL antibody on osteoblasts in this chapter which may contribute to the impaired new bone formation observed in MRONJ.

The direct effects of BPs on osteoblasts have been investigated. Many studies have suggested the inhibitory effects of BPs on osteoblasts and their functions. It has been shown that

ZA increases apoptosis and inhibits proliferation of osteoblasts *in vitro.(85–87)* On the other hand, the studies on anti-RANKL antibody are very limited and inconclusive. Mosch et al. show that anti-RANKL antibody has no significant effect on cell proliferation and osteogenic differentiation-related genes including *Runx2*, *Alp*, and *Col1* in osteoblasts *in vitro(88)*, which is similar to my findings. MSCs, which can differentiate into osteoblasts, express *Rank*, thus, it is possible that RANKL may upregulate osteoblast-related pathways via an autocrine regulatory loop.*(84)* Nevertheless, the expression of *Rank* is downregulated over time as MSCs differentiate to osteoblasts.*(89)* These findings are supported by my qPCR data showing that MC3T3 cells did not express *Rank* at the RNA level during differentiating into mature osteoblasts, while *Rankl* and *Opg* were still detected. The absence of RANK, which is the receptor of RANKL, likely explains why there is no significant effect of RANKL inhibition by anti-RANKL antibody on MC3T3 osteoblasts, even though they express *Rankl*.

Osteoblasts and their functions are also observed in the MRONJ animal models. Interestingly, newly-formed bone in the extraction socket has largely been used as a surrogate of osteoblast's bone formation function rather than studying osteoblast numbers and their other markers in the MRONJ models. Although various methods have been utilized to induce BRONJ in rodents, decreased bone filling in the tooth socket is commonly observed among these animal models.*(26, 46, 90)* In contrast, the inhibitory effects on new bone formation remain inconclusive in the DRONJ models using anti-RANKL antibody monotherapy. The impaired bone formation is only seen when anti-RANKL antibody is used with other chemotherapeutic drugs such as cyclophosphamide to induce DRONJ.*(40)* My *in vitro* findings that anti-RANKL antibody has no significant effect on osteogenic differentiation of osteoblast support the data from our *in vivo* MRONJ model that new bone formation is not affected by anti-RANKL antibody monotherapy

(Ct vs. Ab group). Taking all these data together, the effects of anti-RANKL antibody treatment on RANKL autocrine/paracrine regulatory loop in osteoblasts are less likely to play a major role in DRONJ pathophysiology.

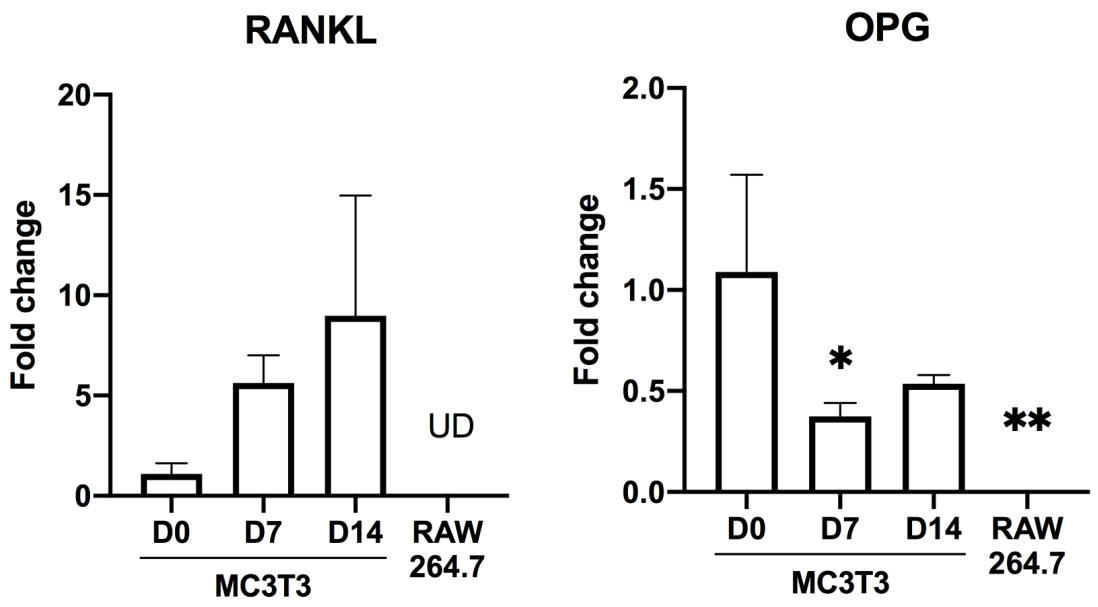

Figure 4.1. MC3T3 cells expressed *Rankl* and *Opg*, but not *Rank*.

(A) *Rankl* and **(B)** *Opg* gene expressions of MC3T3 cells treated with OSM for 0, 7, and 14 days (D0, D7, and D14) as a fold change to D0. Both *Rankl* and *Opg* expressions were undetected in RAW 264.7 cells which are a negative control for both genes. (UD = undetectable, *$p<0.05$, **$p<0.01$)

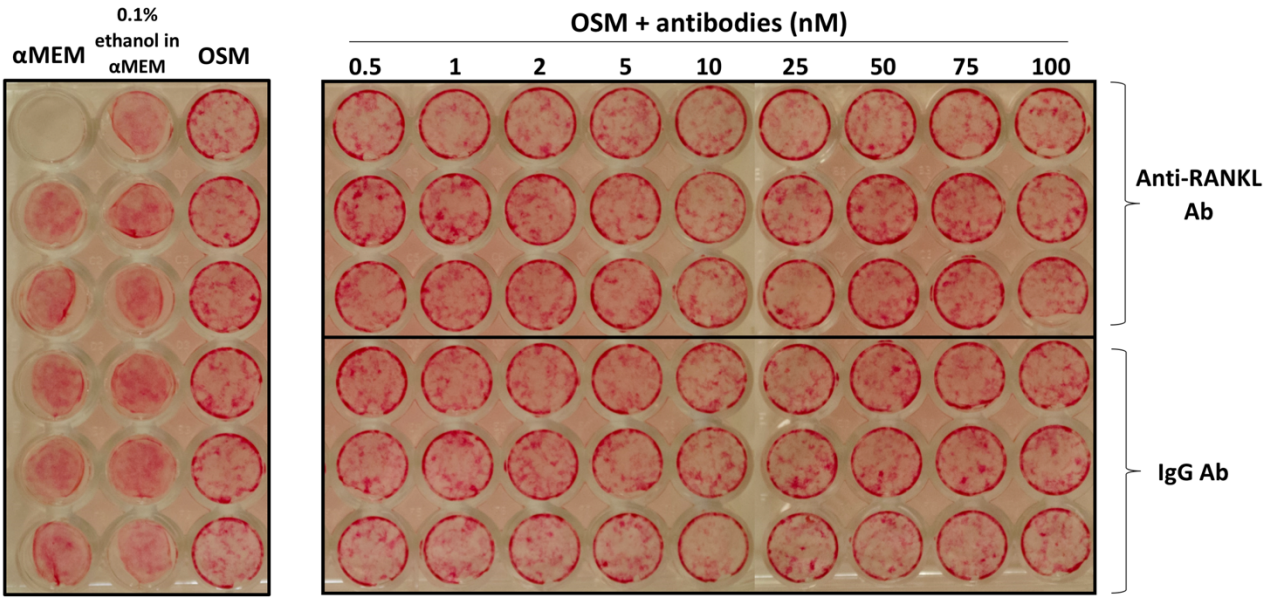

Figure 4.2. Qualitative assessment of ALP activity showed no significant difference among MC3T3 cells treated with various concentrations of anti-RANKL antibody.

MC3T3 cells were treated with OSM concurrently to different concentrations of either anti-RANKL or isotype control IgG antibody for 14 days. There was no significant difference of the ALP activity as shown in red areas among all treated groups. (αMEM as a negative control, 0.1% ethanol in αMEM as a vehicle control, and OSM as a positive control for ALP)

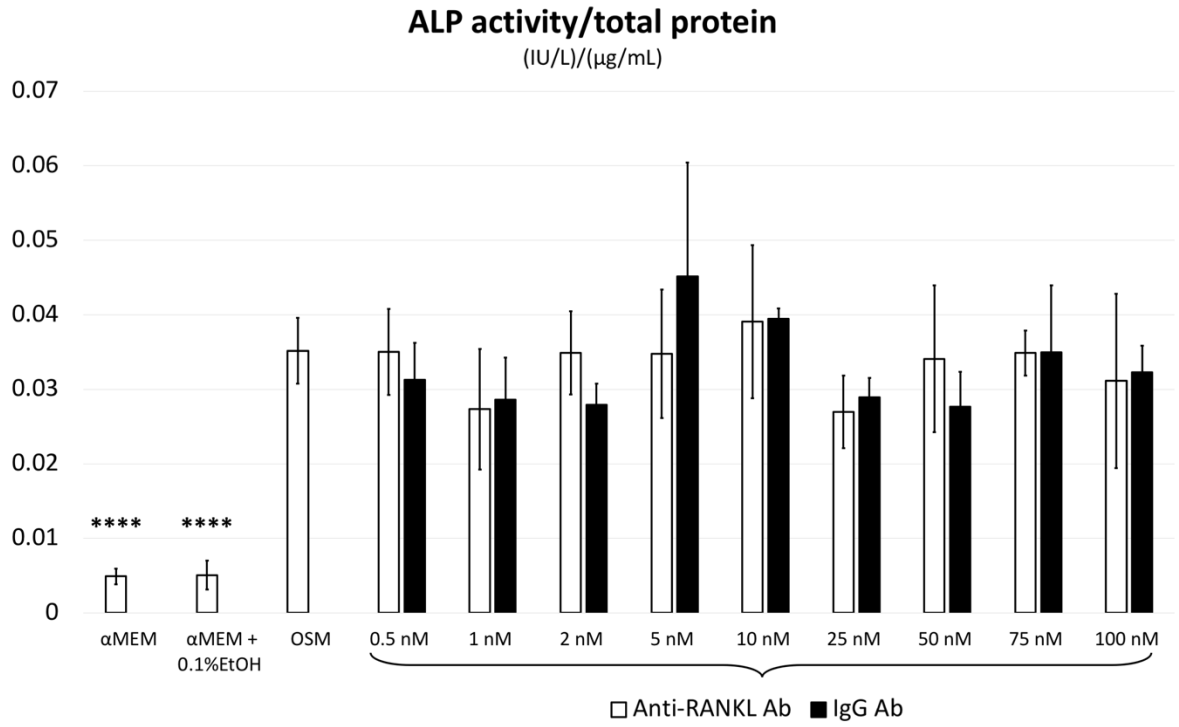

Figure 4.3. Quantitative assessment of ALP activity showed no significant difference among MC3T3 cells treated with various concentrations of anti-RANKL antibody.

MC3T3 cells were treated with OSM concurrently to different concentrations of either anti-RANKL or isotype control IgG antibody for 14 days. There was no significant difference of the ALP activity normalized to total proteins among all groups with antibody treatment. (****$p<0.0001$, αMEM as a negative control, 0.1% ethanol in αMEM as a vehicle control, and OSM as a positive control for ALP)

Genes	Assay ID	Size (bp)
MC3T3 and M0 studies		
Tnfrsf11a (Rank)	Mm00437132_m1	65
Tnfrsf11 (Rankl)	Mm00441906_m1	66
Tnfrsf11b (Opg)	Mm00435454_m1	71
M1-related genes		
Nos2 (iNOS)	Mm00440502_m1	66
Tnfa	Mm00443258_m1	81
Il1b	Mm00434228_m1	90
M2-related genes		
Mrc1 (CD206)	Mm01329362_m1	147
Arg1	Mm00475988_m1	65
Ym1 (Chil3)	Mm00657889_mH	90
Potential RPM markers		
Ifi205	Mm01315309_m1	99
Cxcl9	Mm00434946_m1	64
Mycl	Mm00493155_m1	80
Mmp25	Mm01309189_m1	107
Traf1	Mm00493827_m1	78
Lad1	Mm00504923_m1	60
Osteoclast-related genes		
Tnfrsf11a (Rank)	Mm00437132_m1	65
Traf6	Mm00493836_m1	72
Nfatc1	Mm00479445_m1	75
Dcstamp	Mm04209236_m1	105
Ocstamp	Mm00512445_m1	73
Acp5 (TRAP)	Mm00475698_m1	79
Ctsk	Mm00484039_m1	73

Table 4.1. TaqMan gene expression assays (Applied Biosystems) used for RT-qPCR

Chapter 5. ROLES OF RANKL IN MACROPHAGE POLARIZATION AND MEDICATION-RELATED OSTEONECROSIS OF THE JAW

5.1 INTRODUCTION

Macrophages, a mononuclear myeloid lineage cell, are one of the key inflammatory cells which play crucial roles in healing.*(91)* They are heterogeneous and capable of polarizing into broad spectrum of cell types depending on the functions and healing phases. Unpolarized macrophages (M0) can polarize to pro-inflammatory M1 which releases several cytokines such as IL-1, IL-2, IL-6, IL-12, TNF-α, and IFN-γ playing roles in inflammation, pathogen clearance, and activation of immune system in the early phase of wound healing.*(10, 11)* While, anti-inflammatory M2 promotes tissue repair, extracellular matrix deposition and new bone formation by releasing in IL-10, CCL-18, CCL-12, BMP-2, TGF-β, osteopontin, and 1,25-dihydroxy-vitamin D3 during the late phase of wound healing.*(12–14)* Moreover, macrophages also act as mediators which controls the functions of nearby cells such as osteoblasts and osteocytes.*(91)* Therefore, the equilibrium of macrophage populations and their functions is required for successful healing.

The disruption of M1 and M2 equilibrium leads to impaired bone healing in several oral diseases. Periodontitis is a chronic inflammatory disease with a clinical feature of alveolar bone loss caused by altered host immune response to bacteria biofilm.*(92)* Gram-negative bacteria in biofilm release lipopolysaccharide (LPS) and other bacterial factors, which recruit inflammatory cells and induce M1 polarization as well as secretion of proinflammatory cytokines.*(92)* Several studies have shown that increased numbers of overall macrophages are observed locally at bone-

loss sites in patients with periodontitis as well as increased M1/M2 ratio and increased M1-related cytokine secretion including IFN-γ, TNF-α, IL-6, and IL-12.*(23, 24)* Several *in vitro* studies also support that M1 and their proinflammatory cytokines inhibit osteogenic differentiation of MSCs and mineralization.*(48)*

Macrophage alteration is also one of the potential mechanisms underlying MRONJ pathophysiology.*(3, 39)* MRONJ lesions exhibit necrotic bones as well as impaired hard and soft tissue healing.*(3)* While osteoclasts play a role in necrotic bone resorption as explained in the previous chapter, macrophages play both direct and indirect roles in pathogen clearance, recruitment of inflammatory cells, and tissue formation.*(10–14)* Hence, the disruption of M1 and M2 equilibrium may potentially contribute to MRONJ. Indeed, increased M1/M2 ratio has been observed in both BRONJ animal models and patients associating with the severity of the disease.*(20–22)* Several studies have shown that BPs can induce M1 polarization via several mechanisms including toll-like receptor 4 (TLR-4) and IL-17.*(20, 22)* On the other hand, the roles of macrophages in DRONJ pathophysiology have still not been fully understood. Unlike BRONJ, only a few studies have observed macrophage alteration in DRONJ. Paschalidi et. al. reported an increased M1/M2 ratio in DRONJ patients*(93)*, while Tamaki et. al. observed an increased M1/M2 ratio only in the combined treatment of anti-RANKL antibody and cyclophosphamide, but not in anti-RANKL antibody monotherapy in DRONJ animal model.*(40)* Thus, more studies on the roles of macrophages in DRONJ pathophysiology need to be further investigated.

In contrast to BRONJ, robust and reliable DRONJ animal models have not been established and the effects of RANKL and anti-RANKL antibody on macrophage polarization remains elusive. Most studies have focused on the effects of RANKL (in the presence of M-CSF) on osteoclast differentiation from osteoclastic precursors, and how osteoclast inhibition caused by anti-RANKL

antibody contributes to DRONJ pathophysiology. However, the effects of RANKL on macrophages (in the absence of M-CSF) needs to be further explored in order to fully understand how anti-RANKL antibody plays a role in DRONJ pathophysiology. Macrophages are heterogenous and can polarize and differentiate into various types of cells. Nevertheless, it remains unknown as to whether RANKL can induce osteoclast differentiation if myeloid precursors have already committed to a specific macrophage cell lineage. In addition, it has been shown that RANKL can upregulate the expression of proinflammatory and M1-related genes such as *Il1b*, *Il6*, *Tnfa*, and *iNOS* in BMDMs.*(49)* However, this upregulation is at a significantly lower magnitude compared to the effects of classical M1 inducers, including LPS and IFN-γ.*(49)* As the previous study only focuses on a few M1-related genes, it is possible that RANKL may induce a gene expression profile and phenotype which is different from other macrophage population.

In this chapter, I investigated the effects of RANKL in the absence of M-CSF on macrophage polarization; I have termed the resulting cells as "RANKL – polarized macrophages (RPMs)". *I hypothesized that RPMs have a different gene expression profile and functions compared to M0, M1, M2 macrophages and osteoclasts.* To test this hypothesis, the gene expression profile, potential markers, related pathways, and osteoclast differentiation potency of RPMs were analyzed using RNA sequencing (RNA-seq), RT-qPCR, and bioinformatics analysis. Additionally, I also investigated how the absence of RANKL affects macrophage polarization *in vivo*. The tissue sections of MRONJ model from the previous chapter were utilized to determine the effects of anti-RANKL antibody on macrophage polarization *in vivo*. *I hypothesized that the absence of RANKL leads to increased M1/M2 ratio in the MRONJ model.* These data will altogether provide important pieces to fulfill the understanding of the roles of macrophages in DRONJ pathophysiology which is currently much needed in the field.

5.2 MATERIALS & METHODS

5.2.1 *Bone marrow derived cell isolation and macrophage differentiation*

Six- to twelve-week-old C57BL/6 wild-type mice were utilized for bone marrow derived (BMD) cell isolation as previously described.*(41)* In brief, mice were sacrificed, and tibiae and femora were collected. Both ends of tibiae and femora were cut open and RPMI 1640 media (Gibco™, 11875119) containing 20% fetal bovine serum and 100 U/mL of penicillin/streptomycin were used to flush BMD cells from the bone marrow from both ends of the bones using a 25-gauge needle and syringe. BMD cells were plated at 2×10^6 cells/well in 6-well plates and cultured in RPMI 1640 media containing 20% fetal bovine serum and 100 U/mL of penicillin/streptomycin. Cells were treated with 10 ng/mL recombinant mouse M-CSF (R&D Systems, 416-ML) for 7 days to differentiate BMD cells into unpolarized macrophages (M0) for further experiments. Fresh media and treatments were added once on Day 4.

5.2.2 *Cell culture*

To study the effects of RANKL on macrophage polarization, M0 macrophages were treated with various inducers in RPMI 1640 media containing 100 U/mL of penicillin/streptomycin with no serum nor M-CSF for 2, 6, and 24 hours. Treatments of 20 ng/mL recombinant mouse RANKL (R&D Systems, 426-TEC), 50 ng/mL LPS (Sigma, L4391) + 40 ng/mL IFN-γ (Peprotech, 315-05), and 20 ng/mL IL-4 (Peprotech, 214-14) were used for RPM, M1, and M2 polarization respectively. Additionally, M0 macrophages were treated with 100 ng/mL RANKL for 24 hours to determine if there is any dose-dependent effect of RANKL. To study the effects of RANKL on M1 and M2 inducers, M0 macrophages were treated with 20 ng/mL RANKL concurrently with

LPS + IFN-γ and IL-4 respectively for 2 and 24 hours. M0 and vehicle (PBS) groups were included as controls in both experiments. These cells were used for RT-qPCR and RNA-seq later.

To investigate the osteoclast differentiation potency of M0 macrophages, M0 macrophages were treated with 20 ng/mL recombinant mouse RANKL and 10 ng/mL recombinant mouse M-CSF in RPMI 1640 media containing 20% fetal bovine serum and 100 U/mL of penicillin/streptomycin for 5 days. Osteoclasts derived from BMD cells treated with the same doses of RANKL and M-CSF were used as a positive control. Fresh media and treatments were changed once on Day 3. These cells were used for RT-qPCR and TRAP staining later. For TRAP staining, sterilized coverslips were placed into the wells before seeding cells.

5.2.3 *RNA isolation and RT-qPCR*

RNA extraction was performed with a RNeasy mini kit (Qiagen). Cells were washed twice with PBS and lysed by Buffer RLT from the kit. Cell lysate was kept at -80 °C until further use. RNA was extracted from cell lysate following manufacturer's instructions. cDNA was synthesized from 250 ng RNA using an Omniscript RT Kit (Qiagen). qPCR was performed on cDNA using TaqMan gene expression assays (Applied Biosystems) for RPM, M1, M2, and osteoclast-related genes shown in **Table 4.1**, and QuantStudio 6 Pro Real-Time PCR System (Applied Biosystems). RNA expressions were reported as fold changes to M0 macrophages unless stated in the text using ΔΔCT method normalized to 18s rRNA (Applied Biosystems, 4308329).

5.2.4 *RNA sequencing*

M0 macrophages were treated with either RANKL (for RPM) or PBS (for a vehicle control; Veh) for 2 and 6 hours as explained above. Five sample groups including M0, Veh-2h, RPM-2h, Veh-6h, RPM-6h were used in this study. Cells were isolated from the same C57BL/6 wild-type

mouse for all conditions, and cells were cultured and treated in three wells of 6-well plates for each condition (n=3 per group). RNA was extracted as explained above and used for RNA-seq.

RNA quality measurement, library preparation, and RNA-seq were performed by BGI (Shenzhen, China). RNA concentration, 28S/18S, and RNA Integrity Number (RIN) were determined using a 2,100 Bioanalyzer (Agilent Technologies). All the RNA samples were qualified with 28S/18S $\geq$ 1.0 and RIN $\geq$ 7.0 and used for library construction. PE100 sequencing were performed using the BGISEQ platform. On average, the samples generated about 4.47 Gb bases per sample. Reads with low quality, adaptor sequences and high levels of N base were filtered, and the remaining reads were mapped to the reference genome and gene using HISAT and Bowtie2 respectively. The average mapping ratio with reference genome is 96.55%, while the average mapping ratio with gene is 86.39%. In total, 16,571 genes were identified. These genes were used in bioinformatics analysis using Dr. Tom analysis platform (BGI, Shenzhen, China) and IPA (Qiagen).

5.2.5 *Bioinformatics analysis of RNA-sequencing data*

Dr. Tom analysis platform (BGI, Shenzhen, China) was used to analyze and compare between RPM-2h vs. Veh-2h, RPM-6h vs. Veh-6h, and RPM-6h and RPM-2h for differentially expressed genes (DEGs), KEGG pathway, and Gene Ontology (GO). Genes with $|\log_2 \text{fold change}| \geq 2$ and q-value < 0.05 were considered significant DEGs. Several significant DEGs with both high values of upregulated fold change and statistical difference were selected as potential RPM markers, and RT-qPCR was used to confirm the difference at the RNA level among groups. For KEGG pathway and GO enrichment analysis, the phyper function in R software was used to perform the enrichment analysis according to the classification, calculate the p-value, and the q-

value was obtained by correction of the p-value. Q-value ≤ 0.05 was regarded as a significant enrichment.

For Qiagen IPA analysis, a dataset containing genes from RNA-seq with $|\log_2 \text{fold change}| \geq 1$ and q-value < 0.05 was uploaded into the application. This dataset was used for canonical pathway, upstream regulator, and diseases and functions analysis, as well as, analysis match.

5.2.6 *TRAP staining*

Cells were washed with PBS twice and fixed with 10% neutral buffered formalin for 10 minutes at room temperature. Cells were then incubated for 10-15 minutes with TRAP staining solution at 37°C, according to manufacturer's protocol (Sigma-Aldrich, 387A). Nuclei were counterstained with 0.5% methyl green (Sigma, 323829) for 5 minutes. Coverslips with attached cells were removed from the wells and mounted to glass slides with Aqua-Mount (Thermo Fisher Scientific). Images were obtained using an upright microscope (Nikon E800).

5.2.7 *Immunofluorescence staining*

To study M1 and M2 macrophages in the MRONJ mouse model, a double-staining of F4/80 & iNOS and F4/80 & CD206 was used to visualize M1 and M2 respectively. MRONJ tissue sections were deparaffinized and rehydrated with TBS-Tween (TBS-T; 0.05 M Tris buffer, 0.15 M NaCl, 0.1% Tween 20, pH 7.6). For antigen retrieval, the sections were incubated with sodium citrate buffer (10 mM sodium citrate, 0.05% Tween 20, pH 6.0) at 65 °C for 40 minutes, then cooled down at the room temperature for 20 minutes. Permeabilization was performed with 0.1% Triton X-100 in PBS, pH 7.4 for 10 minutes following by background blocking with 4% normal donkey serum (NDS) and 1% bovine serum albumin (BSA) in PBS for 30 minutes. Tissues sections were incubated with primary antibodies including rat anti-mouse F4/80 antibody

(BioLegend, 123101; 1:100 dilution) with either rabbit iNOS polyclonal antibody (Invitrogen, PA1-036; 1:100 dilution) or rabbit CD206 polyclonal antibody (Proteintech, 18704-1-AP; 1:500 dilution) in 2% NDS and 1% BSA in PBS at 4°C overnight. Slides were rinsed three times in TBS-T for 5 minutes. Tissues sections were then incubated with Cy3 AffiniPure Donkey Anti-Rat IgG secondary antibody (Jackson ImmunoResearch Laboratories, Inc., 712-165-153; 1:200 dilution) and Alexa 488 AffiniPure Donkey Anti-Rabbit IgG secondary antibody (Jackson ImmunoResearch Laboratories, Inc., 711-545-152; 1:200 dilution) for 30 minutes at room temperature. Slides were then rinsed three times in TBS-T for 5 minutes and once in Milli-Q water. Nuclei were counterstained with 300 nM DAPI Dilactate (Life Technologies) for 5 minutes. Slides were rinsed with Milli-Q water and PBS before mounting with ProLong Gold Antifade Mountant (Thermo Fisher Scientific). Images were obtained using an upright microscope (Nikon E800) and overlaid using Adobe Photoshop.

5.2.8 *Macrophage quantitation*

Two uniformly spaced (approximately 100 μm) tissue sections were selected per sample for M1 quantitation and another two sections per sample for M2 quantitation; both M1 and M2 sections were adjacent. Region of interest (ROI) included connective tissue above the tooth sockets and unfilled sockets in early-term samples (terminated 1 week after tooth extraction), while only connective tissue above the tooth sockets in final-term samples (terminated 3 weeks after tooth extraction). NIS-Elements software (BR 4.30.02 64-bit, Nikon) was used to set two different thresholds for M1 and M2. Mononuclear cells which passed the thresholds were considered M1 or M2. Numbers of macrophages in ROI (#M1 or #M2/mm^2) were quantitated for M1 and M2 using adjacent sections, and M1/M2 ratios were calculated from these values.

5.2.9 *Statistical analysis*

Results are expressed as mean ± SD. GraphPad Prism version 8.4.1 was used to perform Kolmogorov-Smirnov test to test normality of data, student's *t*-test to compare means of two individual groups with equal variances, student's *t*-test with Welch's correction to compare means of two individual groups with unequal variances, and one-way ANOVA with post-hoc Tukey test to compare means of three or more individual groups. Triplicates were used per group (n=3) unless stated and a value of $p < 0.05$ was considered statistically significant.

5.3 RESULTS

5.3.1 *RANKL treatment had a small but significant effect on M1 and M2 marker expression in M0, but did not significantly alter the effect of classical M1 and M2 inducers on polarized gene expression.*

I hypothesized that RANKL potentially polarizes M0 macrophages into RPMs which may have different gene expression profiles and phenotypes compared to M0, M1, and M2. Therefore, several M1 and M2 markers were investigated in RPMs to identify if their expression was different from that expected following classical M1 and M2 induction. In order to polarize into RPMs, M0 macrophages must express RANK which is a receptor of RANKL. I first confirmed that M0 macrophages expressed *Tnfrsf11a (Rank)* at the RNA level. Interestingly, *Rank* expression in M0 was decreased over time when cultured in media without M-CSF **(Figure 5.1)**. As expected, M0 did not express *Tnfrsf11 (Rankl)* and *Tnfrsf11b (Opg)*. These findings confirmed that M0 macrophages could be polarized into RPMs by RANKL.

Next, expressions of several M1 (*Nos2, Tnfa,* and *Il1b*) and M2 markers (*Mrc1, Arg1,* and *Ym1*) were studied in RPMs at 2, 6, and 24 hours. As a result, RANKL significantly upregulated

the expressions of *iNOS* at 24 hours, and *Tnfa* at 6 and 24 hours in RPMs compared to M0 and vehicle control **(Figure 5.2)**. On the other hand, RANKL had no significant effects on *Mrc1, Arg1,* and *Ym1* expressions at all timepoints as these expressions were downregulated in both RPMs and vehicle control **(Figure 5.3)**. Although the effects of RANKL were statistically significant, the upregulations of M1 markers in RPMs were in much lower level compared to M1 polarized by LPS and IFN-γ **(Table 5.1)**. Moreover, there was no significant difference on the effects on M1 and M2 markers in RPMs between normal (20 ng/mL) and high dose (100 ng/mL) of RANKL treatments **(Figure 5.2, Figure 5.3)**.

Additionally, the effects of RANKL on polarizing ability of classical M1 (LPS+IFN-γ) and M2 inducers (IL-4) were determined. The upregulation trend of M1 markers and downregulation trend of M2 markers were observed in M1+RANKL and M2+RANKL respectively. Nevertheless, these effects were not significantly different except *Ym1* in M2+RANKL at 24 hours **(Figure 5.4)**. Taking all these *in vitro* data together, RANKL slightly upregulates M1 markers without a dose-dependent manner, while does not alter the effect of classical M1 and M2 inducers on polarized gene expression. However, the upregulations induced by RANKL in RPMs are in much lower level compared to M1.

5.3.2 *Potential RPM markers were upregulated in RPMs, however, in much lower level compared to M1*

As I showed that RANKL only has slight effects on M1 and M2 markers in RPMs, RNA-seq was used to identify other upregulated genes in RPMs since their gene expression profile has not been previously studied. Differentially expressed genes (DEGs) of RPMs compared to M0 and vehicle control groups at 2 and 6 hours were identified. Several DEGs with both high values of upregulated fold change and statistical difference were selected as potential RPM markers **(Figure**

5.5). RT-qPCR was performed to validate that all the potential RPM markers including *Ifi205, Cxcl9, Mycl, Mmp25, Lad1,* and *Traf1* were significantly upregulated at the RNA level compared to M0 at both 2 and 6 hours. However, the significant difference between RPMs and vehicle controls were observed in *Mycl, Mmp25, Lad1,* and *Traf1* at 2 hours, and *Cxcl9, Mycl, Mmp25,* and *Traf1* at 6 hours **(Figure 5.6)**. I then compared these genes to M1 and M2 and identified whether the expressions were higher in RPMs. Surprisingly, all potential RPM markers, except *Mycl*, were also upregulated in M1 in much higher level at both timepoints **(Table 5.2)**. Thus, both cell culture and RNA-seq data exhibit the upregulatory effects of RANKL on several genes in RPMs, albeit the expressions are much lower compared to M1. In addition to the potential RPM markers, I also studied the pre-osteoclast and osteoclast markers in the RNA-seq dataset including *Calcr, Ca2, Ctsk, Mmp9, Spp1, Acp5, Itgb1, Itgb3, Itgav, Cd14, Adgre1, Fcgr2a, Fcgr2b, Fcgr3,* and *Spn*. Interestingly, these genes were either not present in the dataset or not included in DEGs. This suggests that RPMs are unlikely to differentiate into osteoclasts.

5.3.3 *IPA analysis of RPM RNA-sequencing data*

IPA Qiagen were used to analyze canonical pathways, upstream regulators, and diseases and functions. The analysis was used to compared RPM at 2 hours to vehicle control at 2 hours (RPM-2h vs. Veh-2h), RPM at 6 hours to vehicle control at 6 hours (RPM-6h vs. Veh-6h), and RPM at 6 hours to RPM at 2 hours (RPM-6h vs. RPM-2h). The most activated and inhibited pathways in RPMs were neuroinflammation signaling (z-score = 3.441) and ferroptosis signaling (z-score = -2.333) respectively at 2 hours **(Figure 5.7)**, while neuroinflammation signaling (z-score = 2.646) and tumor microenvironment (z-score = -1) respectively at 6 hours **(Figure 5.8)**. Interestingly, neuroinflammation signaling was the most activated pathway in both timepoints, however, it was downregulated over time in RPM-6h vs. RPM-2h **(Figure 5.9)**.

Next, upstream regulators were analyzed. This analysis predicted upstream molecules which may be causing the observed gene expression changes in the RPM RNA-seq dataset. For RPM-2h vs. Veh-2h, some top activated regulators were LPS, TNF, and IFN-γ, while top inhibited regulators were PTGER4 and IL10RA **(Table 5.3)**. For RPM-6h vs. Veh-6h, some top activated regulators were LPS, STAT1, and TICAM1, while top inhibited regulators were CITED2 and PTGER4 **(Table 5.4)**. Interestingly, LPS which is a potent M1 inducer was predicted as a top activated in both timepoints, however, LPS as well as TNF were downregulated over time in RPM-6h vs. RPM-2h **(Figure 5.10)**.

In addition, diseases and functions were also analyzed. For RPM-2h vs. Veh-2h, some top activations were cell-to-cell signaling and interaction, cellular movement, hematological system development and function, and immune cell trafficking, while top inhibitions were cell death and survival **(Table 5.5)**. For RPM-6h vs. Veh-6h, top activations were similar to 2 hours timepoint, while top inhibitions were infectious diseases and cell signaling **(Table 5.6)**. Interestingly, these top activated diseases and functions were downregulated over time in RPM-6h vs. RPM-2h **(Figure 5.10)**.

Lastly, I compared my RPM RNA-seq dataset to the other murine cell datasets on the IPA database using analysis match function. At both timepoints, the RPM dataset was similar to murine BMD M1 macrophage datasets; however, the overall expression was lower in our dataset compared to M1 datasets. Moreover, the RPM dataset was different from M2, neutrophil, and dendritic cell datasets **(Figure 5.11).** In summary, IPA analysis shows that RANKL has similar effects to M1 inducers such as LPS supporting the cell culture and RT-qPCR data. However, the effects of RANKL were smaller and decreased over time.

5.3.4 *GO enrichment and KEGG pathway analysis of RPM RNA-sequencing data*

In addition to IPA Qiagen, Dr. Tom analysis platform was used to analyze GO enrichment and KEGG pathway. Upregulated and downregulated DEGs were used separately for different analyses for each timepoint. The results of GO enrichment analysis in biological process category are shown in **Figure 5.12**. For the analysis using upregulated DEGs, immune system process is the most significantly enriched term for both RPM-2h vs. Veh-2h and RPM-6h vs. Veh-6h. The other interesting shared terms between these two groups included cellular response to LPS, inflammatory response, and immune response. For the analysis using downregulated DEGs, the enriched terms were varied for both timepoints. Some interesting shared terms were endocytosis and positive regulation of transcription by RNA polymerase II. Interestingly, cellular response to LPS and inflammatory response were the enriched term when using downregulated DEGs in RPM-6h vs. RPM-2h. This suggests that these processes were decreased over time after the RANKL treatment. Moreover, immune system process was the enriched term in both analyses using upregulated and downregulated DEGs in RPM-6h vs. RPM-2h. This suggests that genes involved in this process were both upregulated and downregulated over time after the RANKL treatment.

Next, KEGG pathway analysis was conducted and the results are shown in **Figure 5.13**. For the analysis using upregulated DEGs, the common significantly enriched terms for both RPM-2h vs. Veh-2h and RPM-6h vs. Veh-6h included TNF, NOD-like receptor, and NF-kappa B signaling pathways, and osteoclast differentiation. For the analysis using downregulated DEGs, the enriched terms were varied for both timepoints; the interesting shared term was parathyroid hormone synthesis. Interestingly, osteoclast differentiation was the enriched term in both analyses using upregulated and downregulated DEGs in RPM-6h vs. RPM-2h. This suggests that genes involved in this process were both upregulated and downregulated over time after the RANKL

treatment. In summary, these data suggest that processes related to inflammatory response are decreased over time, while genes related to immune system process and osteoclast differentiation are both upregulated and downregulated over time after the RANKL treatment.

5.3.5 *M0 macrophages were able to differentiate into osteoclasts by M-CSF and RANKL treatment*

It has been well established that BMD cells can differentiate into osteoclasts by the induction of M-CSF and RANKL; however, it has remained intriguing if M0 macrophages have this ability. As none of the pre-osteoclast and osteoclast markers were included in DEGs in the RPM RNA-seq data, M0 macrophages treated with RANKL alone are unlikely to differentiate into osteoclasts. Therefore, I investigated if M0 macrophages can differentiate into osteoclasts by the treatment of both M-CSF and RANKL *in vitro* using TRAP staining and RT-qPCR. Surprisingly, both BMD cells and M0 macrophages differentiated into TRAP+ multinucleated osteoclasts after treated by M-CSF and RANKL for 5 days **(Figure 5.14)**. Additionally, cell lysates were collected at several timepoints after the treatment to determine the expression of osteoclastogenesis-related genes. Interestingly, *Tnfrsf11a (Rank)*, early markers (*Nfatc1* and *Traf6*), fusogenic markers (*Ocstamp* and *Dcstamp*), and late markers of osteoclasts (*Acp5* and *Ctsk*) were all comparably upregulated in both treated BMD cells and M0 macrophages compared to the untreated M0 macrophages **(Figure 5.15)**. In contrast to the previous finding, my data show that M0 macrophages have potential to differentiate into osteoclasts by M-CSF and RANKL treatment.

5.3.6 *M1 markers were downregulated over time in M0 macrophages treated by M-CSF and RANKL*

I previously showed that RANKL slightly increased the expression of several M1 markers, however, the effect was decreased over time from 2 to 6 hours. Hereby, I utilized the cell lysates from the osteoclast experiment to identify if those M1 markers were continuously downregulated in the long-term treatment (1 to 5 days) of M-CSF and RANKL. As expect, *Il1b, Tnfa, Traf1,* and *Cxcl9* were downregulated progressively from Day 1 to Day 5 of treatment **(Figure 5.16)**. These data support the findings from the RPM RNA-seq data at 2 and 6 hours.

5.3.7 *Increased M1/M2 ratio was observed in anti-RANKL antibody-treated mice*

Contrary to my hypothesis, the *in vitro* data showed that RANKL upregulates several genes only in a slight level suggesting that RPMs do not express unique markers or gene profile which are distinct from other macrophage phenotypes. However, I observed different stages of MRONJ induced by anti-RANKL antibody in the mouse model mentioned in Chapter 3 **(Table 3.1)**. Interestingly, the groups with RAW264.7 cell delivery either with or without osteoclast induction (Abc and Abcc group) exhibited more advanced stage of MRONJ. In addition to differentiating into osteoclasts, RAW264.7 cells can also be polarized into M1 and M2 macrophages which potentially affects macrophage polarization at the tooth extraction site. As macrophage alteration is also one of the potential mechanisms contributing to MRONJ, I next utilized the MRONJ mouse model to study the effects of the presence and absence of RANKL on macrophage polarization *in vivo*. Immunofluorescence staining was performed to locate M1 (F4/80+iNOS+) and M2 (F4/80+CD206+) macrophages **(Figure 5.17)** at both early and final timepoints (approximately 1 and 3 weeks after tooth extraction respectively). For the early timepoint, quantitative data showed

the increasing trend of overall macrophage numbers in Abc compared to Ct and Ab groups **(Figure 5.18)**. This is as expected since the delivered RAW264.7 cells could proliferate over time in Abc group. Additionally, M1/M2 ratio was significantly increased in Ab and Abc compared to Ct group **(Figure 5.18)**. However, these ratios were equalized over time and had no significant difference among all groups at the final timepoint **(Figure 5.18)**.

5.3.8 *Replenishment of CID-induced osteoclasts did not alter M1/M2 ratio in the MRONJ mouse model*

Lastly, I investigated whether replenishment of osteoclasts has any effect on M1/M2 ratio in the MRONJ mouse model. Using immunofluorescence staining, osteoclasts were identified as F4/80-iNOS+ and/or F4/80-CD206+ cells with three nuclei or more **(Figure 5.19)**. As expected, Abcc group exhibited osteoclasts at the extraction site, while the absence of osteoclasts was observed in Abc group supporting the TRAP staining results shown in the previous chapter. Interestingly, there was no significant difference in M1/M2 ratio between Abc and Abcc groups **(Figure 5.19)**. This suggests that the replenishment of CID-induced osteoclasts did not alter macrophage polarization in the MRONJ mouse model.

5.4 DISCUSSIONS

In this chapter, I first investigated the effects of RANKL on M0 macrophages and characterized the gene expression profile of RPMs using *in vitro* cell culture. In contrast to my hypothesis, both RT-qPCR and RNA-seq data showed that RPMs did not have a unique gene expression profile but exhibited similar gene expressions to M1 macrophages in much lower level. The bioinformatics analysis also showed this similarity in pathways and functions of cells. Interestingly, these M1 gene expressions in RPMs were downregulated over time and RPMs were

able to differentiate into osteoclasts by M-CSF + RANKL treatment. Additionally, I utilized the MRONJ mouse model to study how the presence and absence of RANKL affect macrophage polarization *in vivo*. The increased M1/M2 ratio was observed in Ab and Abc groups in my model which supports previous findings in the BRONJ models.

Unlike the effects of RANKL on osteoclast differentiation, its effects on macrophage polarization have not been thoroughly studied. As M0 macrophages express RANK, RANKL may potentially polarized M0 into another phenotype which is distinct from M1 and M2 macrophages. A previous study has shown that RANKL can slightly upregulate M1 markers, however, only several genes including *Il1b*, *Il6*, *Tnfa*, and *iNOS* were investigated in this study.*(49)* In my study, I utilized RNA-seq not only to study the effects of RANKL on well-established M1 genes, but also to identify potential RPM markers which have not been studied before. My findings support the previous studies that RANKL have similar effects to M1 inducers in upregulating M1 markers rather than polarizing them into a new phenotype. However, my findings additionally exhibit that there are slight upregulatory effects of RANKL on other unpublished genes, pathways, and functions of the cells and these effects are downregulated over time after RANKL treatment, which are novel to the field.

Hematopoietic stem cells (HSCs) can differentiate into various cell lineages such as osteoclast precursors which can differentiate into osteoclasts and macrophages which are a heterogenous population capable of polarizing into different phenotypes.*(91)* However, it has remained intriguing if macrophages have an ability to form osteoclasts when HSCs already committed to the macrophage lineage. Deuell et. al. showed that M0 macrophages did not form osteoclasts after 7 days of M-CSF + RANKL treatment.*(41)* On the contrary, my findings suggest that M0 macrophages can differentiate into osteoclasts after M-CSF + RANKL treatment for 5

days. These M0-derived osteoclasts are TRAP+ multinucleated and express osteoclastogenesis-related genes comparably to BMD-derived osteoclasts. It has been shown that the co-stimulation of M-CSF and RANKL is required for proliferation, survival, and differentiation of osteoclasts.*(94)* Despite the controversial outcomes, I hereby show that M0 macrophages have potential to differentiate into osteoclasts similarly to osteoclast precursors. It has been shown that several factors including BMD cell density and RANKL concentration may affect osteoclast differentiation *in vitro(95)*, therefore, it is possible that these different settings between Deuell et. al.'s study and mine may explain the different findings.

In addition to the effects of RANKL on macrophage polarization *in vitro*, the MRONJ mouse model was utilized to study the effects of RANKL *in vivo*. It has been well established that bisphosphates can induce M1 polarization via several pathways such as TLR-4 and IL-17 resulting in the increased M1/M2 ratio in the BRONJ models.*(20, 22)* In contrast, whether anti-RANKL antibody has similar effects in MRONJ remains inconclusive. Therefore, I investigated the macrophage polarization in Ct, Ab, and Abc groups which represent different MRONJ stages as explained in **Table 3.1**. My findings show that the absence of RANKL leads to the increased M1/M2 ratio either with or without the addition of RAW264.7 cells. These data indeed show the similarity in macrophage alteration between BRONJ and DRONJ models. Interestingly, the difference of these ratios was significant only in the early timepoint (1 week after tooth extraction), while they were neutralized and comparable among all groups in the final timepoint (3 weeks after tooth extraction). Dynamic M1 and M2 polarization has been observed in chronic inflammation and healing after tooth extraction.*(92, 96, 97)* For instance, rheumatoid arthritis, an autoimmune disease characterized by chronic inflammation of synovial joints, exhibits a temporal pattern of M1 and M2 polarization which M1 population is predominant at the later timepoint of the

disease*(96)* similarly to my findings in the MRONJ model. However, whether the temporal pattern of M1 and M2 polarization plays a role in the MRONJ progression has not been studied. Thus, future studies on the macrophage alteration at various timepoints to study temporal expression patterns of specific cytokines and M1 and M2 polarization will be useful to fully understand the disease pathophysiology and progression. Furthermore, my *in vitro* data suggesting the slight effects of RANKL on macrophage polarization may explain why the M1/M2 ratio was not significantly affected by the absence of RANKL in a long term in the MRONJ mouse model.

As I previously showed that osteoclast replenishment restores bone resorptive ability in the MRONJ model, I further investigate if it has any effect on macrophage polarization in this chapter. As a result, M1/M2 ratios are not significantly different between Abc and Abcc groups suggesting that osteoclast replenishment does not alter M1 and M2 macrophage polarization. Delivered RAW264.7 cells have potential to differentiate into osteoclasts, M1, and M2 macrophages. Although CID can induce osteoclast differentiation in these cells, this induction might not be able to overcome the M1 polarization induced by proinflammatory cytokines which are most likely abundant at the extraction site.*(8)* Moreover, these findings indeed support the clinical features of Abc and Abcc groups. Besides the decreased necrotic bone area in Abcc group, impaired new bone formation and epithelial closure are not improved compared to Abc group despite osteoclast replenishment. This suggests that the dominance of M1 macrophages may potentially play an important role in MRONJ pathophysiology in addition to osteoclast inhibition.

Taking that RANKL slightly upregulates several M1 and downregulates several M2 gene expressions *in vitro*, one would expect to observe less M1 and more M2 polarization in the absence of RANKL. Interestingly, increased M1/M2 ratio is observed in the MRONJ mouse model induced by anti-RANKL antibody which is counterintuitive to what the *in vitro* data suggest. As mentioned

above, it could be that the direct effects of RANKL on macrophage polarization are very small which may not mainly contribute to the macrophage alteration observed in the MRONJ mouse model. This suggests that RANKL possibly has more significant effects on other cell types besides macrophages which indirectly contribute to the increased M1/M2 ratio. Cui Z et. al. recently showed that RANKL promotes Th17 cell differentiation of naïve CD4+ T cells while downregulates IFN-γ which is one of the potent M1 inducers. Additionally, the blockage of RANK-RANKL interaction by RANK-Fc inhibits Th17 cell differentiation and increases IFN-γ expression.*(98)* This shows one of the possibilities that the absence of RANKL may enhance M1 polarization by the increased IFN-γ expression. Additionally, accumulation of necrotic bone and incomplete epithelial closure may facilitate bacteria invasion at the extraction site and potentially enhance M1 polarization by LPS and other proinflammatory cytokines. Thus, it is important to investigate the effects of the RANKL on the various cell types in the future as they may indirectly affect macrophage polarization which potentially contributes to the MRONJ pathophysiology.

In conclusion, the effects of the presence and absence of RANKL are summarized in **Figure 5.20**. M0 macrophages have potential to differentiate into osteoclasts, RPMs, M1, and M2 macrophages by different inducers during healing processes. In normal wound healing, the *in vitro* data suggest that M0 macrophages can be polarized into RPMs which express a low level of M1 markers by RANKL and can be differentiated into osteoclasts by M-CSF + RANKL with downregulated M1-related genes and upregulated osteoclast-related genes over time. However, whether RPMs can differentiate into osteoclasts has to be further investigated. On the other hand, the *in vivo* data suggest that anti-RANKL antibody treatment inhibits RPM polarization and osteoclast differentiation and leads to the predominance of M1 macrophages as the increased M1/M2 ratio is observed. Nevertheless, the mechanisms on how the absence of RANKL increases

M1/M2 ratio need to be further investigated. Additionally, more robust MRONJ model with later stages of disease is required in future studies and transcriptomic tools such as single cell RNA-seq and spatial transcriptomics can be tremendously helpful to study numerous cells of interest and identify undiscovered novel cell types which potentially contributes to MRONJ pathophysiology and progression.

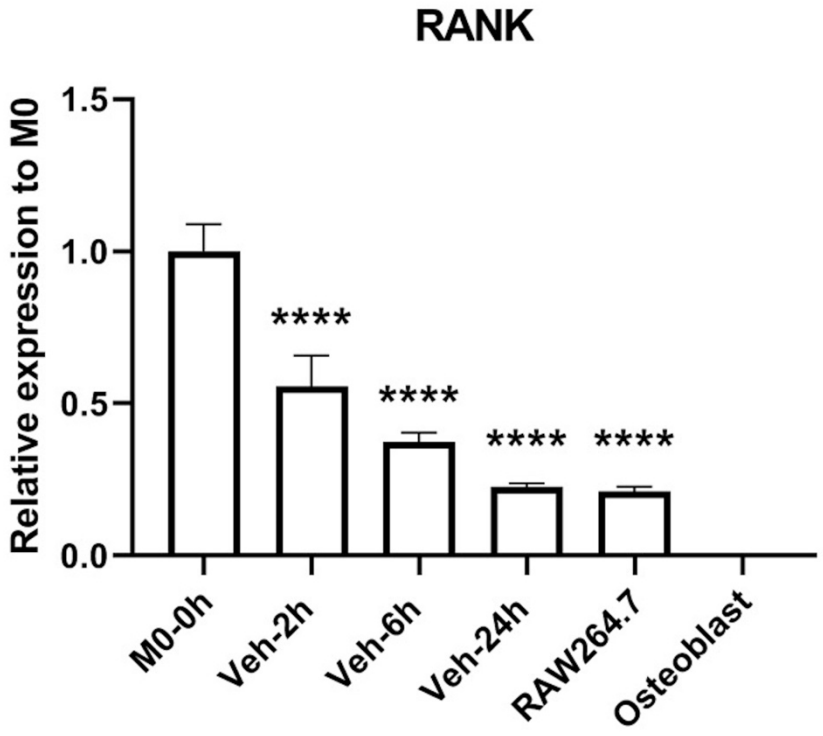

Figure 5.1. *Rank* expression was observed in M0 macrophages, however, was downregulated in the absence of M-CSF over time.

Rank expression is shown as a fold change to M0 macrophages (M0-0h). The expression was significantly downregulated from 2 to 24 hours in vehicle control groups (Veh) in the absence of M-CSF. (****$p<0.0001$ compared to M0, RAW264.7 cells as a positive control, and osteoblasts as a negative control for *Rank*)

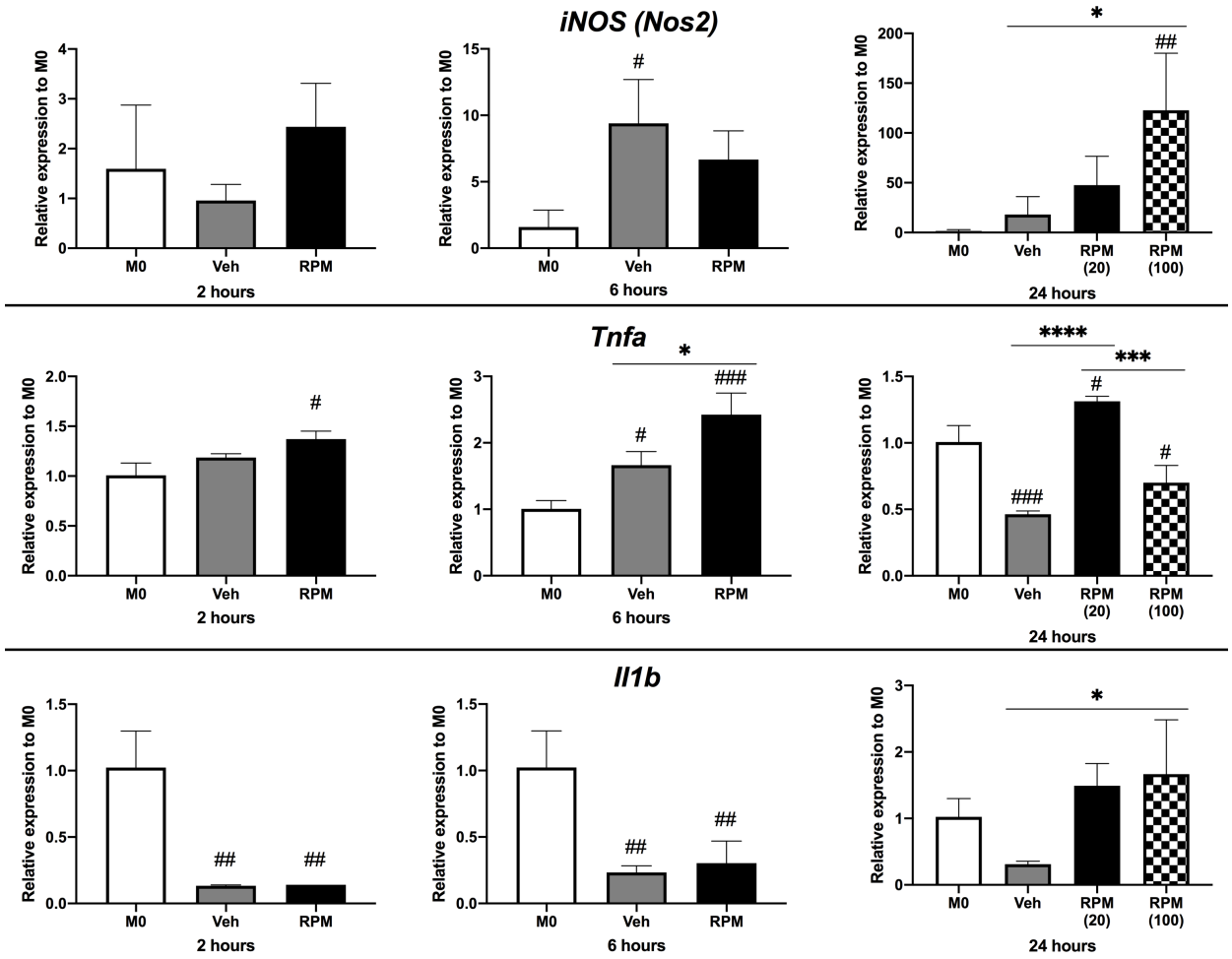

Figure 5.2. RANKL treatment significantly upregulated classical M1 markers.

iNOS, Tnfa, and Il1b expressions at 2, 6, and 24 hours after RANKL treatment are shown as a fold change to M0 macrophages (M0). These expressions were significantly upregulated in RPM for *iNOS* at 24 hours, and *Tnfa* at 6 and 24 hours compared to vehicle control group (Veh). Additionally, there was no significant difference between normal (20 ng/mL) and high dose (100 ng/mL) RANKL treatments on these genes at 24 hours. (#$p<0.05$, ##$p<0.01$, and ###$p<0.001$ compared to M0; *$p<0.05$, ***$p<0.001$, and ****$p<0.0001$ compared between indicated groups)

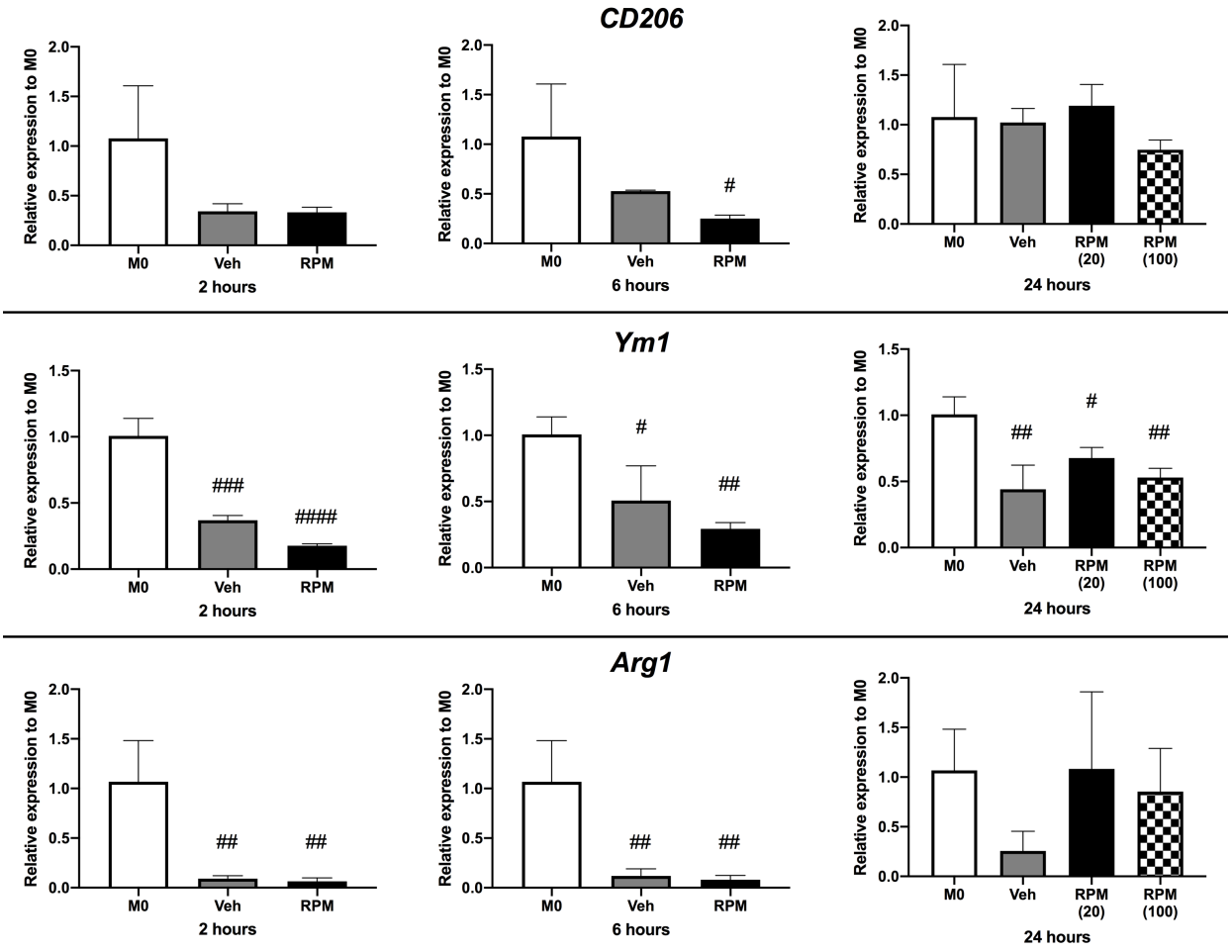

Figure 5.3. RANKL treatment had no significant effects on classical M2 markers.

CD206, Ym1, and Arg1 expressions at 2, 6, and 24 hours after RANKL treatment are shown as a fold change to M0 macrophages (M0). These expressions were significantly downregulated in both RPM and vehicle control group (Veh) compared to M0 at various timepoints. However, these effects were not significantly different between RPM and Veh. Additionally, there was no significant difference between normal (20 ng/mL) and high dose (100 ng/mL) RANKL treatments on these genes at 24 hours. (#$p<0.05$, ##$p<0.01$, ###$p<0.001$, and ####$p<0.0001$ compared to M0)

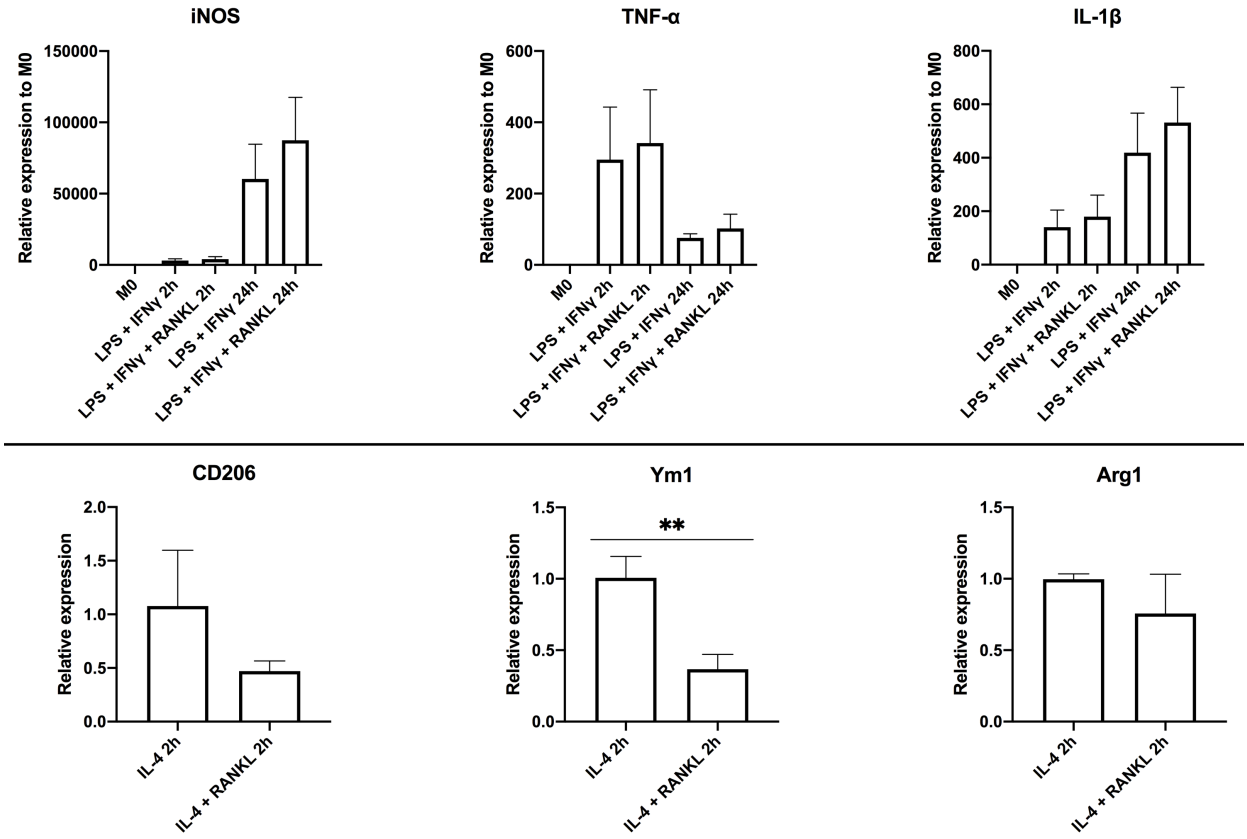

Figure 5.4. RANKL treatment had no significant effects on the polarizing ability of classical M1 and M2 inducers.

M1 gene expressions (*iNOS, Tnfa, and Il1b*) at 2 and 24 hours, and M2 gene expressions (*CD206, Ym1, and Arg1*) at 2 hours after RANKL treatment in addition to classical M1 and M2 inducers are shown as a fold change to M0 and M2 macrophages (IL-4 2h) respectively. Addition of RANKL treatment to M1 and M2 inducers had no significant effects on these genes except *Ym1*. (**p<0.01)

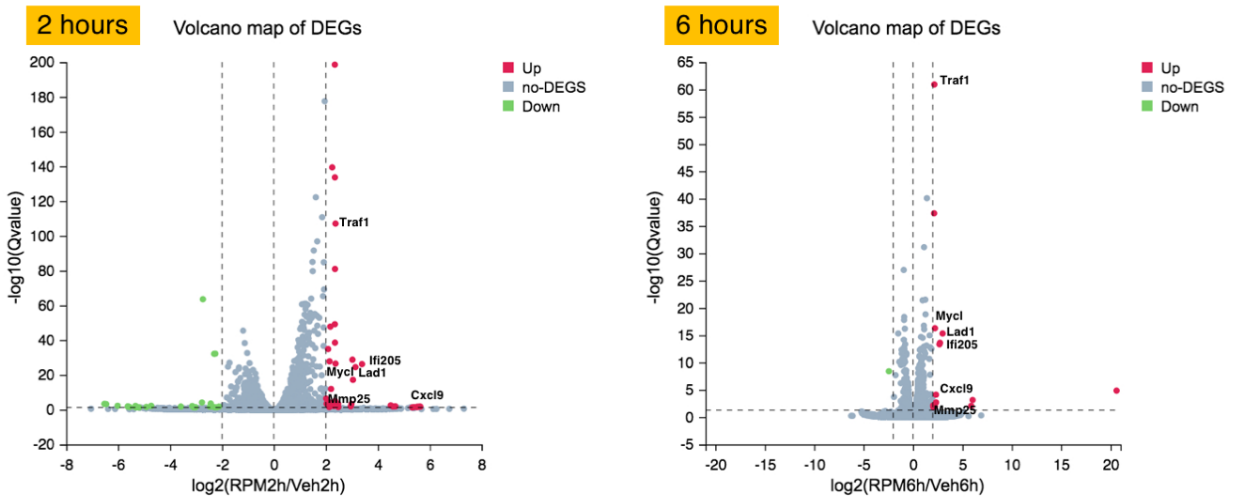

Figure 5.5. Volcano plots of differentially expressed genes (DEGs) of RPM

Several genes including *Ifi205, Cxcl9, Mycl, Mmp25, Lad1,* and *Traf1* were selected as potential RPM markers from DEGs of RPM compared to vehicle control groups at 2 and 6 hours. The x-axis represents the fold change of the difference after conversion to log2, and the y-axis represents the significance value after conversion to log10. Red represents DEGs upregulated, blue represents DEGs downregulated, and gray represents non-DEGs.

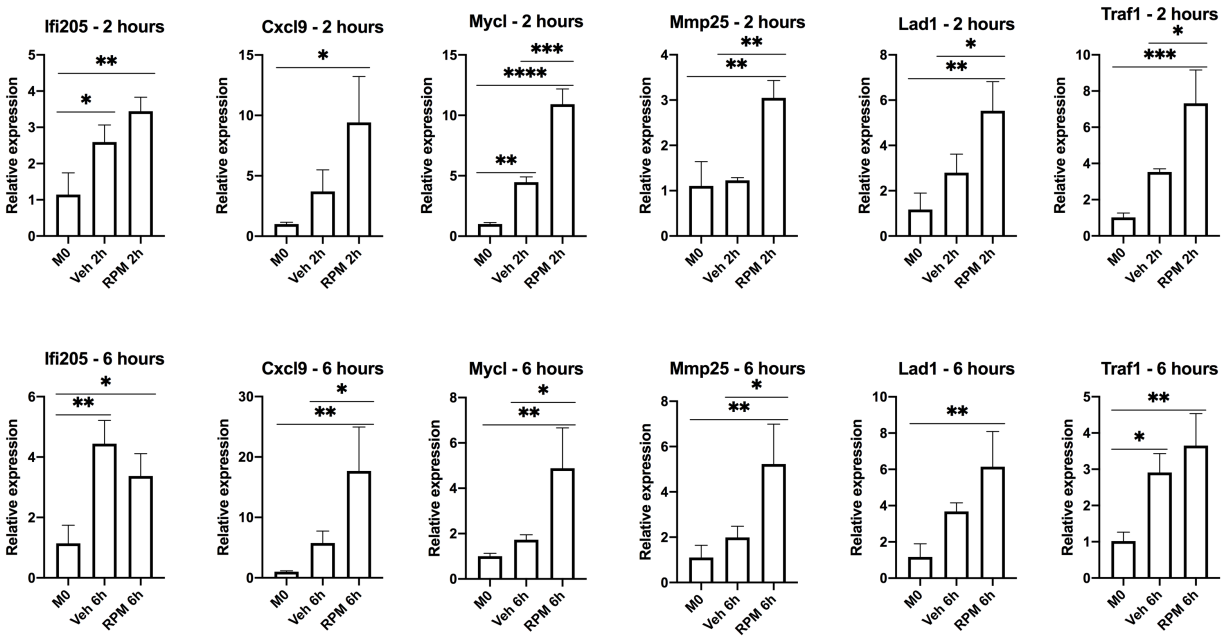

Figure 5.6. RT-qPCR data validated the upregulation of potential RPM markers in RPMs. The upregulation of *Ifi205, Cxcl9, Mycl, Mmp25, Lad1,* and *Traf1* which were selected as potential RPM markers from RNA-seq data at 2 and 6 hours were validated in RPMs using RT-qPCR. (*p<0.05, ** p<0.01, ***p<0.001, and ****p<0.0001)

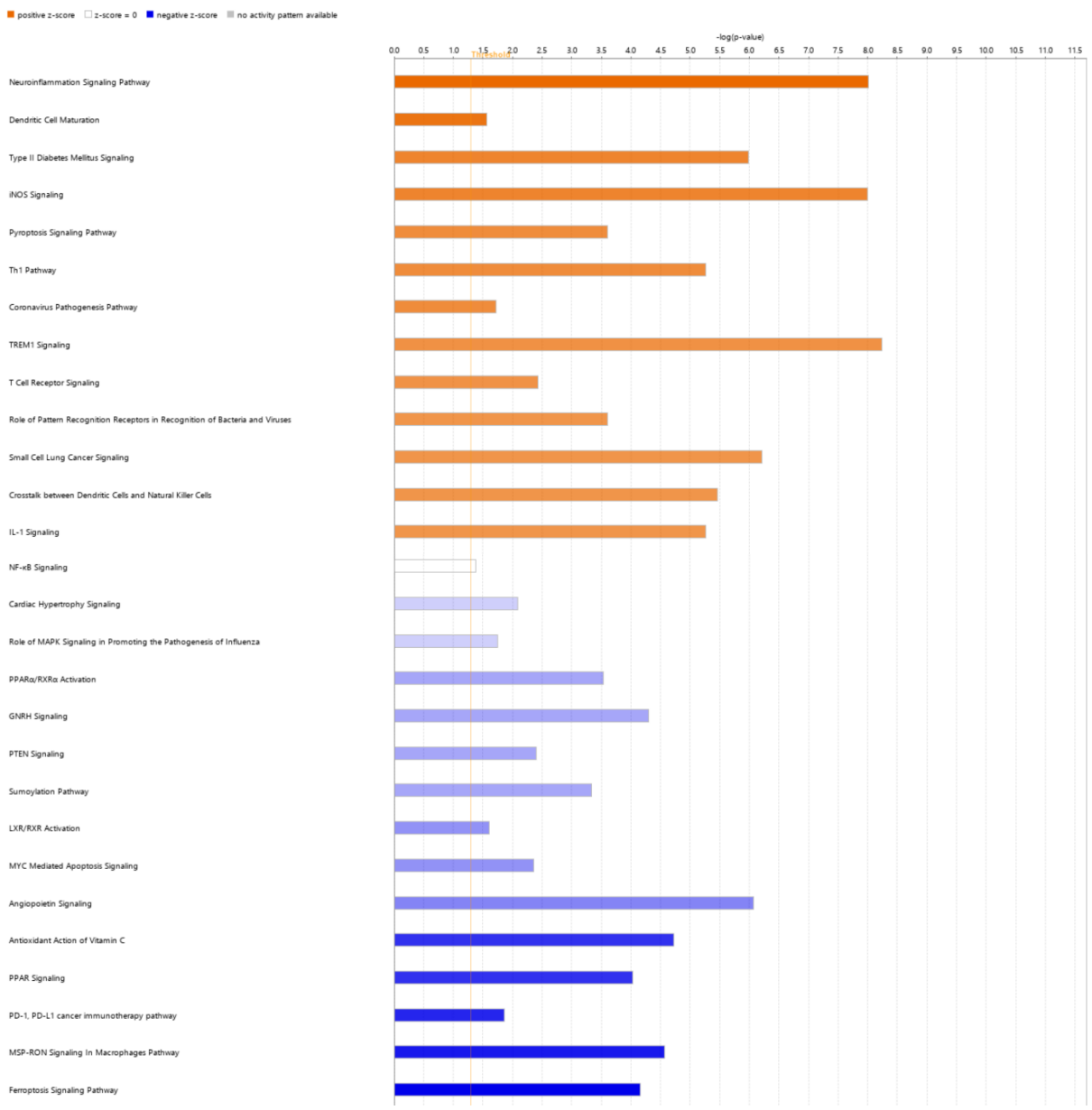

Figure 5.7. Canonical pathway analysis of RPM-2h vs. Veh-2h

Canonical pathways were analyzed in RPM-2h vs. Veh-2h using Qiagen IPA. The x-axis represents the pathways, and the y-axis represents the -log of the p-value which is calculated by the right-tailed Fisher's Exact Test. Orange represents positive z-score indicating predicted pathway activation, blue represents negative z-score indicating predicted pathway inhibition, white represents z-score = 0, and gray represents no prediction.

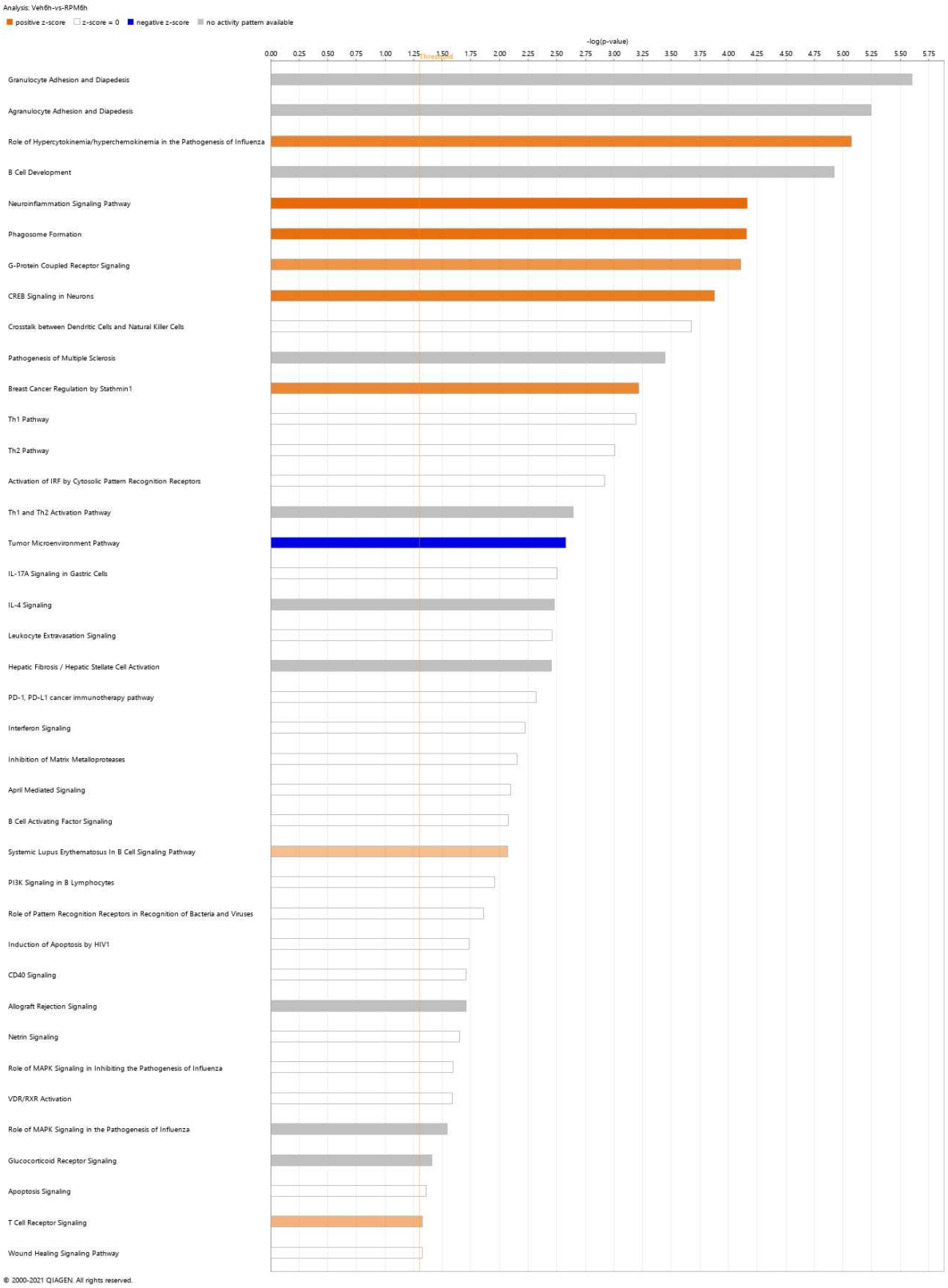

Figure 5.8. Canonical pathway analysis of RPM-6h vs. Veh-6h

Canonical pathways were analyzed in RPM-6h vs. Veh-6h using Qiagen IPA. The x-axis represents the pathways, and the y-axis represents the -log of the p-value which is calculated by the right-tailed Fisher's Exact Test. Orange represents positive z-score indicating predicted pathway activation, blue represents negative z-score indicating predicted pathway inhibition, white represents z-score = 0, and gray represents no prediction.

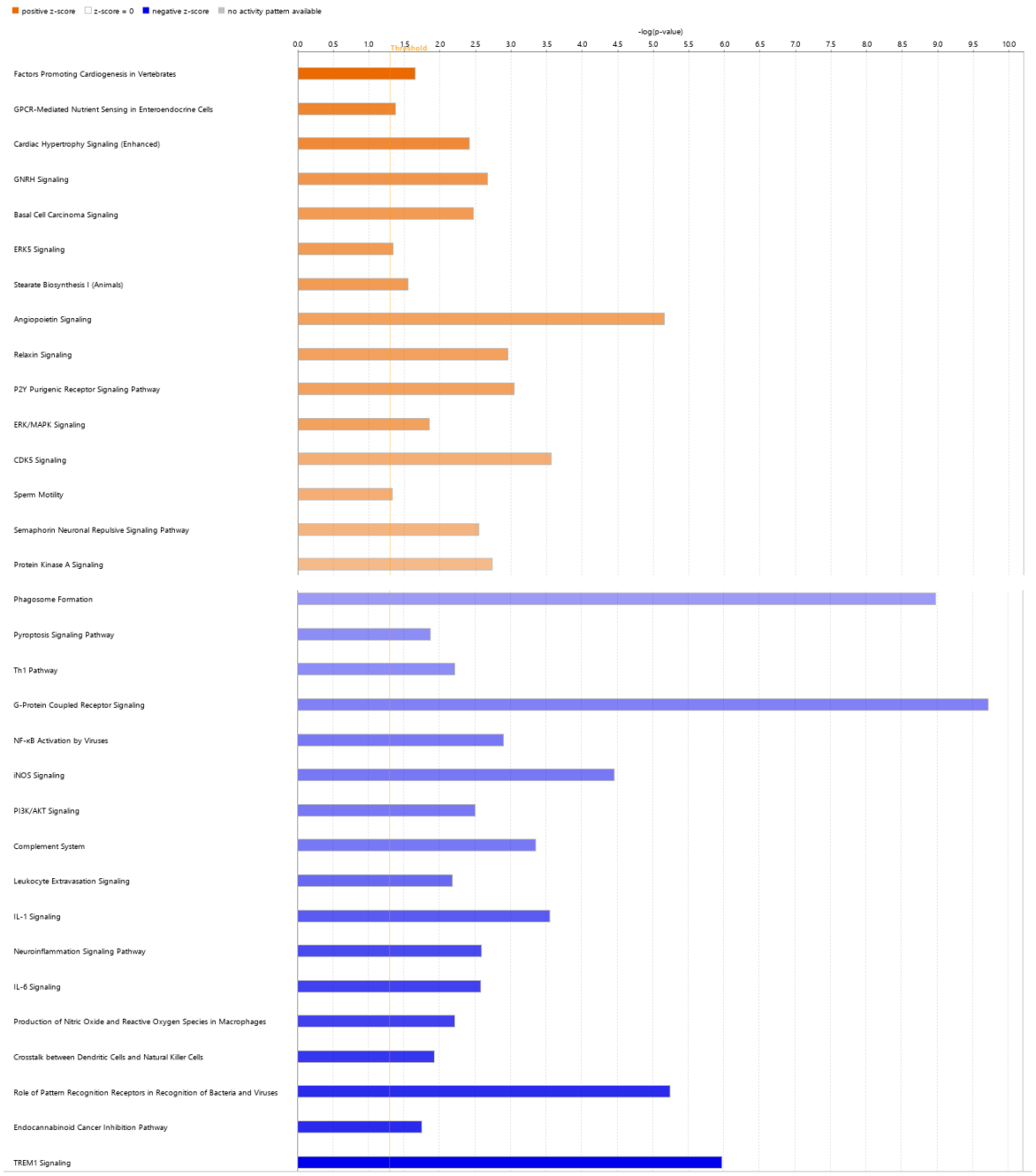

Figure 5.9. Canonical pathway analysis of RPM-6h vs. RPM-2h

Canonical pathways were analyzed in RPM-6h vs. RPM-2h using Qiagen IPA. The x-axis represents the pathways, and the y-axis represents the -log of the p-value which is calculated by the right-tailed Fisher's Exact Test. Orange represents positive z-score indicating predicted pathway activation, blue represents negative z-score indicating predicted pathway inhibition, white represents z-score = 0, and gray represents no prediction.

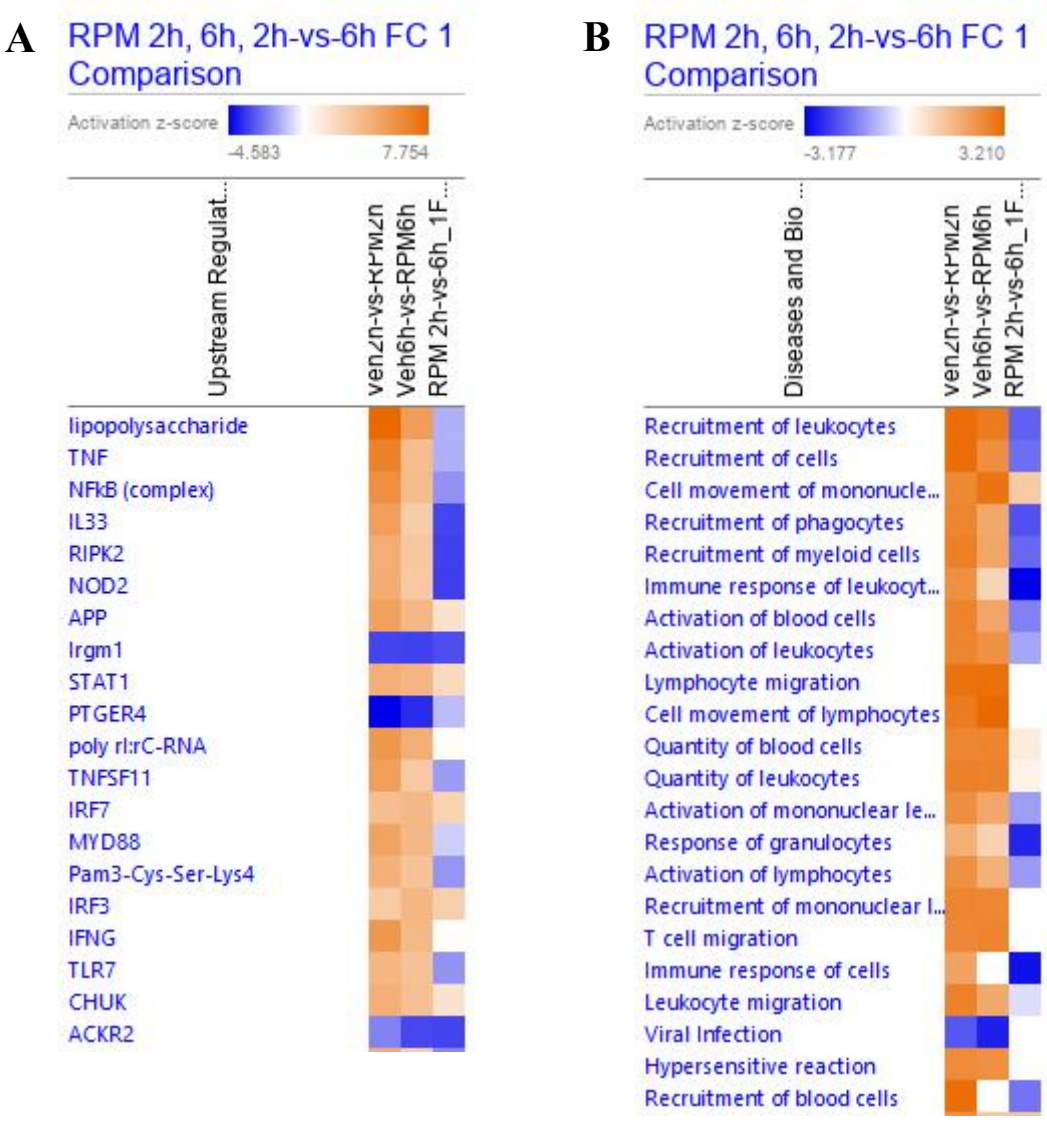

Figure 5.10. The predicted upstream regulators and activated diseases and functions were downregulated over time in RPM.

(A) Upstream regulators and **(B)** diseases and functions were analyzed in RPM-2h vs. Veh-2h, RPM-6h vs. Veh-6h, and RPM-6h vs. RPM-2h and displayed as heatmaps using Qiagen IPA. Most of them were downregulated in RPM-6h vs. RPM-2h. Orange represents positive z-score indicating predicted activation, blue represents negative z-score indicating predicted inhibition, and white represents z-score = 0.

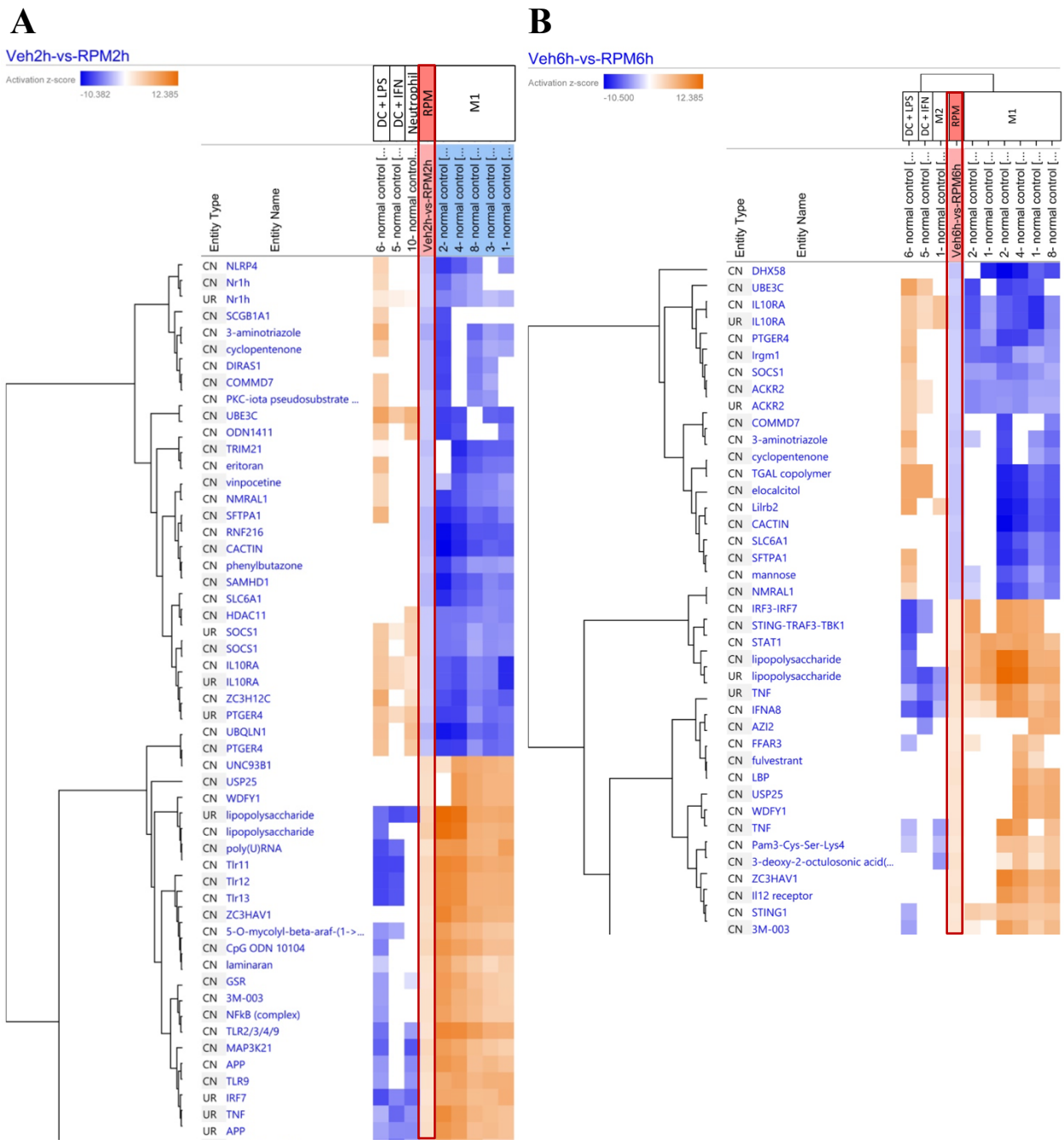

Figure 5.11. IPA analysis match showed similarity between RPMs and M1 macrophages. IPA analysis match was performed to compare the RPM RNA-seq dataset at **(A)** 2 hours and **(B)** 6 hours to the other murine cells datasets on the IPA Qiagen database. Upstream regulators (UR) and casual networks (CN) were used for the comparisons and displayed as heatmaps. The analysis showed similarity between RPMs and M1 macrophages in both timepoints, however, the expressions in RPMs were much lower. Additionally, these expressions were different from other

cell types including M2 macrophages, neutrophils, and dendritic cells (DC). Orange represents positive z-score indicating predicted activation, blue represents negative z-score indicating predicted inhibition, and white represents z-score = 0.

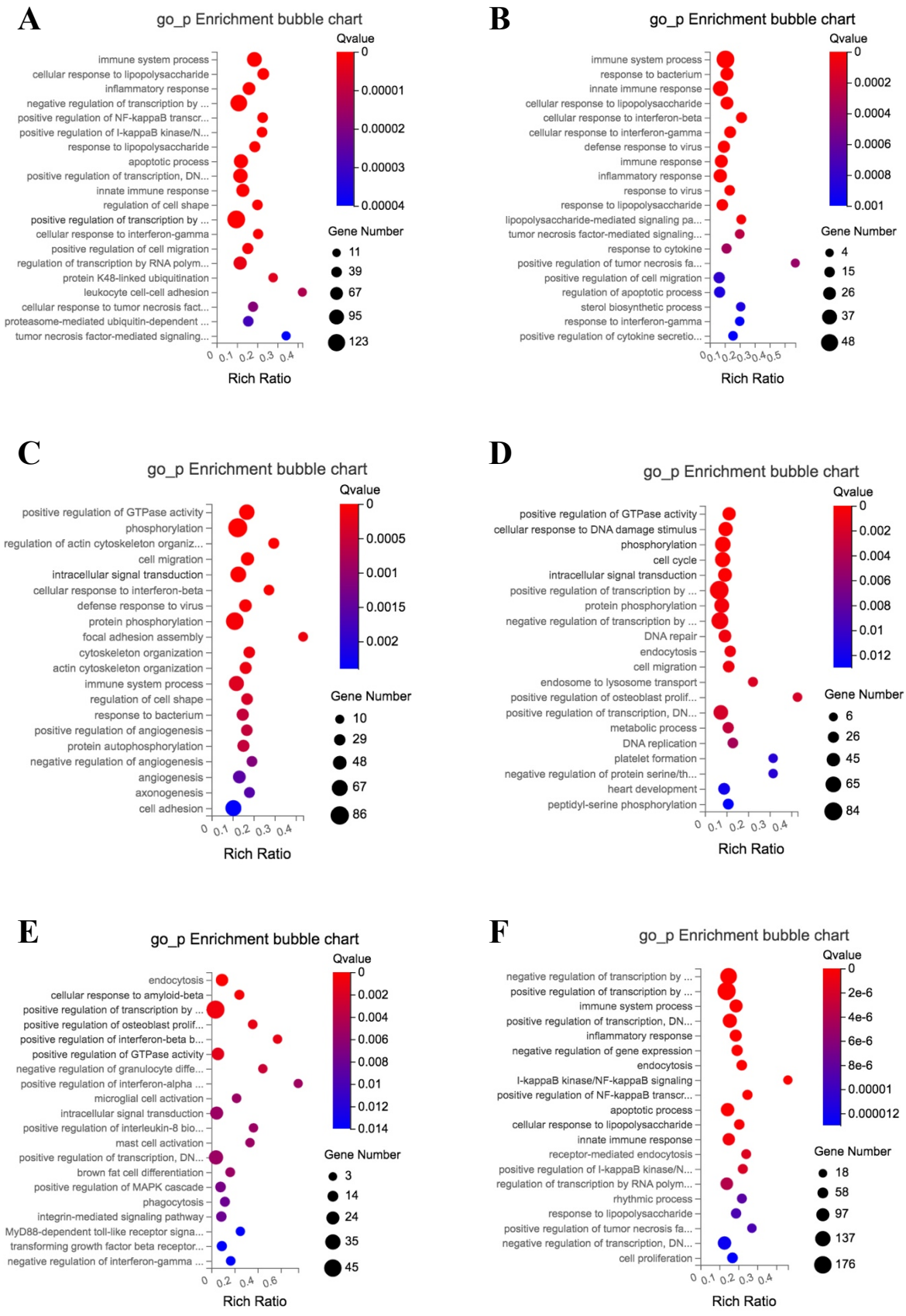
A
go_p Enrichment bubble chart
immune system process
cellular response to lipopolysaccharide
inflammatory response
negative regulation of transcription by ...
positive regulation of NF-kappaB transcr...
positive regulation of I-kappaB kinase/N...
response to lipopolysaccharide
apoptotic process
positive regulation of transcription, DN...
innate immune response
regulation of cell shape
positive regulation of transcription by ...
cellular response to interferon-gamma
positive regulation of cell migration
regulation of transcription by RNA polym...
protein K48-linked ubiquitination
leukocyte cell-cell adhesion
cellular response to tumor necrosis fact...
proteasome-mediated ubiquitin-dependent ...
tumor necrosis factor-mediated signaling...
0 0.1 0.2 0.3 0.4
Rich Ratio
Qvalue
0
0.00001
0.00002
0.00003
0.00004
Gene Number
11
39
67
95
123
B
go_p Enrichment bubble chart
immune system process
response to bacterium
innate immune response
cellular response to lipopolysaccharide
cellular response to interferon-beta
cellular response to interferon-gamma
defense response to virus
immune response
inflammatory response
response to virus
response to lipopolysaccharide
lipopolysaccharide-mediated signaling pa...
tumor necrosis factor-mediated signaling...
response to cytokine
positive regulation of tumor necrosis fa...
positive regulation of cell migration
regulation of apoptotic process
sterol biosynthetic process
response to interferon-gamma
positive regulation of cytokine secretio...
0 0.1 0.2 0.3 0.4 0.5
Rich Ratio
Qvalue
0
0.0002
0.0004
0.0006
0.0008
0.001
Gene Number
4
15
26
37
48
C
go_p Enrichment bubble chart
positive regulation of GTPase activity
phosphorylation
regulation of actin cytoskeleton organiz...
cell migration
intracellular signal transduction
cellular response to interferon-beta
defense response to virus
protein phosphorylation
focal adhesion assembly
cytoskeleton organization
actin cytoskeleton organization
immune system process
regulation of cell shape
response to bacterium
positive regulation of angiogenesis
protein autophosphorylation
negative regulation of angiogenesis
angiogenesis
axonogenesis
cell adhesion
0 0.1 0.2 0.3 0.4
Rich Ratio
Qvalue
0
0.0005
0.001
0.0015
0.002
Gene Number
10
29
48
67
86
D
go_p Enrichment bubble chart
positive regulation of GTPase activity
cellular response to DNA damage stimulus
phosphorylation
cell cycle
intracellular signal transduction
positive regulation of transcription by ...
protein phosphorylation
negative regulation of transcription by ...
DNA repair
endocytosis
cell migration
endosome to lysosome transport
positive regulation of osteoblast prolif...
positive regulation of transcription, DN...
metabolic process
DNA replication
platelet formation
negative regulation of protein serine/th...
heart development
peptidyl-serine phosphorylation
0 0.1 0.2 0.3 0.4
Rich Ratio
Qvalue
0
0.002
0.004
0.006
0.008
0.01
0.012
Gene Number
6
26
45
65
84
E
go_p Enrichment bubble chart
endocytosis
cellular response to amyloid-beta
positive regulation of transcription by ...
positive regulation of osteoblast prolif...
positive regulation of interferon-beta b...
positive regulation of GTPase activity
negative regulation of granulocyte diffe...
positive regulation of interferon-alpha ...
microglial cell activation
intracellular signal transduction
positive regulation of interleukin-8 bio...
mast cell activation
positive regulation of transcription, DN...
brown fat cell differentiation
positive regulation of MAPK cascade
phagocytosis
integrin-mediated signaling pathway
MyD88-dependent toll-like receptor signa...
transforming growth factor beta receptor...
negative regulation of interferon-gamma ...
0 0.2 0.4 0.6
Rich Ratio
Qvalue
0
0.002
0.004
0.006
0.008
0.01
0.012
0.014
Gene Number
3
14
24
35
45
F
go_p Enrichment bubble chart
negative regulation of transcription by ...
positive regulation of transcription by ...
immune system process
positive regulation of transcription, DN...
inflammatory response
negative regulation of gene expression
endocytosis
I-kappaB kinase/NF-kappaB signaling
positive regulation of NF-kappaB transcr...
apoptotic process
cellular response to lipopolysaccharide
innate immune response
receptor-mediated endocytosis
positive regulation of I-kappaB kinase/N...
regulation of transcription by RNA polym...
rhythmic process
response to lipopolysaccharide
positive regulation of tumor necrosis fa...
negative regulation of transcription, DN...
cell proliferation
0 0.1 0.2 0.3 0.4
Rich Ratio
Qvalue
0
2e-6
4e-6
6e-6
8e-6
0.00001
0.000012
Gene Number
18
58
97
137
176

Figure 5.12. GO enrichment analysis of the RPM RNA-seq dataset

GO enrichment analysis in biological process category using upregulated DEGs of **(A)** RPM 2h vs. Veh 2h, **(B)** RPM 6h vs. Veh 6h, **(C)** RPM 6h vs. RPM 2h and downregulated DEGs of **(D)** RPM 2h vs. Veh 2h, **(E)** RPM 6h vs. Veh 6h, **(F)** RPM 6h vs. RPM 2h is shown as bubble charts. X-axis represents the enrichment ratio (the ratio of the number of genes annotated to an entry in the selected gene set to the total number of genes annotated to the entry in the species, calculated as Rich Ratio = Term Candidate Gene Number/Term Gene Number). Y-axis represents GO terms. The size of the bubble represents the number of DEGs annotated to the GO term. The color of the bubble represents the enriched statistical significance; red shows lower q-value, while blue shows higher q-value.

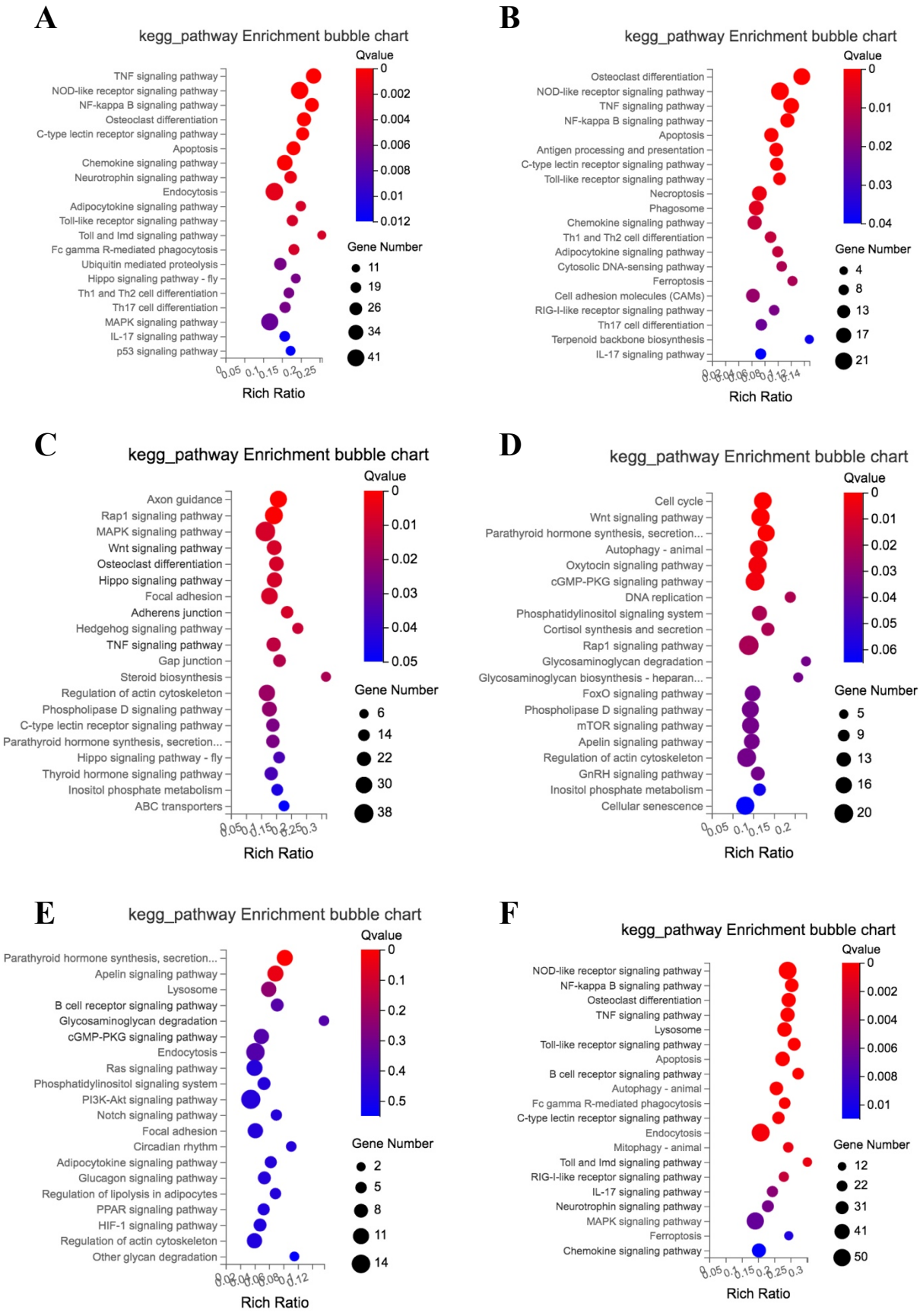
A
kegg_pathway Enrichment bubble chart
Qvalue
0
0.002
0.004
0.006
0.008
0.01
0.012
Gene Number
11
19
26
34
41
TNF signaling pathway
NOD-like receptor signaling pathway
NF-kappa B signaling pathway
Osteoclast differentiation
C-type lectin receptor signaling pathway
Apoptosis
Chemokine signaling pathway
Neurotrophin signaling pathway
Endocytosis
Adipocytokine signaling pathway
Toll-like receptor signaling pathway
Toll and Imd signaling pathway
Fc gamma R-mediated phagocytosis
Ubiquitin mediated proteolysis
Hippo signaling pathway - fly
Th1 and Th2 cell differentiation
Th17 cell differentiation
MAPK signaling pathway
IL-17 signaling pathway
p53 signaling pathway
0.05 0.1 0.15 0.2 0.25
Rich Ratio
B
kegg_pathway Enrichment bubble chart
Qvalue
0
0.01
0.02
0.03
0.04
Gene Number
4
8
13
17
21
Osteoclast differentiation
NOD-like receptor signaling pathway
TNF signaling pathway
NF-kappa B signaling pathway
Apoptosis
Antigen processing and presentation
C-type lectin receptor signaling pathway
Toll-like receptor signaling pathway
Necroptosis
Phagosome
Chemokine signaling pathway
Th1 and Th2 cell differentiation
Adipocytokine signaling pathway
Cytosolic DNA-sensing pathway
Ferroptosis
Cell adhesion molecules (CAMs)
RIG-I-like receptor signaling pathway
Th17 cell differentiation
Terpenoid backbone biosynthesis
IL-17 signaling pathway
0.08 0.1 0.12 0.14
Rich Ratio
C
kegg_pathway Enrichment bubble chart
Qvalue
0
0.01
0.02
0.03
0.04
0.05
Gene Number
6
14
22
30
38
Axon guidance
Rap1 signaling pathway
MAPK signaling pathway
Wnt signaling pathway
Osteoclast differentiation
Hippo signaling pathway
Focal adhesion
Adherens junction
Hedgehog signaling pathway
TNF signaling pathway
Gap junction
Steroid biosynthesis
Regulation of actin cytoskeleton
Phospholipase D signaling pathway
C-type lectin receptor signaling pathway
Parathyroid hormone synthesis, secretion...
Hippo signaling pathway - fly
Thyroid hormone signaling pathway
Inositol phosphate metabolism
ABC transporters
0.05 0.1 0.15 0.2 0.25 0.3
Rich Ratio
D
kegg_pathway Enrichment bubble chart
Qvalue
0
0.01
0.02
0.03
0.04
0.05
0.06
Gene Number
5
9
13
16
20
Cell cycle
Wnt signaling pathway
Parathyroid hormone synthesis, secretion...
Autophagy - animal
Oxytocin signaling pathway
cGMP-PKG signaling pathway
DNA replication
Phosphatidylinositol signaling system
Cortisol synthesis and secretion
Rap1 signaling pathway
Glycosaminoglycan degradation
Glycosaminoglycan biosynthesis - heparan...
FoxO signaling pathway
Phospholipase D signaling pathway
mTOR signaling pathway
Apelin signaling pathway
Regulation of actin cytoskeleton
GnRH signaling pathway
Inositol phosphate metabolism
Cellular senescence
0.05 0.1 0.15 0.2
Rich Ratio
E
kegg_pathway Enrichment bubble chart
Qvalue
0
0.1
0.2
0.3
0.4
0.5
Gene Number
2
5
8
11
14
Parathyroid hormone synthesis, secretion...
Apelin signaling pathway
Lysosome
B cell receptor signaling pathway
Glycosaminoglycan degradation
cGMP-PKG signaling pathway
Endocytosis
Ras signaling pathway
Phosphatidylinositol signaling system
PI3K-Akt signaling pathway
Notch signaling pathway
Focal adhesion
Circadian rhythm
Adipocytokine signaling pathway
Glucagon signaling pathway
Regulation of lipolysis in adipocytes
PPAR signaling pathway
HIF-1 signaling pathway
Regulation of actin cytoskeleton
Other glycan degradation
0.08 0.1 0.12
Rich Ratio
F
kegg_pathway Enrichment bubble chart
Qvalue
0
0.002
0.004
0.006
0.008
0.01
Gene Number
12
22
31
41
50
NOD-like receptor signaling pathway
NF-kappa B signaling pathway
Osteoclast differentiation
TNF signaling pathway
Lysosome
Toll-like receptor signaling pathway
Apoptosis
B cell receptor signaling pathway
Autophagy - animal
Fc gamma R-mediated phagocytosis
C-type lectin receptor signaling pathway
Endocytosis
Mitophagy - animal
Toll and Imd signaling pathway
RIG-I-like receptor signaling pathway
IL-17 signaling pathway
Neurotrophin signaling pathway
MAPK signaling pathway
Ferroptosis
Chemokine signaling pathway
0.05 0.1 0.15 0.2 0.25 0.3
Rich Ratio

Figure 5.13. KEGG pathway analysis of the RPM RNA-seq dataset

KEGG pathway analysis using upregulated DEGs of **(A)** RPM 2h vs. Veh 2h, **(B)** RPM 6h vs. Veh 6h, **(C)** RPM 6h vs. RPM 2h and downregulated DEGs of **(D)** RPM 2h vs. Veh 2h, **(E)** RPM 6h vs. Veh 6h, **(F)** RPM 6h vs. RPM 2h is shown as bubble charts. X-axis represents the enrichment ratio (the ratio of the number of genes annotated to an entry in the selected gene set to the total number of genes annotated to the entry in the species, calculated as Rich Ratio = Term Candidate Gene Number/Term Gene Number). Y-axis represents KEGG pathways. The size of the bubble represents the number of DEGs annotated to the pathway. The color of the bubble represents the enriched statistical significance; red shows lower q-value, while blue shows higher q-value.

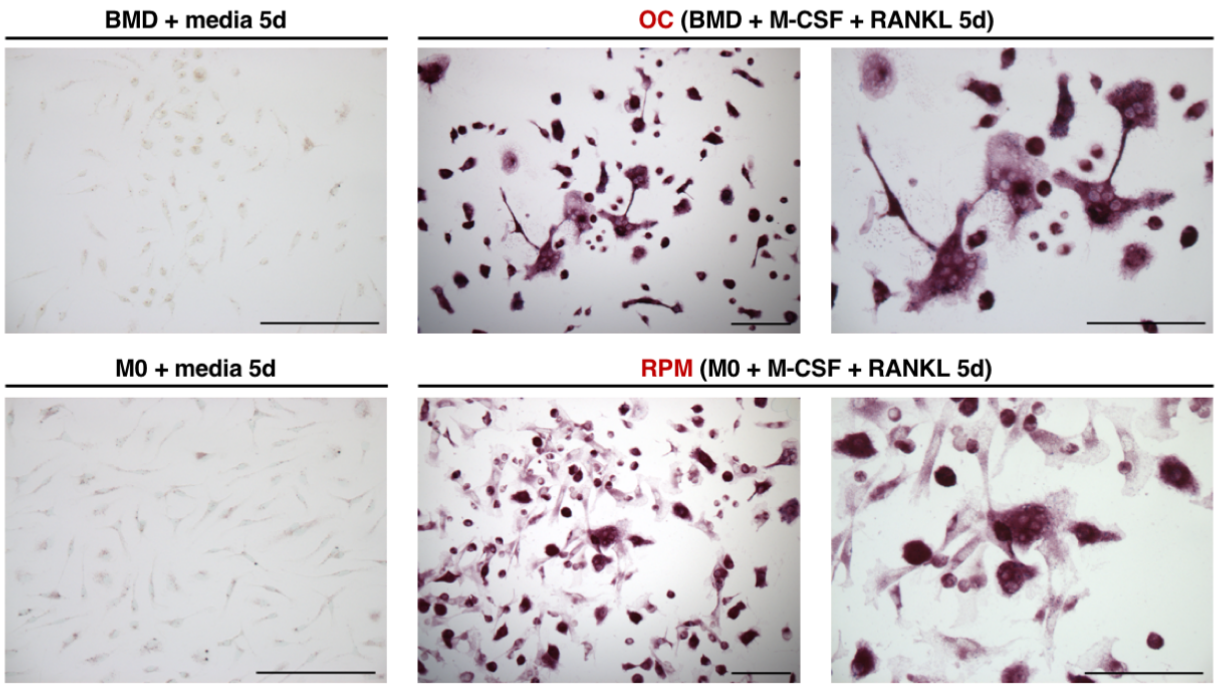

Figure 5.14. Both BMD cells and M0 macrophages were able to differentiate into osteoclasts. BMD cells and M0 macrophages were treated with M-CSF and RANKL for 5 days following by TRAP staining. Both BMD cells and M0 macrophages were able to differentiate into TRAP+ multinucleated osteoclasts (OCs), while negative controls of both cells exhibited TRAP- mononucleated cells. (Scale bar = 100 μm)

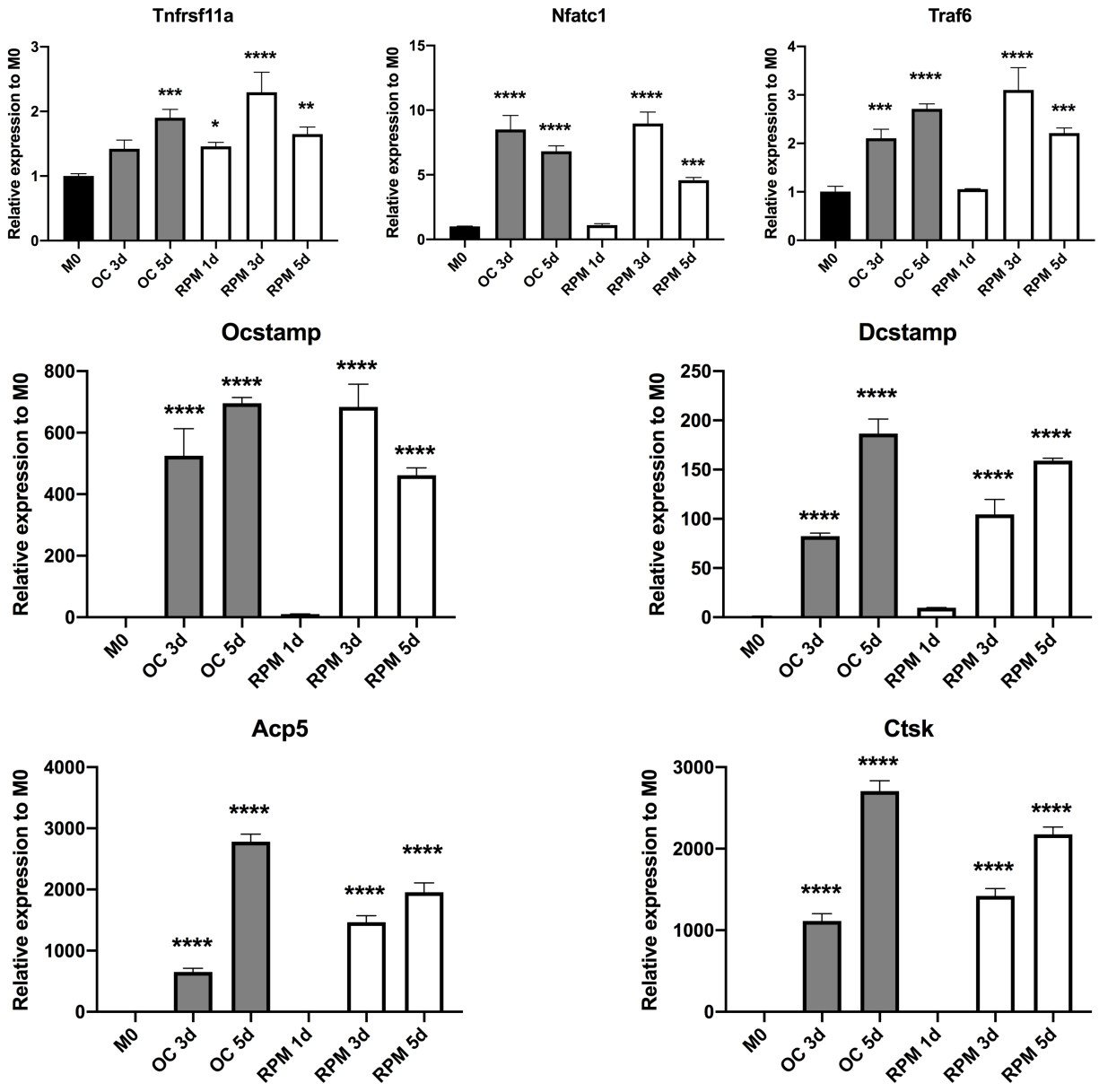

Figure 5.15. Osteoclastogenesis-related genes were upregulated in both osteoclasts and RPMs.

The expressions of *Tnfrsf11a*, *Nfatc1, Traf6*, *Ocstamp*, *Dcstamp*, *Acp5,* and *Ctsk* which are shown as fold changes to M0 macrophages were comparably upregulated in both osteoclasts (OC; BMD cells + M-CSF + RANKL) and RPMs (M0 + M-CSF + RANKL) after 3 and 5 days of treatments. (*p<0.05, ** p<0.01, ***p<0.001, and ****p<0.0001 compared to M0)

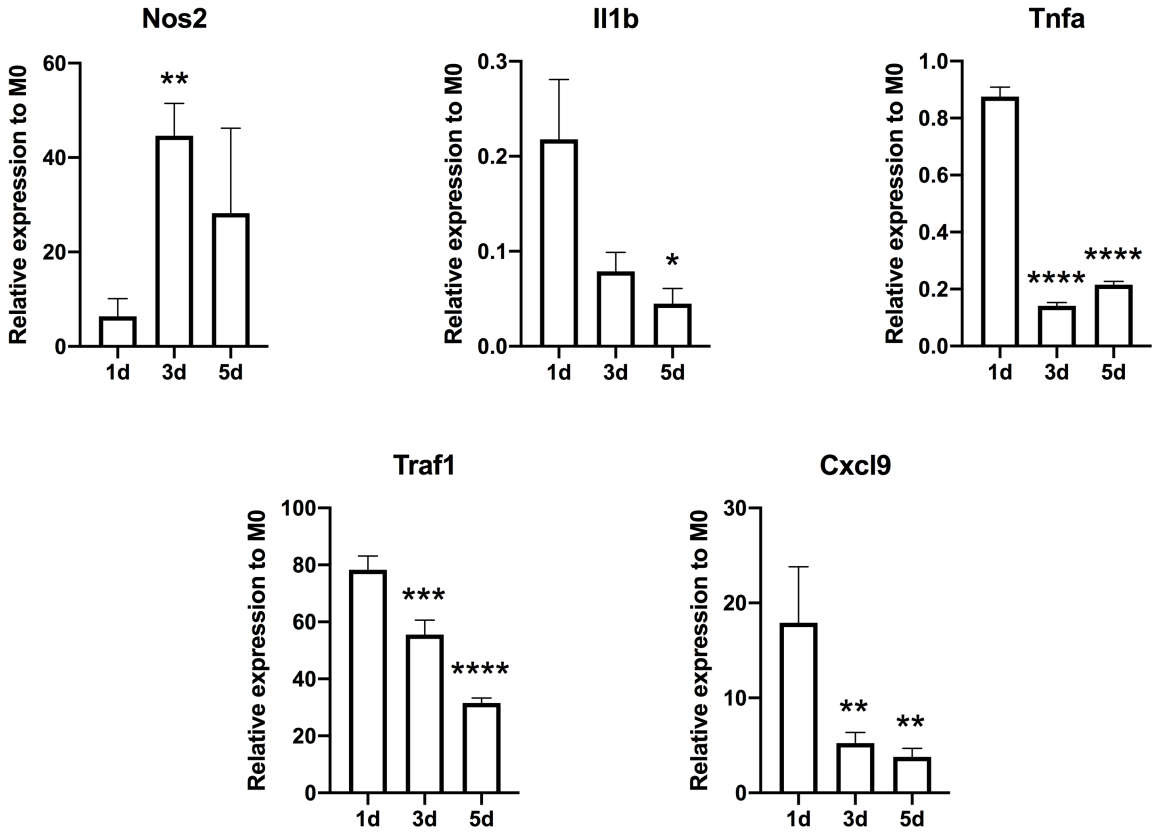

Figure 5.16. M1 markers were downregulated over time in RPMs.

Several M1 markers including *Nos2, Il1b, Tnfa, Traf1,* and *Cxcl9* were investigated in RPMs after 1, 3, and 5 days (1d – 5d) of M-CSF + RANKL treatments and shown as fold changes to M0 macrophage. All genes except *Nos2* were significantly downregulated over time. (*$p<0.05$, ** $p<0.01$, ***$p<0.001$, and ****$p<0.0001$ compared to 1d)

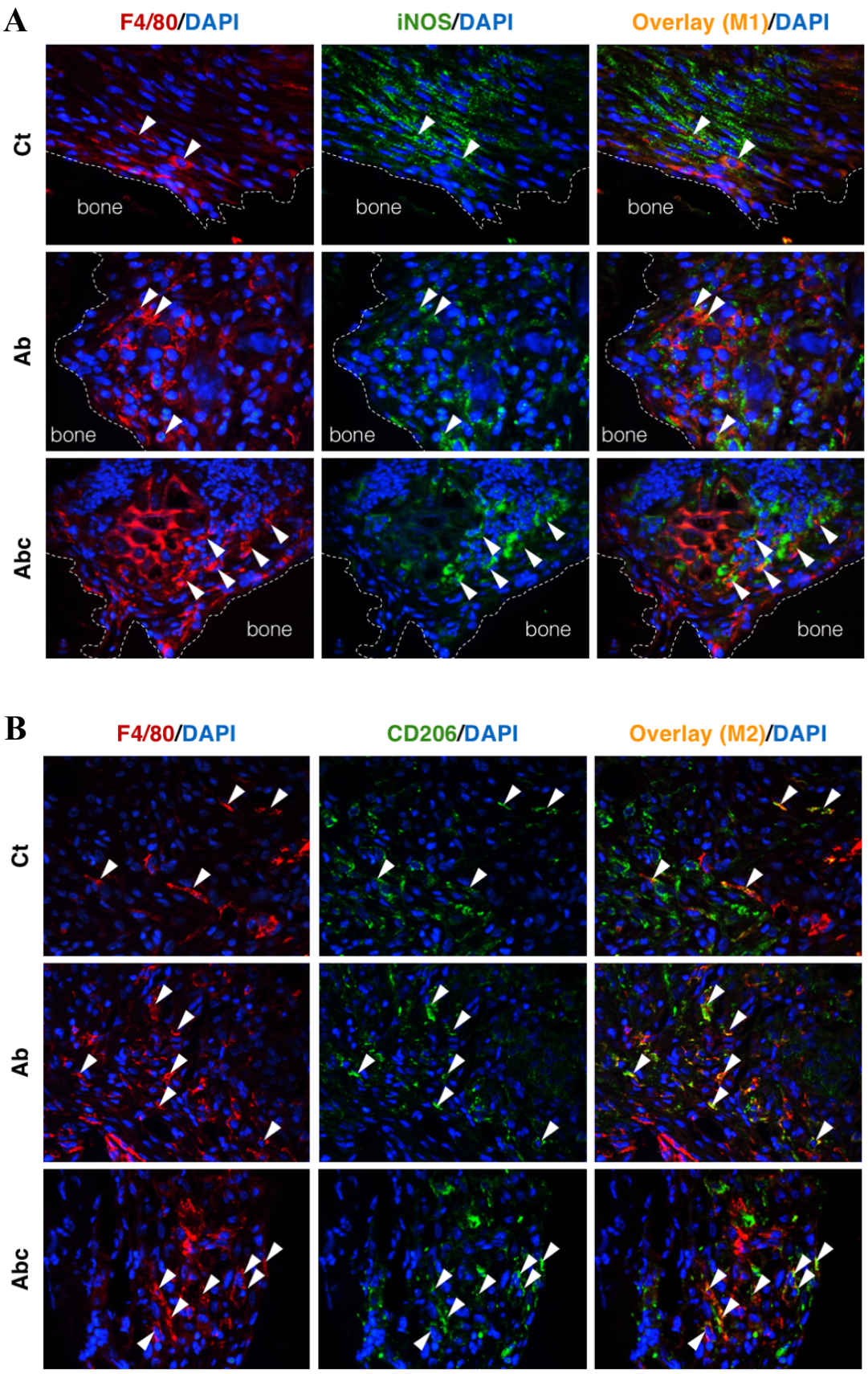
A
F4/80/DAPI
iNOS/DAPI
Overlay (M1)/DAPI
Ct
Ab
Abc
bone
B
F4/80/DAPI
CD206/DAPI
Overlay (M2)/DAPI
Ct
Ab
Abc

Figure 5.17. Double immunofluorescence staining of M1 and M2 macrophages in the early-timepoint MRONJ mouse model

Double immunofluorescence staining was used to locate **(A)** M1 and **(B)** M2 macrophages in the MRONJ mouse model. M1 was identified as F4/80+iNOS+ mononuclear cells, while M2 was identified as F4/80+CD206+ mononuclear cells. All images were taken at 40X magnification. (Red represents F4/80; green represents iNOS in panel A and CD206 in panel B; blue represents DAPI; white arrowheads represent M1 in panel A and M2 in panel B.)

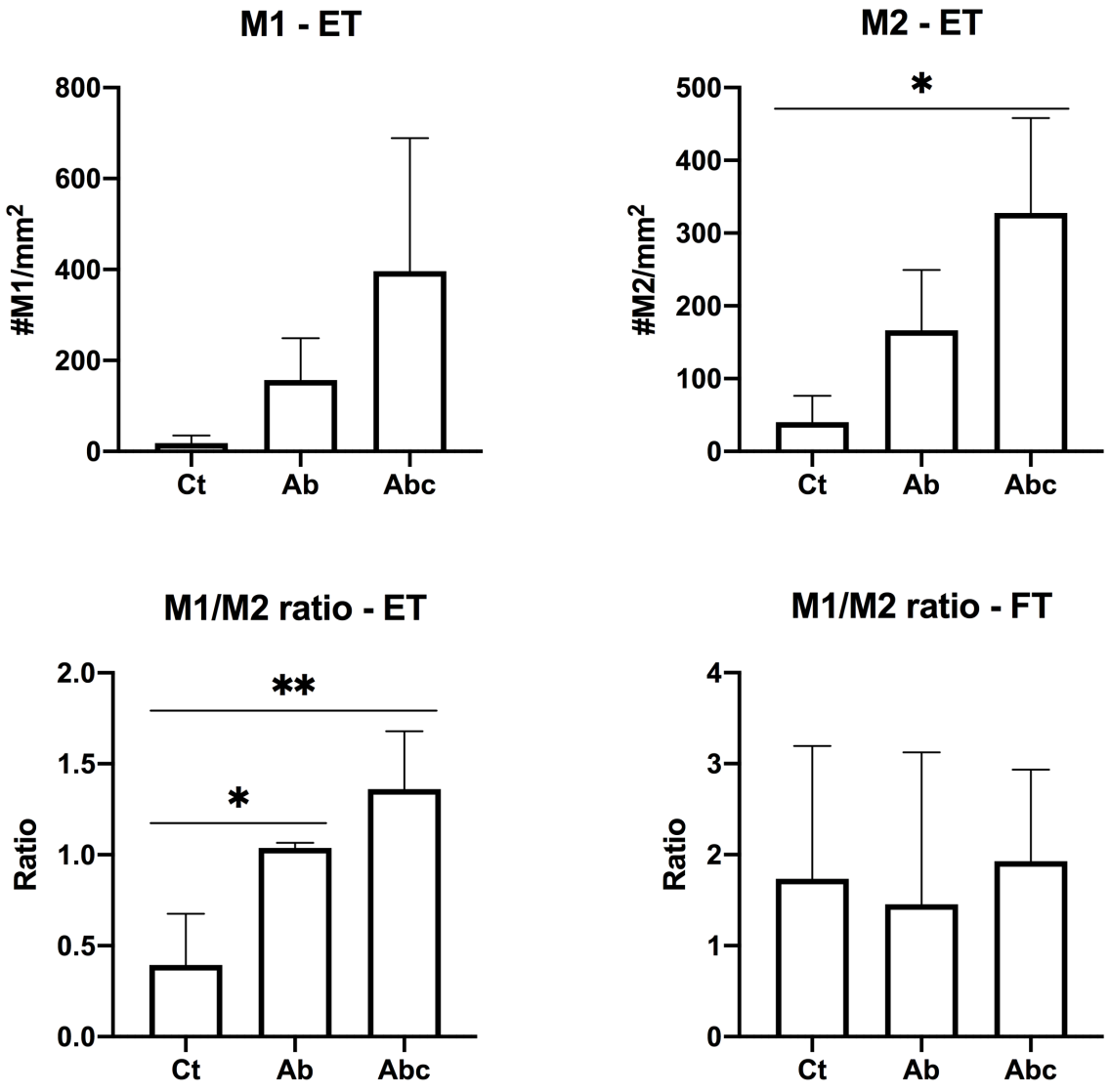

Figure 5.18. M1/M2 ratio was significantly increased in Ab and Abc groups at the early timepoint.

M1 and M2 macrophages were quantified, normalized to a total area (#/mm2), and used to calculate M1/M2 ratio. In the early timepoint (ET), the increasing trend of both M1 and M2 macrophage numbers was observed in both Ab and Abc groups. In addition, M1/M2 ratio was significantly increased in Ab and Abc compared to Ct group. However, these ratios were comparable among all groups at the final timepoint (FT). (n=3 per group; *$p<0.05$ and ** $p<0.01$)

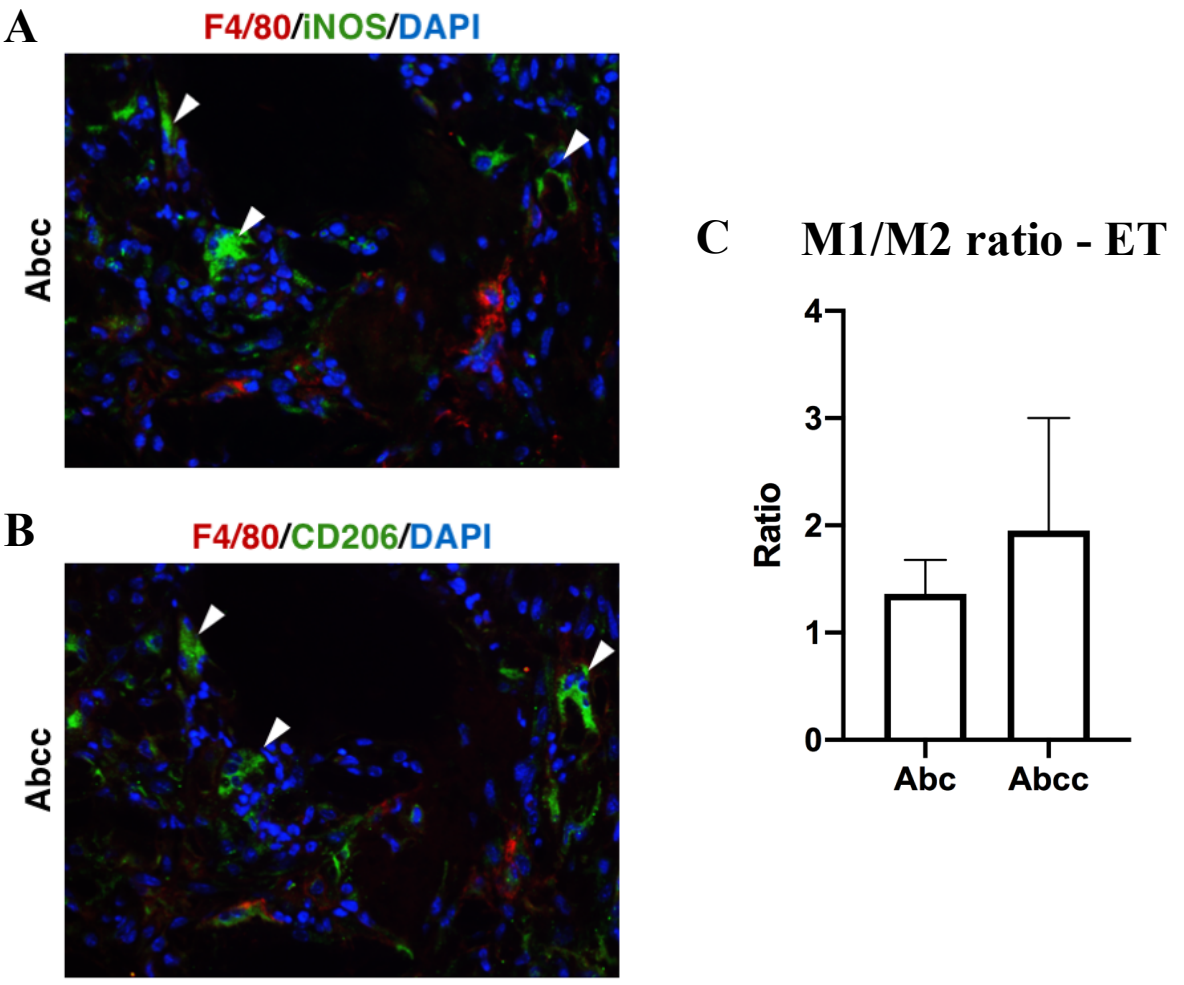

Figure 5.19. Replenishment of CID-induced osteoclasts did not alter M1/M2 ratio in the MRONJ mouse model

Double immunofluorescence staining of **(A)** F4/80 & iNOS and **(B)** F4/80 & CD206. Osteoclasts were identified as F4/80-iNOS+ and/or F4/80-CD206+ with three nuclei or more. All images were taken at 40X magnification. (Red represents F4/80; green represents iNOS in panel A and CD206 in panel B; blue represents DAPI; white arrowheads represent osteoclasts.) **(C)** Quantitation of M1/M2 ratio; there was no significant difference in M1/M2 ratio between Abc and Abcc groups in the early timepoint (ET). (n=3 per group)

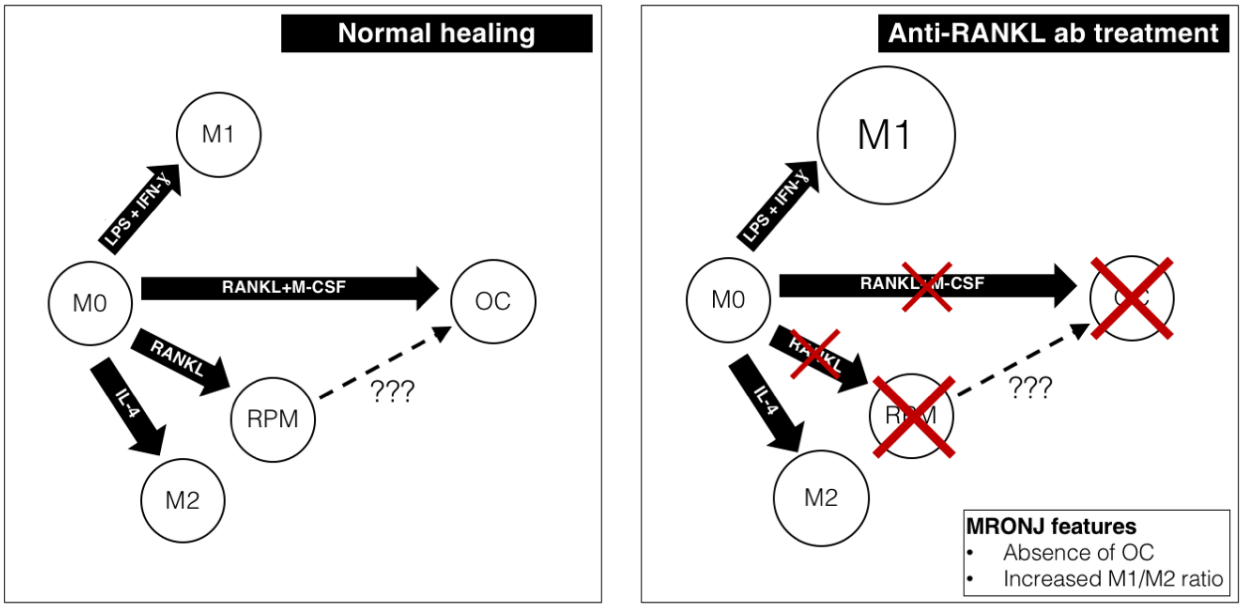

Figure 5.20. Proposed diagram of the effects of RANKL on macrophage polarization

(A) In normal wound healing, the *in vitro* data suggest that M0 macrophages can be polarized into RPMs which express a low level of M1 markers by RANKL and can be differentiated into osteoclasts (OCs) by M-CSF + RANKL with downregulated M1-related genes and upregulated osteoclast-related genes over time. However, whether RPMs can differentiate into osteoclasts has to be further investigated. **(B)** The *in vivo* data suggest that anti-RANKL antibody treatment inhibits RPM polarization and osteoclast differentiation and leads to the predominance of M1 macrophages as the increased M1/M2 ratio is observed. However, the mechanisms on how the absence of RANKL increases M1/M2 ratio have to be further investigated.

Genes	Fold changes to M0 (mean ± SD)				
	M0	**Veh**	**RPM**	**M1**	**M2**
2 hours timepoint					
Nos2 (iNOS)	1.59 ± 1.28	0.96 ± 0.33	2.44 ± 0.87	243.89 ± 22.22	18.35 ± 3.78
Tnfa	1.01 ± 0.13	1.19 ± 0.04	1.37 ± 0.08	317.48 ± 74.05	180.13 ± 20.91
Il1b	1.02 ± 0.28	0.13 ± 0.00	0.14 ± 0.00	74.12 ± 26.81	139.21 ± 19.55
Mrc1 (CD206)	1.08 ± 0.53	0.34 ± 0.08	0.33 ± 0.05	0.60 ± 0.10	0.83 ± 0.16
Arg1	1.07 ± 0.41	0.09 ± 0.03	0.06 ± 0.03	0.08 ± 0.06	1.67 ± 0.30
Ym1 (Chil3)	1.01 ± 0.13	0.37 ± 0.04	0.17 ± 0.01	0.85 ± 0.14	1.08 ± 0.05
6 hours timepoint					
Nos2 (iNOS)	1.59 ± 1.28	9.40 ± 3.30	6.67 ± 2.16	1,189.45 ± 162.68	46.24 ± 4.60
Tnfa	1.01 ± 0.13	1.66 ± 0.21	2.42 ± 0.33	194.10 ± 7.14	48.58 ± 1.01
Il1b	1.02 ± 0.28	0.23 ± 0.05	0.30 ± 0.17	41.35 ± 1.68	68.44 ± 9.64
Mrc1 (CD206)	1.08 ± 0.53	0.53 ± 0.01	0.25 ± 0.03	0.15 ± 0.01	0.35 ± 0.06
Arg1	1.07 ± 0.41	0.12 ± 0.07	0.08 ± 0.04	0.04 ± 0.02	1.61 ± 0.34
Ym1 (Chil3)	1.01 ± 0.13	0.51 ± 0.26	0.29 ± 0.05	0.29 ± 0.04	1.23 ± 0.10
24 hours timepoint					
Nos2 (iNOS)	1.59 ± 1.28	18.02 ± 18.13	47.52 ± 29.10	10,216.23 ± 228.37	778.58 ± 31.96
Tnfa	1.01 ± 0.13	0.46 ± 0.02	1.31 ± 0.04	33.48 ± 1.16	11.79 ± 1.54
Il1b	1.02 ± 0.28	0.31 ± 0.05	1.49 ± 0.34	633.36 ± 96.30	297.90 ± 19.47
Mrc1 (CD206)	1.08 ± 0.53	1.02 ± 0.14	1.19 ± 0.22	0.01 ± 0.00	0.11 ± 0.05
Arg1	1.07 ± 0.41	0.26 ± 0.19	1.08 ± 0.77	14.10 ± 3.74	728.91 ± 28.12
Ym1 (Chil3)	1.01 ± 0.13	0.44 ± 0.18	0.67 ± 0.08	0.10 ± 0.03	8.35 ± 1.23

Table 5.1. M1 and M2 gene expressions in RPMs compared to M1 and M2 macrophages

Genes	Fold changes to M0 (mean ± SD)				
	M0	**Veh**	**RPM**	**M1**	**M2**
2 hours timepoint					
Ifi205	1.14 ± 0.60	2.59 ± 0.47	3.44 ± 0.39	334.94 ± 69.75	54.10 ± 16.85
Cxcl9	1.01 ± 0.14	3.71 ± 1.78	9.42 ± 3.80	133,061.59 ± 11,350.80	70.93 ± 59.67
Mycl	1.01 ± 0.13	4.47 ± 0.43	10.92 ± 1.26	4.04 ± 1.40	1.50 ± 0.14
Mmp25	1.11 ± 0.53	1.23 ± 0.06	3.05 ± 0.38	67.34 ± 9.94	8.12 ± 0.76
Lad1	1.17 ± 0.73	2.80 ± 0.82	5.53 ± 1.28	16.10 ± 4.72	52.70 ± 2.31
Traf1	1.02 ± 0.25	3.53 ± 0.17	7.32 ± 1.84	48.63 ± 7.68	28.11 ± 2.90
6 hours timepoint					
Ifi205	1.14 ± 0.60	4.44 ± 0.77	3.37 ± 0.74	128.73 ± 3.82	111.09 ± 10.62
Cxcl9	1.01 ± 0.14	5.76 ± 1.97	17.69 ± 7.26	84,662.65 ± 10,102.48	32.09 ± 3.59
Mycl	1.01 ± 0.13	1.73 ± 0.22	4.88 ± 1.78	3.31 ± 0.49	1.57 ± 0.05
Mmp25	1.11 ± 0.53	1.99 ± 0.50	5.23 ± 1.76	940.66 ± 60.83	70.10 ± 5.05
Lad1	1.17 ± 0.73	3.68 ± 0.47	6.15 ± 1.94	139.75 ± 29.98	350.36 ± 46.83
Traf1	1.02 ± 0.25	2.91 ± 0.52	3.65 ± 0.88	45.92 ± 3.12	46.98 ± 6.05

Table 5.2. Potential RPM marker expressions in RPMs compared to M1 and M2 macrophages

Upstream Regulator	Molecule Type	Predicted Activation State	Activation z-score	p-value
TOP 15 ACTIVATED				
lipopolysaccharide	chemical drug	Activated	7.754	2.37E-43
TNF	cytokine	Activated	6.447	3.1E-26
NFkB (complex)	complex	Activated	5.738	2.58E-19
poly rI:rC-RNA	biologic drug	Activated	5.351	8.92E-20
IFNG	cytokine	Activated	5.328	1.59E-25
IL33	cytokine	Activated	4.982	4.66E-28
TNFSF11	cytokine	Activated	4.958	6.98E-29
APP	other	Activated	4.891	5.58E-13
IL1B	cytokine	Activated	4.888	7.32E-23
MYD88	other	Activated	4.724	1.48E-16
BHLHE40	transcription regulator	Activated	4.372	2.94E-10
TLR4	transmembrane receptor	Activated	4.371	1.62E-13
TLR3	transmembrane receptor	Activated	4.357	2.72E-10
NOD2	other	Activated	4.264	2.72E-26
RELA	transcription regulator	Activated	4.261	1.73E-19
TOP 15 INHIBITED				
pyrrolidine dithiocarbamate	chemical reagent	Inhibited	-2.747	3.27E-05
PP2/AG1879 tyrosine kinase inhibitor	chemical drug	Inhibited	-2.778	2.64E-05
CISH	other	Inhibited	-2.828	1.03E-05
prednisolone	chemical drug	Inhibited	-2.887	0.000228
Bay 11-7082	chemical - kinase inhibitor	Inhibited	-2.935	4.17E-06
CITED2	transcription regulator	Inhibited	-3.129	8.89E-11
troglitazone	chemical drug	Inhibited	-3.325	0.000489
SB203580	chemical drug	Inhibited	-3.329	1.02E-10
MAP3K8	kinase	Inhibited	-3.344	7.95E-11
dopamine	chemical - endogenous mammalian	Inhibited	-3.352	5.5E-09
Irgm1	other	Inhibited	-3.37	1.37E-08
ADRB	group	Inhibited	-3.45	1.3E-07
mir-21	microRNA	Inhibited	-3.787	1.54E-05
IL10RA	transmembrane receptor	Inhibited	-4.465	3.12E-20
PTGER4	G-protein coupled receptor	Inhibited	-4.583	1.47E-21

Table 5.3. Upstream regulator analysis of RPM-2h vs. Veh-2h

Upstream Regulator	Molecule Type	Predicted Activation State	Activation z-score	p-value
TOP 15 ACTIVATED				
lipopolysaccharide	chemical drug	Activated	5.02	5.85E-19
poly rI:rC-RNA	biologic drug	Activated	4.14	4.5E-18
STAT1	transcription regulator	Activated	3.799	2.07E-16
TICAM1	other	Activated	3.767	1.86E-18
IRF3	transcription regulator	Activated	3.762	4.01E-16
TLR3	transmembrane receptor	Activated	3.658	1.55E-14
APP	other	Activated	3.644	2.99E-09
IRF7	transcription regulator	Activated	3.644	9.77E-16
MYD88	other	Activated	3.638	2.24E-15
IFNG	cytokine	Activated	3.574	6.89E-15
ZBTB10	other	Activated	3.533	7.75E-15
NFkB (complex)	complex	Activated	3.487	4.94E-09
TNF	cytokine	Activated	3.464	3.15E-12
Interferon alpha	group	Activated	3.371	5.57E-17
TLR9	transmembrane receptor	Activated	3.366	2.21E-12
TOP 15 INHIBITED				
dexamethasone	chemical drug	Inhibited	-2.361	3.77E-07
SB203580	chemical drug	Inhibited	-2.399	8.31E-07
filgrastim	biologic drug	Inhibited	-2.414	1.97E-05
mir-21	microRNA	Inhibited	-2.415	0.000432
NGLY1	enzyme	Inhibited	-2.425	1.99E-09
TREX1	enzyme	Inhibited	-2.426	1.28E-10
IRGM	enzyme	Inhibited	-2.63	4.3E-10
ADRB	group	Inhibited	-2.646	5.76E-07
DUSP1	phosphatase	Inhibited	-2.726	4.28E-12
IL10RA	transmembrane receptor	Inhibited	-3.16	2.96E-20
ACKR2	G-protein coupled receptor	Inhibited	-3.317	9.53E-18
Irgm1	other	Inhibited	-3.419	6.04E-16
SOCS1	other	Inhibited	-3.668	5.03E-17
PTGER4	G-protein coupled receptor	Inhibited	-3.828	5.67E-18
CITED2	transcription regulator	Inhibited	-4.181	4.99E-20

Table 5.4. Upstream regulator analysis of RPM-6h vs. Veh-6h

Categories	Diseases or Functions Annotation	Activation z-score	p-value
TOP 15 ACTIVATED			
Cell-To-Cell Signaling and Interaction, Cellular Movement	Recruitment of cells	3.11	5.05E-12
Cell-To-Cell Signaling and Interaction, Cellular Movement	Recruitment of blood cells	3.106	3.78E-10
Cell-To-Cell Signaling and Interaction, Cellular Movement, Hematological System Development and Function, Immune Cell Trafficking	Recruitment of leukocytes	3.106	1.06E-09
Hematological Disease, Infectious Diseases, Organismal Injury and Abnormalities	Endotoxin shock response	3.102	8.93E-07
Connective Tissue Disorders, Inflammatory Disease, Organismal Injury and Abnormalities, Skeletal and Muscular Disorders	Rheumatic Disease	3.054	1.09E-13
Cellular Movement, Hematological System Development and Function, Immune Cell Trafficking	Lymphocyte migration	3.027	1.21E-12
Connective Tissue Disorders, Inflammatory Disease, Inflammatory Response, Organismal Injury and Abnormalities, Skeletal and Muscular Disorders	Inflammation of joint	2.901	6.47E-13
Endocrine System Disorders, Gastrointestinal Disease, Metabolic Disease, Organismal Injury and Abnormalities	Diabetes mellitus	2.898	1.27E-09
Cell-To-Cell Signaling and Interaction, Cellular Growth and Proliferation, Hematological System Development and Function	Induction of T lymphocytes	2.828	1.82E-06
Cellular Movement, Hematological System Development and Function, Immune Cell Trafficking	Cell movement of lymphocytes	2.805	4.45E-13
Inflammatory Disease, Organismal Injury and Abnormalities, Respiratory Disease	Fibrosis of lung	2.762	4.08E-07
Organismal Injury and Abnormalities	Pulmonary fibrosis or aplastic anemia	2.762	3.66E-06
Cellular Movement	Homing of cells	2.761	1.64E-10
Free Radical Scavenging	Metabolism of reactive oxygen species	2.739	2.98E-06
Hematological Disease, Infectious Diseases	Endotoxemia	2.732	3.09E-07
ALL INHIBITED			
Cell Death and Survival	Cell death of leukocyte cell lines	-2.053	8.11E-07
Cell Death and Survival	Apoptosis of leukocyte cell lines	-2.056	5.79E-07
Infectious Diseases	Viral Infection	-2.094	3.81E-08
Connective Tissue Disorders, Hereditary Disorder, Organismal Injury and Abnormalities	Hereditary connective tissue disorder	-2.179	1.28E-06
Cell Death and Survival	Cell death of leukemia cell lines	-2.185	3.08E-06

Table 5.5. Disease and function analysis of RPM-2h vs. Veh-2h

Categories	Diseases or Functions Annotation	Activation z-score	p-value
TOP 15 ACTIVATED			
Cellular Movement, Hematological System Development and Function, Immune Cell Trafficking	Cell movement of lymphocytes	3.21	1.79E-09
Cellular Movement, Hematological System Development and Function, Immune Cell Trafficking	Lymphocyte migration	3.049	2.87E-09
Cellular Movement, Hematological System Development and Function, Immune Cell Trafficking	Cell movement of mononuclear leukocytes	2.977	2.14E-09
Cell-To-Cell Signaling and Interaction, Cellular Movement, Hematological System Development and Function, Immune Cell Trafficking	Recruitment of leukocytes	2.815	3.14E-08
Hematological System Development and Function, Tissue Morphology	Quantity of leukocytes	2.646	3.41E-11
Hematological System Development and Function, Tissue Morphology	Quantity of blood cells	2.629	5.91E-11
Cell-mediated Immune Response, Cellular Movement, Hematological System Development and Function, Immune Cell Trafficking	T cell migration	2.624	9.58E-09
Cellular Movement, Hematological System Development and Function, Immune Cell Trafficking	Cellular infiltration by lymphocytes	2.622	9.36E-10
Cell-To-Cell Signaling and Interaction, Hematological System Development and Function, Immune Cell Trafficking, Inflammatory Response	Activation of phagocytes	2.603	0.000066
Cell-To-Cell Signaling and Interaction, Hematological System Development and Function	Activation of myeloid cells	2.588	0.000206
Cell-mediated Immune Response, Cell-To-Cell Signaling and Interaction, Cellular Movement, Hematological System Development and Function, Immune Cell Trafficking	Recruitment of T lymphocytes	2.564	2.48E-08
Cell-To-Cell Signaling and Interaction, Cellular Movement, Hematological System Development and Function, Immune Cell Trafficking	Recruitment of mononuclear leukocytes	2.56	9.21E-08
Cell-To-Cell Signaling and Interaction, Cellular Movement	Recruitment of cells	2.396	1.18E-08
Cell-To-Cell Signaling and Interaction, Cellular Growth and Proliferation, Hematological System Development and Function	Stimulation of leukocytes	2.386	8.44E-07
Immunological Disease	Hypersensitive reaction	2.377	4.35E-05
ALL INHIBITED			
Infectious Diseases	Replication of Flaviviridae	-2.157	2.03E-05
Cell Signaling	Replication of viral replicon	-2.216	1.8E-06
Infectious Diseases	Viral Infection	-2.79	0.001
Infectious Diseases	Replication of virus	-2.917	0.00143

Table 5.6. Disease and function analysis of RPM-6h vs. Veh-6h

Chapter 6. CONCLUSION

The pathophysiology of MRONJ which often occurs after tooth extraction has remained elusive resulting in lack of effective curative treatments. In my thesis, I investigated the effects of antiresorptive drugs on various cell types involving in the healing processes following tooth extraction which may potentially contribute to MRONJ pathophysiology. Firstly, the roles of osteoclasts in MRONJ were studied. I showed that the osteoclast differentiation of iRANK cells, the engineered cells which have been developed in the lab, can be controlled by CID and is resistant to the inhibition by anti-RANKL antibody *in vitro*. Additionally, I utilized the iRANK cells in the loss-and-gain of bone resorptive function study in the MRONJ mouse model induced by tooth extraction and anti-RANK antibody and showed that the replenishment of osteoclasts reduced necrotic bone area *in vivo*. However, the other MRONJ features including impaired new bone formation and incomplete epithelial closure did not improve suggesting that there are potentially other mechanisms contributing to MRONJ pathophysiology in addition to osteoclast inhibition.

Secondly, I identified the effects of antiresorptive drugs on osteoblasts, a bone forming cell. Although the impaired new bone formation has been observed in both BRONJ and DRONJ, most studies only focus on the inhibitory effects of BPs on osteoblasts and their functions. In my thesis, I determined the effects of anti-RANKL antibody on osteogenic differentiation of MC3T3 pre-osteoblast cell line via the autocrine/paracrine regulatory loop of RANKL *in vitro*. Interestingly, I showed that MC3T3 cells do not express RANK, a receptor of RANKL, which supports the finding that anti-RANKL antibody did not have any significant effect on osteogenic differentiation of MC3T3 cells. Additionally, these *in vitro* findings support the data from my MRONJ mouse model that there was no significant difference in newly-formed bone area between control and anti-RANKL antibody-treated group. (Ct vs. Ab group). Altogether, these data suggest that anti-

RANKL antibody is unlikely to have any significant effects on the osteogenic differentiation of osteoblasts and new bone formation.

Lastly, I investigated the roles of macrophages in MRONJ. To understand how anti-RANKL antibody affects macrophage polarization in MRONJ context, I started by identifying the effects of RANKL on macrophage polarization using isolated murine bone marrow-derived (BMD) cells *in vitro*. In contrast to my hypothesis that RANKL may induce BMD cells into RANKL-polarized macrophage (RPM) phenotype, which is distinct from M1 and M2 macrophages, I discovered that several genes were upregulated in RPMs similarly to M1 macrophages, however, in much lower level. I further showed that unpolarized macrophages (M0) are able to differentiate into osteoclasts similarly to BMD cells by the treatment of M-CSF and RANKL. Additionally, previous studies have shown that BPs can induce M1 polarization and an increased M1/M2 ratio is observed in BRONJ animal models and patients with the impaired bone formation lesions. Thus, I determined the M1/M2 ratio in my MRONJ mouse model and observed the increased M1/M2 ratio in both Ab and Abc groups representing stage 0 and stage 1 MRONJ respectively. Taking both *in vitro* and *in vivo* data together, RANKL upregulates several M1-related genes in RPMs, but only at the low level *in vitro* suggesting that the absence of RANKL may potentially have more significant effects on other cell types which may indirectly affect macrophage polarization resulting in the increased M1/M2 ratio observed in my MRONJ mouse model.

In summary, my thesis focuses on the alteration of osteoclasts, osteoblasts, and macrophages caused by antiresorptive drugs which contributes to MRONJ pathophysiology. Osteoclast inhibition and increased M1/M2 ratio were observed in my MRONJ mouse model induced by anti-RANKL antibody treatment. This helps filling out the huge gap in the field that both inhibited bone remodeling and inflammation also contribute to DRONJ pathophysiology

similarly to BRONJ which has already been shown by many previous studies. Most importantly, my thesis paves the way of engineered osteoclasts as a study tool and potential cell therapy approach for MRONJ treatment which is urgently required in the field.

Chapter 7. FUTURE STUDIES

Although the MRONJ model was successfully developed utilizing tooth extraction and anti-RANKL antibody in my thesis, this model (Ab group) only exhibits mild lesions representing stage 0 MRONJ in humans. For future studies, more robust MRONJ models are required to study the disease progression and develop proper treatments for a late-stage MRONJ. Several recent studies as well as my findings suggest that inflammation is essential in addition to bone remodeling inhibition in order to induce MRONJ. Therefore, the extraction of the teeth with pre-existing inflammatory environment can potentially establish more robust MRONJ models such as the experimental periodontitis model (placing ligature around the teeth to induce inflammation before tooth extraction).

Osteoclast inhibition has been proposed as a potential mechanism leading to MRONJ, thus, the proposed cell therapy of the engineered osteoclasts may serve as a novel treatment strategy for MRONJ. Utilizing the iRANK osteoclasts in my thesis proves this hypothesis, however, replenishment of osteoclasts alone does not completely heal MRONJ lesions. It has been shown that the disturbed macrophage population exhibited as the increased number of overall macrophages and the increased M1/M2 ratio contributes to bone pathologies including periodontitis and BRONJ. In my thesis, I also showed that M1/M2 ratio was increased in my MRONJ mouse model (Ab and Abc groups) and restoring osteoclasts without decreasing this ratio did not improve impaired bone formation and incomplete epithelial closure (Abcc group). Therefore, the proposed cell therapy needs to be modified in several possible aspects. Since iRANK cells not only have potential to differentiate into osteoclasts, but can also polarize into M1 and M2 macrophages, delivery of iRANK cells can disturb the macrophage population equilibrium. Therefore, delivery of enriched iRANK osteoclasts should be considered in the future studies to

maintain physiological macrophage number and M1/M2 ratio while restoring the bone resorptive function. Additionally, inflammation in MRONJ should be explored thoroughly in the future studies such as the contribution of bacteria invasion and necrotic bone to macrophage alteration and MRONJ progression, as well as, approaches to control inflammation in MRONJ such as delivery of cytokine cocktail to decrease M1/M2 ratio to the optimal level.

Lastly, the recent studies have suggested that MRONJ is multifactorial disease and the pathophysiology is contributed by many mechanisms. Only osteoclasts, osteoblasts, and macrophages involving in bone remodeling inhibition and inflammation were investigated in this thesis. Thus, the future studies should explore other mechanisms, for instance, angiogenesis inhibition, innate or acquired immune dysfunction, and genetic factors and cells involved in these processes including but not limited to endothelial cells, T-cells, and dendritic cells. Transcriptomics approaches such as single-cell RNA sequencing and spatial transcriptomics along with robust MRONJ models can be a beneficial tool to study various types of cells potentially contributing to MRONJ pathophysiology.

BIBLIOGRAPHY

1. S. L. Ruggiero, T. B. Dodson, J. Fantasia, R. Goodday, T. Aghaloo, B. Mehrotra, F. O'Ryan, American Association of Oral and Maxillofacial Surgeons, American Association of Oral and Maxillofacial Surgeons position paper on medication-related osteonecrosis of the jaw--2014 update., *J. Oral Maxillofac. Surg.* **72**, 1938–56 (2014).

2. A. Khan, A. Morrison, A. Cheung, W. Hashem, J. Compston, Osteonecrosis of the jaw (ONJ): diagnosis and management in 2015., *Osteoporos. Int.* (2015), doi:10.1007/s00198-015-3335-3.

3. S. L. Ruggiero, T. B. Dodson, T. Aghaloo, E. R. Carlson, B. B. Ward, D. Kademani, American Association of Oral and Maxillofacial Surgeons' Position Paper on Medication-Related Osteonecrosis of the Jaws—2022 Update*J. Oral Maxillofac. Surg.* **80** (2022), doi:10.1016/j.joms.2022.02.008.

4. S. L. Ruggiero, T. B. Dodson, L. A. Assael, R. Landesberg, R. E. Marx, B. Mehrotra, American Association of Oral and Maxillofacial Surgeons Position Paper on Bisphosphonate-Related Osteonecrosis of the Jaws-2009 Update, *J. Oral Maxillofac. Surg.* **67** (2009), doi:10.1016/j.joms.2009.01.009.

5. A. D. Anastasilakis, S. A. Polyzos, P. Makras, B. Aubry-Rozier, S. Kaouri, O. Lamy, Clinical Features of 24 Patients With Rebound-Associated Vertebral Fractures After Denosumab Discontinuation: Systematic Review and Additional Cases, *J. Bone Miner. Res.* **32** (2017), doi:10.1002/jbmr.3110.

6. S. R. Cummings, S. Ferrari, R. Eastell, N. Gilchrist, J. E. B. Jensen, M. McClung, C. Roux, O. Törring, I. Valter, A. T. Wang, J. P. Brown, Vertebral Fractures After Discontinuation of

Denosumab: A Post Hoc Analysis of the Randomized Placebo-Controlled FREEDOM Trial and Its Extension, *J. Bone Miner. Res.* **33** (2018), doi:10.1002/jbmr.3337.

7. E. Tsourdi, B. Langdahl, M. Cohen-Solal, B. Aubry-Rozier, E. F. Eriksen, N. Guañabens, B. Obermayer-Pietsch, S. H. Ralston, R. Eastell, M. C. Zillikens, Discontinuation of Denosumab therapy for osteoporosis: A systematic review and position statement by ECTS*Bone* **105** (2017), doi:10.1016/j.bone.2017.08.003.

8. A. E. Vieira, C. E. Repeke, S. De Barros Ferreira, P. M. Colavite, C. C. Biguetti, R. C. Oliveira, G. F. Assis, R. Taga, A. P. F. Trombone, G. P. Garlet, Intramembranous bone healing process subsequent to tooth extraction in mice: Micro-computed tomography, histomorphometric and molecular characterization, *PLoS One* **10** (2015), doi:10.1371/journal.pone.0128021.

9. M. G. Araújo, C. O. Silva, M. Misawa, F. Sukekava, Alveolar socket healing: What can we learn?, *Periodontol. 2000* **68** (2015), doi:10.1111/prd.12082.

10. M. Genin, F. Clement, A. Fattaccioli, M. Raes, C. Michiels, M1 and M2 macrophages derived from THP-1 cells differentially modulate the response of cancer cells to etoposide, *BMC Cancer* **15** (2015), doi:10.1186/s12885-015-1546-9.

11. D. M. Mosser, The many faces of macrophage activation, *J. Leukoc. Biol.* **73** (2003), doi:10.1189/jlb.0602325.

12. M. Kreutz, R. Andreesen, S. Krause, A. Szabo, E. Ritz, H. Reichel, 1,25-dihydroxyvitamin D3 production and vitamin D3 receptor expression are developmentally regulated during differentiation of human monocytes into macrophages, *Blood* **82** (1993), doi:10.1182/blood.v82.4.1300.bloodjournal8241300.

13. F. Takahashi, K. Takahashi, K. Shimizu, R. Cui, N. Tada, H. Takahashi, S. Soma, M. Yoshioka, Y. Fukuchi, Osteopontin is strongly expressed by alveolar macrophages in the lungs of acute

respiratory distress syndrome, *Lung* **182** (2004), doi:10.1007/s00408-004-0309-1.

14. C. M. Champagne, J. Takebe, S. Offenbacher, L. F. Cooper, Macrophage cell lines produce osteoinductive signals that include bone morphogenetic protein-2, *Bone* **30** (2002), doi:10.1016/S8756-3282(01)00638-X.

15. L. Cardoso, B. C. Herman, O. Verborgt, D. Laudier, R. J. Majeska, M. B. Schaffler, Osteocyte Apoptosis Controls Activation of Intracortical Resorption in Response to Bone Fatigue, *J. Bone Miner. Res.* **24** (2009), doi:10.1359/jbmr.081210.

16. O. Verborgt, G. J. Gibson, M. B. Schaffler, Loss of osteocyte integrity in association with microdamage and bone remodeling after fatigue in vivo, *J. Bone Miner. Res.* **15** (2000), doi:10.1359/jbmr.2000.15.1.60.

17. J. I. Aguirre, L. I. Plotkin, S. A. Stewart, R. S. Weinstein, A. M. Parfitt, S. C. Manolagas, T. Bellido, Osteocyte apoptosis is induced by weightlessness in mice and precedes osteoclast recruitment and bone loss, *J. Bone Miner. Res.* **21** (2006), doi:10.1359/jbmr.060107.

18. W. D. Clark, E. L. Smith, K. A. Linn, J. R. Paul-Murphy, P. Muir, M. E. Cook, Osteocyte apoptosis and osteoclast presence in chicken radii 0-4 days following osteotomy, *Calcif. Tissue Int.* **77** (2005), doi:10.1007/s00223-005-0074-z.

19. L. Trombelli, R. Farina, A. Marzola, L. Bozzi, B. Liljenberg, J. Lindhe, Modeling and remodeling of human extraction sockets, *J. Clin. Periodontol.* **35** (2008), doi:10.1111/j.1600-051X.2008.01246.x.

20. W. Zhu, R. Xu, J. Du, Y. Fu, S. Li, P. Zhang, L. Liu, H. Jiang, Zoledronic acid promotes TLR-4-mediated M1 macrophage polarization in bisphosphonate-related osteonecrosis of the jaw, *FASEB J.* **33** (2019), doi:10.1096/fj.201801791RR.

21. J. Kaneko, T. Okinaga, H. Hikiji, W. Ariyoshi, D. Yoshiga, M. Habu, K. Tominaga, T.

Nishihara, Zoledronic acid exacerbates inflammation through M1 macrophage polarization, *Inflamm. Regen.* **38** (2018), doi:10.1186/s41232-018-0074-9.

22. S. Shi, Q. Zhang, I. Atsuta, S. Liu, C. Chen, S. Shi, A. D. Le, IL-17-mediated M1/M2 macrophage alteration contributes to pathogenesis of bisphosphonate-related osteonecrosis of the jaws, *Clin. Cancer Res.* **19** (2013), doi:10.1158/1078-0432.CCR-13-0042.

23. L. N. Zhou, C. S. Bi, L. N. Gao, Y. An, F. Chen, F. M. Chen, Macrophage polarization in human gingival tissue in response to periodontal disease, *Oral Dis.* **25** (2019), doi:10.1111/odi.12983.

24. C. Garaicoa-Pazmino, T. Fretwurst, C. H. Squarize, T. Berglundh, W. V. Giannobile, L. Larsson, R. M. Castilho, Characterization of macrophage polarization in periodontal disease, *J. Clin. Periodontol.* **46** (2019), doi:10.1111/jcpe.13156.

25. T. Kim, S. Kim, M. Song, C. Lee, H. Yagita, D. W. Williams, E. C. Sung, C. Hong, K. H. Shin, M. K. Kang, N. H. Park, R. H. Kim, Removal of Pre-Existing Periodontal Inflammatory Condition before Tooth Extraction Ameliorates Medication-Related Osteonecrosis of the Jaw–Like Lesion in Mice, *Am. J. Pathol.* **188** (2018), doi:10.1016/j.ajpath.2018.06.019.

26. A. Soundia, D. Hadaya, N. Esfandi, I. Gkouveris, R. Christensen, S. M. Dry, O. Bezouglaia, F. Pirih, N. Nikitakis, T. Aghaloo, S. Tetradis, Zoledronate Impairs Socket Healing after Extraction of Teeth with Experimental Periodontitis, *J. Dent. Res.* **97** (2018), doi:10.1177/0022034517732770.

27. T. L. Aghaloo, B. Kang, E. C. Sung, M. Shoff, M. Ronconi, J. E. Gotcher, O. Bezouglaia, S. M. Dry, S. Tetradis, Periodontal disease and bisphosphonates induce osteonecrosis of the jaws in the rat., *J. Bone Miner. Res.* **26**, 1871–82 (2011).

28. F. J. Rodríguez-Lozano, R. Oñate-Sánchez, M. Gonzálvez-García, M. Vallés-Bergadá, C. M.

Martínez, B. Revilla-Nuin, J. Guerrero-Gironés, J. M. Moraleda, D. García-Bernal, Allogeneic bone marrow mesenchymal stem cell transplantation in tooth extractions sites ameliorates the incidence of osteonecrotic jaw-like lesions in zoledronic acid-treated rats, *J. Clin. Med.* **9** (2020), doi:10.3390/jcm9061649.

29. P. Barba-Recreo, J. L. Del Castillo Pardo De Vera, T. Georgiev-Hristov, E. Ruiz Bravo-Burguillos, A. Abarrategi, M. Burgueño, M. García-Arranz, Adipose-derived stem cells and platelet-rich plasma for preventive treatment of bisphosphonate-related osteonecrosis of the jaw in a murine model, *J. Cranio-Maxillofacial Surg.* **43** (2015), doi:10.1016/j.jcms.2015.04.026.

30. S. Kuroshima, M. Sasaki, K. Nakajima, S. Tamaki, H. Hayano, T. Sawase, Transplantation of Noncultured Stromal Vascular Fraction Cells of Adipose Tissue Ameliorates Osteonecrosis of the Jaw–Like Lesions in Mice, *J. Bone Miner. Res.* **33** (2018), doi:10.1002/jbmr.3292.

31. T. Tamari, R. Elimelech, G. Cohen, T. Cohen, O. Doppelt, L. Eskander-Hashoul, H. Zigdon-Giladi, Endothelial Progenitor Cells inhibit jaw osteonecrosis in a rat model: A major adverse effect of bisphosphonate therapy, *Sci. Rep.* **9** (2019), doi:10.1038/s41598-019-55383-5.

32. S. Kuroshima, K. Nakajima, M. Sasaki, I. Takashi, Y. Sumita, T. Asahara, I. Asahina, T. Sawase, Systemic administration of quality- A nd quantity-controlled PBMNCs reduces bisphosphonate-related osteonecrosis of jaw-like lesions in mice, *Stem Cell Res. Ther.* **10** (2019), doi:10.1186/s13287-019-1308-8.

33. K. Ogata, M. Matsumura, M. Moriyama, W. Katagiri, H. Hibi, S. Nakamura, Cytokine Mixtures Mimicking Secretomes From Mesenchymal Stem Cells Improve Medication-Related Osteonecrosis of the Jaw in a Rat Model, *JBMR Plus* **2** (2018), doi:10.1002/jbm4.10013.

34. C. W. Rementer, M. Wu, W. Buranaphatthana, H. Y. L. Yang, M. Scatena, C. M. Giachelli, An inducible, ligand-independent receptor activator of NF-kB gene to control osteoclast

differentiation from monocytic precursors, *PLoS One* **8** (2013), doi:10.1371/journal.pone.0084465.

35. A. I. Gogakos, M. S. Cheung, J. H. D. Bassett, G. R. Williams, Bone signaling pathways and treatment of osteoporosis*Expert Rev. Endocrinol. Metab.* **4** (2009), doi:10.1586/eem.09.38.

36. J. H. Kim, N. Kim, Signaling Pathways in Osteoclast Differentiation, *Chonnam Med. J.* **52** (2016), doi:10.4068/cmj.2016.52.1.12.

37. J. R. Edwards, M. M. Weivoda, Osteoclasts: Malefactors of disease and targets for treatment, *Discov. Med.* **13** (2012).

38. K. Iwamoto, T. Miyamoto, Y. Sawatani, N. Hosogane, I. Hamaguchi, M. Takami, K. Nomiyama, K. Takagi, T. Suda, Dimer formation of receptor activator of nuclear factor κB induces incomplete osteoclast formation, *Biochem. Biophys. Res. Commun.* **325** (2004), doi:10.1016/j.bbrc.2004.10.024.

39. S. Kuroshima, M. Sasaki, T. Sawase, Medication-related osteonecrosis of the jaw: A literature review*J. Oral Biosci.* **61** (2019), doi:10.1016/j.job.2019.03.005.

40. S. Tamaki, S. Kuroshima, H. Hayano, K. Nakajima, H. Kakehashi, A. Ishisaki, T. Sawase, Dynamic polarization shifting from M1 to M2 macrophages in reduced osteonecrosis of the jaw-like lesions by cessation of anti-RANKL antibody in mice, *Bone* (2020), doi:10.1016/j.bone.2020.115560.

41. K. A. Deuell, A. Callegari, C. M. Giachelli, M. E. Rosenfeld, M. Scatena, RANKL enhances macrophage paracrine pro-calcific activity in high phosphate-treated smooth muscle cells: Dependence on IL-6 and TNF-α, *J. Vasc. Res.* **49** (2012), doi:10.1159/000341216.

42. L. Dunphy, G. Salzano, B. Gerber, J. Graystone, Republished: Medication-related osteonecrosis (MRONJ) of the mandible and maxilla, *Drug Ther. Bull.* (2020), doi:10.1136/dtb.2020.224455rep.

43. M. R. Allen, S. L. Ruggiero, A review of pharmaceutical agents and oral bone health: how osteonecrosis of the jaw has affected the field., *Int. J. Oral Maxillofac. Implants* **29**, e45-57.

44. E. Gaudin, L. Seidel, M. Bacevic, E. Rompen, F. Lambert, Occurrence and risk indicators of medication-related osteonecrosis of the jaw after dental extraction: a systematic review and meta-analysis., *J. Clin. Periodontol.* **42**, 922–932 (2015).

45. N. C. Wright, A. C. Looker, K. G. Saag, J. R. Curtis, E. S. Delzell, S. Randall, B. Dawson-Hughes, The recent prevalence of osteoporosis and low bone mass in the United States based on bone mineral density at the femoral neck or lumbar spine, *J. Bone Miner. Res.* **29** (2014), doi:10.1002/jbmr.2269.

46. D. W. Williams, C. Lee, T. Kim, H. Yagita, H. Wu, S. Park, P. Yang, H. Liu, S. Shi, K.-H. Shin, M. K. Kang, N.-H. Park, R. H. Kim, Impaired bone resorption and woven bone formation are associated with development of osteonecrosis of the jaw-like lesions by bisphosphonate and anti-receptor activator of NF-κB ligand antibody in mice., *Am. J. Pathol.* **184**, 3084–93 (2014).

47. H. Hayano, S. Kuroshima, M. Sasaki, S. Tamaki, M. Inoue, A. Ishisaki, T. Sawase, Distinct immunopathology in the early stages between different antiresorptives-related osteonecrosis of the jaw-like lesions in mice, *Bone* **135** (2020), doi:10.1016/j.bone.2020.115308.

48. L. Gong, Y. Zhao, Y. Zhang, Z. Ruan, The macrophage polarization regulates MSC osteoblast differentiation in vitro, *Ann. Clin. Lab. Sci.* **46** (2016).

49. R. Huang, X. Wang, Y. Zhou, Y. Xiao, RANKL-induced M1 macrophages are involved in bone formation, *Bone Res.* **5** (2017), doi:10.1038/boneres.2017.19.

50. W. Buranaphatthana, A. Yavirach, E. M. Leaf, M. Scatena, H. Zhang, J. Y. An, C. M. Giachelli, Engineered osteoclasts resorb necrotic alveolar bone in anti-RANKL antibody-treated mice, *Bone* **153** (2021), doi:10.1016/j.bone.2021.116144.

51. F. Saad, J. E. Brown, C. Van Poznak, T. Ibrahim, S. M. Stemmer, A. T. Stopeck, I. J. Diel, S. Takahashi, N. Shore, D. H. Henry, C. H. Barrios, T. Facon, F. Senecal, K. Fizazi, L. Zhou, A. Daniels, P. Carri??re, R. Dansey, Incidence, risk factors, and outcomes of osteonecrosis of the jaw: Integrated analysis from three blinded active-controlled phase III trials in cancer patients with bone metastases, *Ann. Oncol.* **23**, 1341–1347 (2012).

52. E. Michael Lewiecki, Denosumab: An investigational drug for the management of postmenopausal osteoporosis*Biol. Targets Ther.* **2**, 645–653 (2008).

53. P. D. Miller, Denosumab: Anti-RANKL antibody*Curr. Osteoporos. Rep.* **7**, 18–22 (2009).

54. P. J. Kostenuik, H. Q. Nguyen, J. McCabe, K. S. Warmington, C. Kurahara, N. Sun, C. Chen, L. Li, R. C. Cattley, G. Van, S. Scully, R. Elliott, M. Grisanti, S. Morony, H. L. Tan, F. Asuncion, X. Li, M. S. Ominsky, M. Stolina, D. Dwyer, W. C. Dougall, N. Hawkins, W. J. Boyle, W. S. Simonet, J. K. Sullivan, Denosumab, a fully human monoclonal antibody to RANKL, inhibits bone resorption and increases BMD in knock-in mice that express chimeric (murine/human) RANKL., *J. Bone Miner. Res.* **24**, 182–95 (2009).

55. R. Rizzoli, U. Yasothan, P. Kirkpatrick, Denosumab, *Nat. Rev. Drug Discov.* **9**, 591–592 (2010).

56. R. G. Russell, M. J. Rogers, J. C. Frith, S. P. Luckman, F. P. Coxon, H. L. Benford, P. I. Croucher, C. Shipman, H. A. Fleisch, The pharmacology of bisphosphonates and new insights into their mechanisms of action., *J. Bone Miner. Res.* **14 Suppl 2**, 53–65 (1999).

57. S. Colucci, V. Minielli, G. Zambonin, N. Cirulli, G. Mori, M. Serra, V. Patella, A. Zambonin Zallone, M. Grano, Alendronate reduces adhesion of human osteoclast-like cells to bone and bone protein-coated surfaces., *Calcif. Tissue Int.* **63**, 230–5 (1998).

58. D. Heymann, B. Ory, F. Gouin, J. R. Green, F. Rédini, Bisphosphonates: new therapeutic

agents for the treatment of bone tumors, *Trends Mol. Med.* **10**, 337–343 (2004).

59. D. E. Hughes, K. R. Wright, H. L. Uy, A. Sasaki, T. Yoneda, G. D. Roodman, G. R. Mundy, B. F. Boyce, Bisphosphonates promote apoptosis in murine osteoclasts in vitro and in vivo., *J. Bone Miner. Res.* **10**, 1478–87 (1995).

60. J. R. Green, P. Clézardin, Mechanisms of Bisphosphonate Effects on Osteoclasts, Tumor Cell Growth, and Metastasis, *Am. J. Clin. Oncol.* **25**, S3–S9 (2002).

61. V. Viereck, G. Emons, V. Lauck, K.-H. Frosch, S. Blaschke, C. Gründker, L. C. Hofbauer, Bisphosphonates pamidronate and zoledronic acid stimulate osteoprotegerin production by primary human osteoblasts., *Biochem. Biophys. Res. Commun.* **291**, 680–6 (2002).

62. B. Pan, A. N. Farrugia, L. B. To, D. M. Findlay, J. Green, K. Lynch, A. C. W. Zannettino, The nitrogen-containing bisphosphonate, zoledronic acid, influences RANKL expression in human osteoblast-like cells by activating TNF-alpha converting enzyme (TACE)., *J. Bone Miner. Res.* **19**, 147–54 (2004).

63. H. Katsarelis, N. P. Shah, D. K. Dhariwal, M. Pazianas, Infection and medication-related osteonecrosis of the jaw., *J. Dent. Res.* **94**, 534–9 (2015).

64. K. M. Kim, Y. Rhee, Y.-D. Kwon, T.-G. Kwon, J. K. Lee, D.-Y. Kim, Medication Related Osteonecrosis of the Jaw: 2015 Position Statement of the Korean Society for Bone and Mineral Research and the Korean Association of Oral and Maxillofacial Surgeons, *J. Bone Metab.* **22**, 151 (2015).

65. E. Sehic, A. Westerlund, M. K. Lagerquist, U. H. Lerner, H. Carlsten, P. Henning, C. Engdahl, Immunoglobulin G complexes without sialic acids enhance osteoclastogenesis but do not affect arthritis-mediated bone loss, *Scand. J. Immunol.* **93** (2021), doi:10.1111/sji.13009.

66. U. Harre, S. C. Lang, R. Pfeifle, Y. Rombouts, S. Frühbeißer, K. Amara, H. Bang, A. Lux, C.

A. Koeleman, W. Baum, K. Dietel, F. Gröhn, V. Malmström, L. Klareskog, G. Krönke, R. Kocijan, F. Nimmerjahn, R. E. M. Toes, M. Herrmann, H. U. Scherer, G. Schett, Glycosylation of immunoglobulin G determines osteoclast differentiation and bone loss, *Nat. Commun.* **6** (2015), doi:10.1038/ncomms7651.

67. Y. Liu, Z. Li, M. Arioka, L. Wang, C. Bao, J. A. Helms, WNT3A accelerates delayed alveolar bone repair in ovariectomized mice, *Osteoporos. Int.* **30** (2019), doi:10.1007/s00198-019-05071-x.

68. I. Glickman, S. Pruzansky, M. Ostrach, The healing of extraction wounds in the presence of retained root remnants and bone fragments. An experimental study, *Am. J. Orthod. Oral Surg.* **33** (1947), doi:10.1016/0096-6347(47)90063-X.

69. G. S. Heithersay Ao, B. Kahler, Healing responses following transverse root fracture: A historical review and case reports showing healing with (a) calcified tissue and (b) dense fibrous connective tissue, *Dent. Traumatol.* **29** (2013), doi:10.1111/edt.12029.

70. J. P. Gorski, Is all bone the same? Distinctive distributions and properties of non-collagenous matrix proteins in lamellar vs. woven bone imply the existence of different underlying osteogenic mechanisms., *Crit. Rev. Oral Biol. Med.* **9**, 201–23 (1998).

71. A. Allegra, V. Innao, N. Pulvirenti, C. Musolino, Antiresorptive agents and anti-angiogenesis drugs in the development of osteonecrosis of the jaw*Tohoku J. Exp. Med.* **248** (2019), doi:10.1620/tjem.248.27.

72. J. D. Kün-Darbois, H. Libouban, G. Mabilleau, F. Pascaretti-Grizon, D. Chappard, Bone mineralization and vascularization in bisphosphonate-related osteonecrosis of the jaw: an experimental study in the rat, *Clin. Oral Investig.* **22** (2018), doi:10.1007/s00784-018-2385-2.

73. M. Q. S. Soares, J. Van Dessel, R. Jacobs, P. S. da Silva Santos, T. M. Cestari, G. P. Garlet,

M. A. H. Duarte, T. S. N. Imada, I. Lambrichts, I. R. F. Rubira-Bullen, Zoledronic Acid Induces Site-Specific Structural Changes and Decreases Vascular Area in the Alveolar Bone, *J. Oral Maxillofac. Surg.* **76** (2018), doi:10.1016/j.joms.2018.03.007.

74. N. A. Chrysanthakopoulos, Reasons for extraction of permanent teeth in Greece: A five-year follow-up study, *Int. Dent. J.* **61** (2011), doi:10.1111/j.1875-595X.2011.00004.x.

75. P. P. L. Fung, G. Bedogni, A. Bedogni, A. Petrie, S. Porter, G. Campisi, J. Bagan, V. Fusco, G. Saia, S. Acham, P. Musto, M. T. Petrucci, P. Diz, G. Colella, M. D. Mignogna, M. Pentenero, P. Arduino, G. Lodi, C. Maiorana, M. Manfredi, P. Hallberg, M. Wadelius, K. Takaoka, Y. Y. Leung, R. Bonacina, M. Schiødt, P. Lakatos, T. Taylor, G. De Riu, G. Favini, S. N. Rogers, M. Pirmohamed, P. Nicoletti, S. Fedele, J. L. López-Cedrún, S. Madsen, G. Sadile, S. Leuci, C. Mirelli, G. Conti, R. Maiavacca, M. Urade, H. Kishimoto, S. Okui, Y. Zushi, M. Yamamura, K. Yoshikawa, G. Mansueto, P. K. E. Magnusson, S. Popat, B. Kirnbauer, B. Obermayer-Pietsch, N. Jakse, U. Mariani, V. Martini, A. Fasciolo, I. De Martino, M. Alessio, J. F. Sanromán, S. Grammatico, G. Siniscalchi, A. Itro, B. Balla, J. P. Kosa, M. Vaszilko, J. Lo, E. Besi, F. D'Aiuto, K. Yong, N. Donos, V. Mercadante, R. Stein, S. D'Sa, E. Varoni, D. Soma, S. Meloni, J. Evely, A. Hanson, F. Giancola, O. Di Fede, V. Panzarella, G. Bettini, E. Merigo, G. Mergoni, P. Vescovi, S. Gandolfo, R. Marino, M. Berrone, A. Gambino, E. Menegatti, R. Broccoletti, E. Hens, L. Bagan, Time to onset of bisphosphonate-related osteonecrosis of the jaws: a multicentre retrospective cohort study, *Oral Dis.* **23** (2017), doi:10.1111/odi.12632.

76. T. Kikuiri, I. Kim, T. Yamaza, K. Akiyama, Q. Zhang, Y. Li, C. Chen, W. J. Chen, S. Wang, A. D. Le, S. Shi, Cell-based immunotherapy with mesenchymal stem cells cures bisphosphonate-related osteonecrosis of the jaw-like disease in mice, *J. Bone Miner. Res.* **25** (2010), doi:10.1002/jbmr.37.

77. R. Elsayed, Z. Kurago, C. W. Cutler, R. M. Arce, J. Gerber, E. Celis, H. Sultan, M. Elashiry, M. Meghil, C. Sun, C. M. Auersvald, M. E. Awad, R. Zeitoun, R. Elsayed, M. Eldin M. Elshikh, C. Isales, M. E. Elsalanty, Role of dendritic cell-mediated immune response in oral homeostasis: A new mechanism of osteonecrosis of the jaw, *FASEB J.* **34** (2020), doi:10.1096/fj.201901819RR.

78. I. Szadvari, O. Krizanova, P. Babula, Athymic nude mice as an experimental model for cancer treatment*Physiol. Res.* **65** (2016), doi:10.33549/physiolres.933526.

79. R. Romano, L. Palamaro, A. Fusco, L. Iannace, S. Maio, I. Vigliano, G. Giardino, C. Pignata, From murine to human Nude/SCID: The thymus, T-Cell development and the missing link*Clin. Dev. Immunol.* **2012** (2012), doi:10.1155/2012/467101.

80. M. Pelleitier, S. Montplaisir, The nude mouse: a model of deficient T-cell function.*Methods Achiev. Exp. Pathol.* **7** (1975).

81. S. Park, K. Kanayama, K. Kaur, H. C. H. Tseng, S. Banankhah, D. T. Quje, J. W. Sayre, A. Jewett, I. Nishimura, Osteonecrosis of the jaw developed in mice: Disease variants regulated by γδ T cells in oral mucosal barrier immunity, *J. Biol. Chem.* **290** (2015), doi:10.1074/jbc.M115.652305.

82. F. M. Chen, H. H. Sun, H. Lu, Q. Yu, Stem cell-delivery therapeutics for periodontal tissue regeneration*Biomaterials* **33** (2012), doi:10.1016/j.biomaterials.2012.05.048.

83. J. Jung, J. S. Park, L. Righesso, A. M. Pabst, B. Al-Nawas, Y. D. Kwon, C. Walter, Effects of an oral bisphosphonate and three intravenous bisphosphonates on several cell types in vitro, *Clin. Oral Investig.* **22** (2018), doi:10.1007/s00784-018-2349-6.

84. F. Schena, C. Menale, E. Caci, L. Diomede, E. Palagano, C. Recordati, M. Sandri, A. Tampieri, I. Bortolomai, V. Capo, C. Pastorino, A. Bertoni, M. Gattorno, A. Martini, A. Villa, E. Traggiai, C. Sobacchi, Murine Rankl−/− Mesenchymal Stromal Cells Display an Osteogenic Differentiation

Defect Improved by a RANKL-Expressing Lentiviral Vector, *Stem Cells* **35** (2017), doi:10.1002/stem.2574.

85. S. Saracino, R. A. Canuto, M. Maggiora, M. Oraldi, M. Scoletta, L. Ciuffreda, A. M. Vandone, S. Carossa, M. Mozzati, G. Muzio, Exposing human epithelial cells to zoledronic acid can mediate osteonecrosis of jaw: An in vitro model, *J. Oral Pathol. Med.* **41** (2012), doi:10.1111/j.1600-0714.2012.01173.x.

86. F. Thibaut, T. Watrin, F. Meary, S. Tricot, V. Legros, P. Pellen-Mussi, D. Chauvel-Lebret, Effects of zoledronic acid on osteoblasts in three-dimensional culture, *J. Dent. Sci.* **10** (2015), doi:10.1016/j.jds.2014.07.004.

87. E. Anitua, M. Zalduendo, M. Troya, G. Orive, PRGF exerts a cytoprotective role in zoledronic acid-treated oral cells, *Clin. Oral Investig.* **20** (2016), doi:10.1007/s00784-015-1528-y.

88. A. Mosch, T. Ettl, A. Mamilos, S. Schreml, S. Spörl, G. Spanier, C. Klingelhöffer, Physiological concentrations of denosumab enhance osteogenic differentiation in human mesenchymal stem cells of the jaw bone, *Arch. Oral Biol.* **101** (2019), doi:10.1016/j.archoralbio.2019.03.005.

89. D. Golden, E. A. Saria, M. F. Hansen, Regulation of Osteoblast Migration Involving Receptor Activator of Nuclear Factor-kappa B (RANK) Signaling, *J. Cell. Physiol.* **230** (2015), doi:10.1002/jcp.25024.

90. A. Soundia, D. Hadaya, N. Esfandi, R. S. de Molon, O. Bezouglaia, S. M. Dry, F. Q. Pirih, T. Aghaloo, S. Tetradis, Osteonecrosis of the jaws (ONJ) in mice after extraction of teeth with periradicular disease, *Bone* **90** (2016), doi:10.1016/j.bone.2016.06.011.

91. B. P. Sinder, A. R. Pettit, L. K. McCauley, Macrophages: Their Emerging Roles in Bone*J. Bone Miner. Res.* **30** (2015), doi:10.1002/jbmr.2735.

92. C. Sima, A. Viniegra, M. Glogauer, Macrophage immunomodulation in chronic osteolytic diseases—the case of periodontitis*J. Leukoc. Biol.* **105** (2019), doi:10.1002/JLB.1RU0818-310R.

93. P. Paschalidi, I. Gkouveris, A. Soundia, E. Kalfarentzos, E. Vardas, M. Georgaki, G. Kostakis, B. M. Erovic, S. Tetradis, C. Perisanidis, N. G. Nikitakis, The role of M1 and M2 macrophage polarization in progression of medication-related osteonecrosis of the jaw, *Clin. Oral Investig.* **25** (2021), doi:10.1007/s00784-020-03602-z.

94. N. Udagawa, M. Koide, M. Nakamura, Y. Nakamichi, T. Yamashita, S. Uehara, Y. Kobayashi, Y. Furuya, H. Yasuda, C. Fukuda, E. Tsuda, Osteoclast differentiation by RANKL and OPG signaling pathways*J. Bone Miner. Metab.* **39** (2021), doi:10.1007/s00774-020-01162-6.

95. M. Motiur Rahman, S. Takeshita, K. Matsuoka, K. Kaneko, Y. Naoe, A. Sakaue-Sawano, A. Miyawaki, K. Ikeda, Proliferation-coupled osteoclast differentiation by RANKL: Cell density as a determinant of osteoclast formation, *Bone* **81** (2015), doi:10.1016/j.bone.2015.08.008.

96. C. C. Kung, S. P. Dai, H. Chiang, H. S. Huang, W. H. Sun, Temporal expression patterns of distinct cytokines and M1/M2 macrophage polarization regulate rheumatoid arthritis progression, *Mol. Biol. Rep.* **47** (2020), doi:10.1007/s11033-020-05422-6.

97. B. Liang, H. Wang, D. Wu, Z. Wang, Macrophage M1/M2 polarization dynamically adapts to changes in microenvironment and modulates alveolar bone remodeling after dental implantation, *J. Leukoc. Biol.* **110** (2021), doi:10.1002/JLB.1MA0121-001R.

98. Z. Cui, R. Feng, Z. Liu, Y. Gong, Y. Zhang, Receptor Activator of Nuclear Factor (Nf)-kb Ligand Promotes T Helper 17 Cell Differentiation through Fas, *Immunol. Invest.* (2021), doi:10.1080/08820139.2021.1948050.

VITA

A. EDUCATION

2017-2022 **Doctor of Philosophy, Oral Health Sciences**, School of Dentistry, University of Washington, USA

Thesis topic: Roles of Osteoclasts and Macrophages in Medication-Related Osteonecrosis of the Jaw Pathophysiology

2016-2017 **Prosthodontics Postgraduate Program**, Chiang Mai University, Thailand

2009-2015 **Doctor of Dental Surgery (Hons)**, Chiang Mai University, Thailand

B. POSITIONS AND HONORS

Positions and Employment

2015-Present **Instructor**, Department of Prosthodontics, Faculty of Dentistry, Chiang Mai University, Thailand

Academic and Professional Honors

2021-2022 **Magnuson scholarship**, School of Dentistry, University of Washington

2020 **AADR Student Research Day Award**, American Association of Dental Research (AADR) 2020

Winner of School of Dentistry Research Day graduate poster competition, School of Dentistry, University of Washington

2019-present **Geriatric sciences for dental care scholarship**, Thai government

2017-2019 **Fulbright scholarship**, U.S. government

2016 **Winner of 21st Century Teaching & Learning Innovation**, Software Aiding in Denture Design for Dental Students, Chiang Mai University, Thailand

2015 **Winner of video competition for dental care in patients with disability**, Faculty of Dentistry, Chiang Mai University, Thailand

C. PUBLICATIONS AND ABSTRACTS

Publications

2021 Buranaphatthana W.*, **Yavirach A.***, Leaf E. M., Scatena M., Zhang H., An J. Y., Giachelli C. M. (2021). Engineered osteoclasts resorb necrotic alveolar bone in anti-RANKL antibody-treated mice. *Bone*, *153*, 116144. (* indicates equal contribution.)

2019 Rungsiyakull P., Kasetwong K., **Yavirach A.**, Sornsuwan T. (2019). Fracture analysis of post material and bonding condition on a cylindrical Glass-Resin Bilayer structure. Journal of International Dental and Medical Research, 12(3), 870–879.

2018 Subsomboon T., Hemwutiphan N., Suphatarkul N., Lomklang N., Lertratanawong P., Choosuk S., Sastraruji T., **Yavirach A.**, Jia-mahasap W., Yavirach P., Chaijareenont P. (2018). Effect of Different Surface Treatments on Shear Bond Strength of Alumina Plate Bonded with Resin Cement. Khon Kaen University Dental Journal, 21(2), 94-106.

Conference Presentations

2022 **A. Yavirach**, W. Buranaphatthana, C. Rementor, C. M. Giachelli, Engineered Osteoclasts: Potential Cell Therapy for Ectopic Calcification, the SFB/JSB Hawaii Joint Symposium, January 2022, Hawaii, USA (poster presentation)

2020 **A. Yavirach***, W. Buranaphatthana*, E. M. Leaf, M. Scatena, H. Zhang, C. M. Giachelli, Engineered Osteoclasts Resorb Necrotic Bone in MRONJ Mouse Model, School of Dentistry Research Day 2020, January 2020, University of Washington (poster presentation, * indicates equal contribution.)

2019 **Yavirach A.**, Software Aiding in Denture Design for Dental Students, the 15th Teaching & Learning Symposium 2019, April 2019, University of Washington (poster presentation)

2016 **Yavirach A.,** "One Special Day for the Special Ones"; the Health Promotion Project for the Disabled at Kuamoong Village, Chiang Mai, Thailand, the 15th Asia Pacific Student Services Association (APSSA) International Conference 2016, June 2016, Chiang Mai, Thailand (oral presentation)